AGH University of Science and Technology
Faculty of Physics and Applied Computer Science

Doctoral thesis

Michał Gałkowski

TEMPORAL AND SPATIAL VARIABILITY OF NITROUS OXIDE IN THE ATMOSPHERE OVER MAŁOPOLSKA REGION: DETERMINATION OF LOADS AND EMISSIONS

Supervisor: prof. dr hab. Kazimierz Różański
Co-supervisor: dr inż. Jarosław Nęcki

Kraków, July 2015

Declaration of the author of this dissertation:

Aware of legal responsibility for making untrue statements I hereby declare that I have written this dissertation myself and all the contents of the dissertation have been obtained by legal means.

Declaration of the thesis Supervisor:

This dissertation is ready to be reviewed.

Niniejszą pracę dedykuję mojej *Żonie*, *Edycie*,
za cierpliwość i wsparcie przez ostatnie cztery lata.

Pragnę szczerze i serdecznie podziękować
profesorowi *Kazimierzowi Różańskiemu*
za nieocenioną pomoc.

Serdecznie dziękuję *Jarosławowi Nęckiemu*,
za wsparcie na każdym etapie
w pracy i poza nią.

Podziękowania składam również
przyjaciołom i kolegom z Zespołu Fizyki Środowiska:
Mirosławowi Zimnochowi,
Jakubowi Bartyzelowi,
Łukaszowi Chmurze,
Damianowi Ziębie,
Klaudii Ciaciek,
za pomoc, poświęcony czas i za to,
że zawsze chciałem wracać do pracy.

Dziękuję również
Kierownictwu Interdyscyplinarnych Studiów Doktoranckich,
a w szczególności *prof. dr hab. Januszowi Adamowskiemu*,
oraz wszystkim pracownikom
Wydziału Fizyki i Informatyki Stosowanej
Akademii Górniczo – Hutniczej im. Stanisława Staszica w Krakowie,
za możliwość pracy i nauki w najlepszych warunkach.

Niniejsza rozprawa doktorska została wykonana w ramach
Programu Operacyjnego Kapitał Ludzki POKL.04.01.01-00-434/08-02
współfinansowanego ze środków Unii Europejskiej.

CONTENTS

1. INTRODUCTION

The nitrous oxide (N_2O), both ozone-depleting and greenhouse gas, has been gaining attention of scientists and policy makers for some years now. Its emissions are reported, along with other greenhouse gases, in the framework of Kyoto Protocol, of which Poland is an Annex I Party. Currently, there is a lack of high-quality information about variability of N_2O in the atmosphere over Central Europe across diverse spatial and temporal scales, as well as about typical levels of emissions of this gas from both natural ecosystems and anthropogenic sources in the region. The presented PhD thesis, "Temporal and spatial variability of nitrous oxide in the atmosphere over Małopolska region: determination of loads and emissions", constitutes an attempt to provide such an information, utilizing a multitude of available sources and methods, including *in-situ* measurements, external emission databases as well as modern numerical tools.

In this introductory chapter, a short overview of the rationale behind this PhD work will be given (section 1.1), together with main goals that were set at the start of this four-year project (section 1.2). In section 1.3, funding sources are acknowledged.

1.1. Rationale.

A multitude of nitrogen compounds circulate through the environment on a variety of spatial and temporal scales. Their lower abundances, when compared to molecular nitrogen (N_2, present mainly in the atmosphere) reflects the overall high reactivity of these substances. They function under a collective name – reactive nitrogen (N_r) – and include a great variety of substances that display a wide range of physical and chemical properties. Anthropogenic activities result in excessive concentrations of some of those substances in selected compartments of the global ecosphere, causing environmental problems such as soil and air quality degradation, ozone depletion, ecosystem changes, ground- and surface water pollution and global warming (Figure 1.1.). These will be discussed in more detail in Chapter 2 of this thesis.

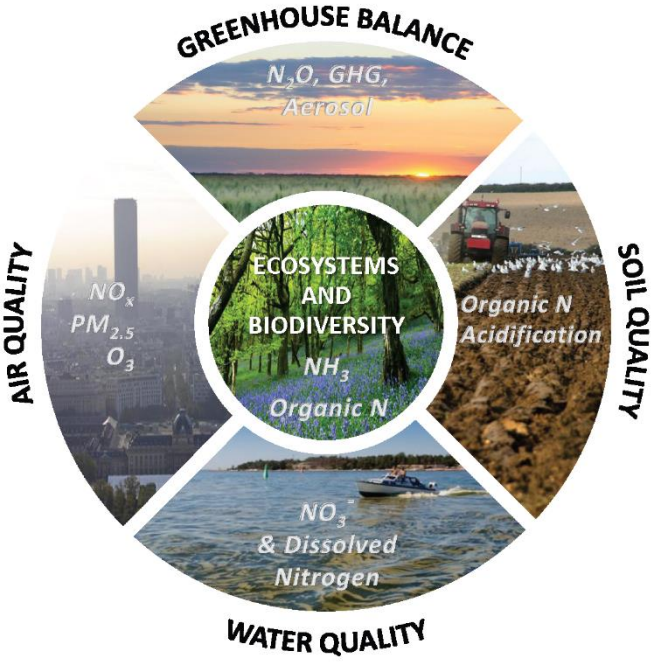

Figure 1.1. Summary of key societal threats of excess reactive nitrogen (N_r) present in the environment. The main chemical forms associated with each threat are shown. Source: Sutton et al. (2011a).

Nitrous oxide plays an important role in the Earth's System, through its interaction with climate, as both a long-lived greenhouse gas (LLGG) and the most important ozone depleting substance (ODS; see Ravishankara et al., 2009, IPCC, 2013). In recognition of this role, N_2O has been included in the international effort to curb the negative effects of growing emissions of LLGGs –

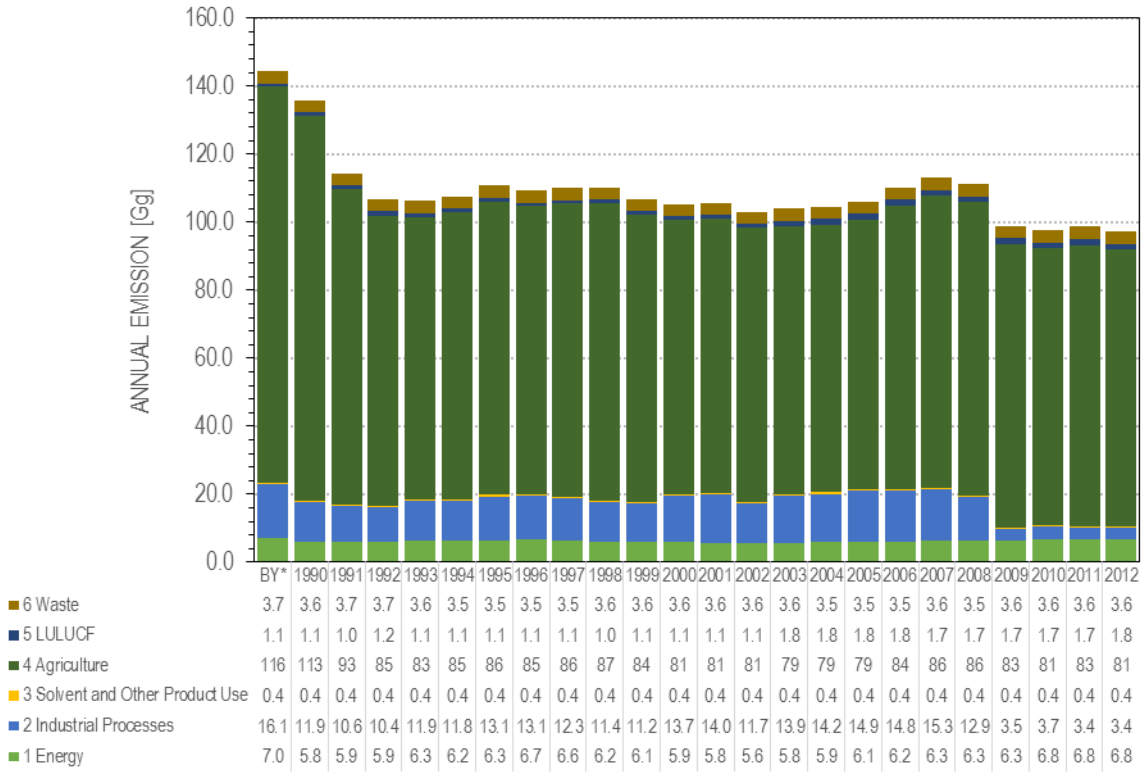

	BY*	1990	1991	1992	1993	1994	1995	1996	1997	1998	1999	2000	2001	2002	2003	2004	2005	2006	2007	2008	2009	2010	2011	2012
6 Waste	3.7	3.6	3.7	3.7	3.6	3.5	3.5	3.5	3.5	3.6	3.6	3.6	3.6	3.6	3.6	3.5	3.5	3.5	3.6	3.5	3.6	3.6	3.6	3.6
5 LULUCF	1.1	1.1	1.0	1.2	1.1	1.1	1.1	1.1	1.1	1.0	1.1	1.1	1.1	1.1	1.8	1.8	1.8	1.8	1.7	1.7	1.7	1.7	1.7	1.8
4 Agriculture	116	113	93	85	83	85	86	85	86	87	84	81	81	81	79	79	79	84	86	86	83	81	83	81
3 Solvent and Other Product Use	0.4	0.4	0.4	0.4	0.4	0.4	0.4	0.4	0.4	0.4	0.4	0.4	0.4	0.4	0.4	0.4	0.4	0.4	0.4	0.4	0.4	0.4	0.4	0.4
2 Industrial Processes	16.1	11.9	10.6	10.4	11.9	11.8	13.1	13.1	12.3	11.4	11.2	13.7	14.0	11.7	13.9	14.2	14.9	14.8	15.3	12.9	3.5	3.7	3.4	3.4
1 Energy	7.0	5.8	5.9	5.9	6.3	6.2	6.3	6.7	6.6	6.2	6.1	5.9	5.8	5.6	5.8	5.9	6.1	6.2	6.3	6.3	6.3	6.8	6.8	6.8

Figure 1.2. National emissions of N_2O by Poland as reported to UNFCCC, grouped by IPCC activity sector. Data for 1989 was not available. BY – base year (1988). LULUCF – Land Use, Land-Use Change and Forestry. Source: UNFCCC (2014)

United Nations Framework Convention on Climate Change (*UNFCCC*), which is best known for the Kyoto Protocol – a global agreement obliging the signatory countries to reduce their national emissions of greenhouse gases by the year 2012 and beyond. Poland is a signatory country of the Kyoto Protocol both as an independent party and through membership in the European Union. Although the Kyoto Protocol is in force, the first commitment period has expired already by the end of 2012, and no new binding agreement has been reached as of the moment of writing this thesis.

The data show that the efforts to reduce Poland's greenhouse gas emissions have been successful to this point, with almost 30% decrease in total LLGG emission between 1988 and 2012, with reduction in total annual releases of all greenhouse gases included in the UNFCCC, including N_2O. As seen in Figure 1.2., the most important contribution to N_2O emissions reported by Poland to UNFCCC is the agriculture (ca. 83.5% of total for 2012), responsible for releases of close to 80 Gg N_2O annually. Of other sectors, most notable additions come from Energy (7.0%), Waste (3.7%) and Industrial Processes (3.5%). The effect of targeted mitigation measures in the industrial sector is clearly visible, where in the years of 2007-2009 several Joint Implementation projects (one of the Flexibility Mechanisms of the Kyoto Protocol) aimed at reducing the N_2O releases from ammonia oxidation installations have been started. These have resulted in 77% reduction of industrial emissions of N_2O – close to 12% of Poland's national total.

On a global scale, reductions have been reported by most signatory countries (LLGG total), with just above 2 Pg CO_2-equivalent being released to the Earth's atmosphere every year (UNFCCC, 2014). These reductions, however, are not sufficient. The most recent, 5th Assessment Report by the Intergovernmental Panel on Climate Change states that "*Global mean temperatures will continue to rise over the 21st century if greenhouse gas (GHG) emissions continue unabated*" (IPCC, 2013). The report predicts that globally averaged temperatures in 2080-2100 will rise by 0.3 to 4.8 °C above the values observed in 1986-2005, depending on the abatement scenarios.

While N_2O is not the most important greenhouse gas, with only 6% increase of the mean radiative forcing related to it, the reduction of its emissions can bring unproportionally large benefits for certain key environmental issues, such as reduction of stratospheric ozone or pollution of water resources by dissolved nitrogen compounds. While the most important processes of the production and destruction of N_2O are known, some important gaps in current scientific knowledge are still present, preventing precise estimation of the N_2O balance on global and regional scales.

Bottom-up budgets of N_2O rely in large part on the emission factors that relate large-scale emissions to certain proxy quantities, based on current scientific understanding of the emission processes. However, limitations of this understanding, stemming from the enormous variety of biogenic and anthropogenic emission sources with their spatial and temporal heterogeneity, make global budgets of N_2O highly uncertain, with confidence interval of the total N_2O emissions reported in the IPCC AR5 ranging from 2.7 to 11.1 Tg N-N_2O yr^{-1} (IPCC, 2013).

Continuing studies of nitrogen cycle on regional and local scales can help to better constraint this important cycle through two main pathways: (i) verification of the reported N_2O releases, and (ii) providing additional, detailed information on the process parameters driving the emissions of N_2O. Regional and local scales are also the most appropriate means of acquiring the knowledge about disaggregated N_2O emissions from specific activity sectors. Generalizations made in the global bottom-up budgets have limited ability to reproduce nation-wide specifics, e.g. regarding the agricultural practices that are the most important driver of N_2O emissions.

1.2. Main goals of the thesis.

The overarching goal of the presented work was to provide a holistic view of nitrous oxide emission and transport patterns on a regional scale, through a case study of Małopolska region in southern Poland. In order to achieve that goal, a methodology was applied that combined gathering of information on the regional emissions from multiple publicly available sources (such as relevant databases and scientific literature) and independent verification with *in-situ* measurements through a variety of statistical analyses as well as numerical transport modelling.

This main goal has been divided into three specific tasks, each focusing on certain aspects of the problem. Each of those tasks have been the focus of one chapter in the presented PhD thesis.

The first task was to provide a consistent, long-term (at least 2 year), high-quality and quality-controlled record of N_2O concentrations in the atmosphere over southern Poland from two observation stations representing two distinctly different conditions – lower tropospheric urban environment and high-mountain, relatively clean environment. These instrumental records formed the basis for statistical analyses of temporal and spatial characteristics of N_2O transport patterns in southern Poland presented in the thesis. They also represent a valuable resource for future studies of this type, e.g. using advanced inverse modelling frameworks. The results achieved under this task are presented in Chapter 3 of the PhD thesis.

The second task was focused on the description of the main N_2O emission sources in Małopolska, together with their respective spatial and temporal patterns. In the scope of this task, *in-situ* measurements of N_2O fluxes from agricultural sources were to be performed, in order to: (i) provide an independent assessment of annual releases of N_2O from this sector and to compare them with

the available database estimates, and (ii) try to determine the main factors that drive these N_2O emissions. Chapter 4 of the thesis contains the description of the methodology and the discussion of the obtained results.

The third task was aimed at coupling the obtained information on atmospheric concentrations and emission sources of nitrous oxide in order to provide quantitative information on spatial and temporal patterns of N_2O emissions and transport. In order to achieve that goal, a modelling framework has been established that utilized the Stochastic Time-Inverted Lagrangian Transport model (STILT), allowing to predict the N_2O concentrations at chosen measurement sites and compare selected scenarios of N_2O emissions with the observations. An attempt has also been made to use the STILT-observations framework to independently verify the emissions from the largest point-type source of N_2O in the Małopolska region, a chemical plant located in Tarnów. These efforts were described in Chapter 5 of this work.

1.3. Funding.

The author would like to gratefully acknowledge all the sources of funding that helped him to perform the research described in the presented PhD thesis.

The N_2O measurements performed at Kasprowy Wierch station (KAS) in the scope of this PhD work have been a part of the NA2/NA3 workpackages of the InGOS project (*Integrated non-CO2 Greenhouse Gas Observing System* - 2011-2015, 7th Framework European Union Project), support from which is kindly acknowledged.

Measurements performed at Kraków station (KRK) and field flux measurements campaigns have been a part of the scientific project "Temporal and spatial variability of nitrous oxide in the atmosphere of southern Poland: estimation of regional loads and fluxes of N_2O", financed by the National Science Centre (decision no. EC-2012/05/N/ST10/03710).

The author of this thesis has been partly supported by the EU Human Capital Operation Program, Polish Project No. POKL.04.0101-00-434/08-00 and by the Doctus programme (Małopolska Scholarship Fund for PhD Students). Doctus programme was partly supported by EU funds from the European Social Fund.

2. THE GLOBAL NITROGEN CYCLE

Starting from the middle of XIX century, growing food demand of increasing human population has resulted in a steady increase of chemically active (reactive) nitrogen compounds (N_r[1]) loads in the environment, initially mainly through the growing usage of crop residues and animal manure as fertilizer. As the industrialization process progressed, however, new pathways of acquiring N_r were required, not only for food security but also for growing military applications (production of munitions). These increased N_r requirements were fulfilled by intense mining of saltpetre (a naturally occurring form of potassium nitrate, KNO_3) and guano deposits in Chile, making western world a "fossil nitrogen economy" (Erisman et al., 2008, Sutton et al., 2008, Sutton et al., 2011a and references therein). The invention of chemical fixation of atmospheric nitrogen by Fritz Haber in 1908 has made the industrial-scale production of artificial ammonia possible, which gave access to practically unlimited supply of mineral fertilizers, and effectively allowed Central Powers to maintain military actions during the First World War after the trade routes to Chile were cut-off by the Allies.

By the 1950, the Haber-Bosch process had replaced the fossil reserves as the main source of N_r for the society, and its global production has been increasing ever since, more than doubling the pre-industrial levels of natural N_r inputs (Galloway et al., 2004, 2008). According to the data of Food and Agriculture Organization, in 2005 the Haber-Bosch process was the source of 121 Tg N yr^{-1} of N_r produced globally (FAO, 2006). It has been estimated that 98 Tg N yr^{-1} of this global supply was introduced directly into the environment in the form of fertilizers (Prud'homme, 2007, Smith, 2010), with the rest being used by industry and its final fate unclear. Rising food demand is also responsible for development of cultivation-induced biological nitrogen fixation (BNF), where specialized crops (e.g. legumes) are being planted specifically to increase N_r availability. BNF is estimated to produce nowadays another 40 Tg N yr^{-1} (Galloway et al., 2008).

Regardless of its source, N_r added to the environment is responsible for both local and large-scale impacts as it "cascades" down through different parts of the global ecosystem (Galloway and Cowling, 2002, Galloway et al., 2003). It has been calculated by Smil (2002, 2004) that over 50 % of new N_r added to agricultural ecosystems is subsequently lost, either to the atmosphere (NO_x, N_2O, NH_3, N_2) or through surface and underground runoff (as dissolved or particulate N_r, mainly as NO_3^-). These compounds will undergo further chemical changes before ultimately being converted back to N_2. The concept of the nitrogen cascade is further discussed in section 2.2.

Nitrous oxide (N_2O) is only one of many forms of nitrogen which are present in the environment. However, as a major long-lived greenhouse gas and the most potent ozone depleting substance, it is critical to understand the processes of its formation and destruction when developing appropriate strategies aimed at diminishing negative impact of greenhouse gases on the climate system. This task, however, cannot be achieved without considering the place of N_2O in the global nitrogen cycle.

[1] In the presented work, the term "reactive nitrogen" is defined following the work by Galloway et al. (2004), i.e. it includes all biologically, photochemically and radiatively active molecules that contain N atoms and are present in the atmosphere and biosphere of Earth. Such a definition is broader than one usually accepted in the atmospheric chemistry community, and include both inorganic reduced forms of N (e.g. NH_3, NH_4^+), inorganic oxidized forms (e.g. N_2O, NO_3^-, HNO_3, NO_2, NO) as well as organic compounds (e.g. urea, proteins, nucleic acids, etc.).

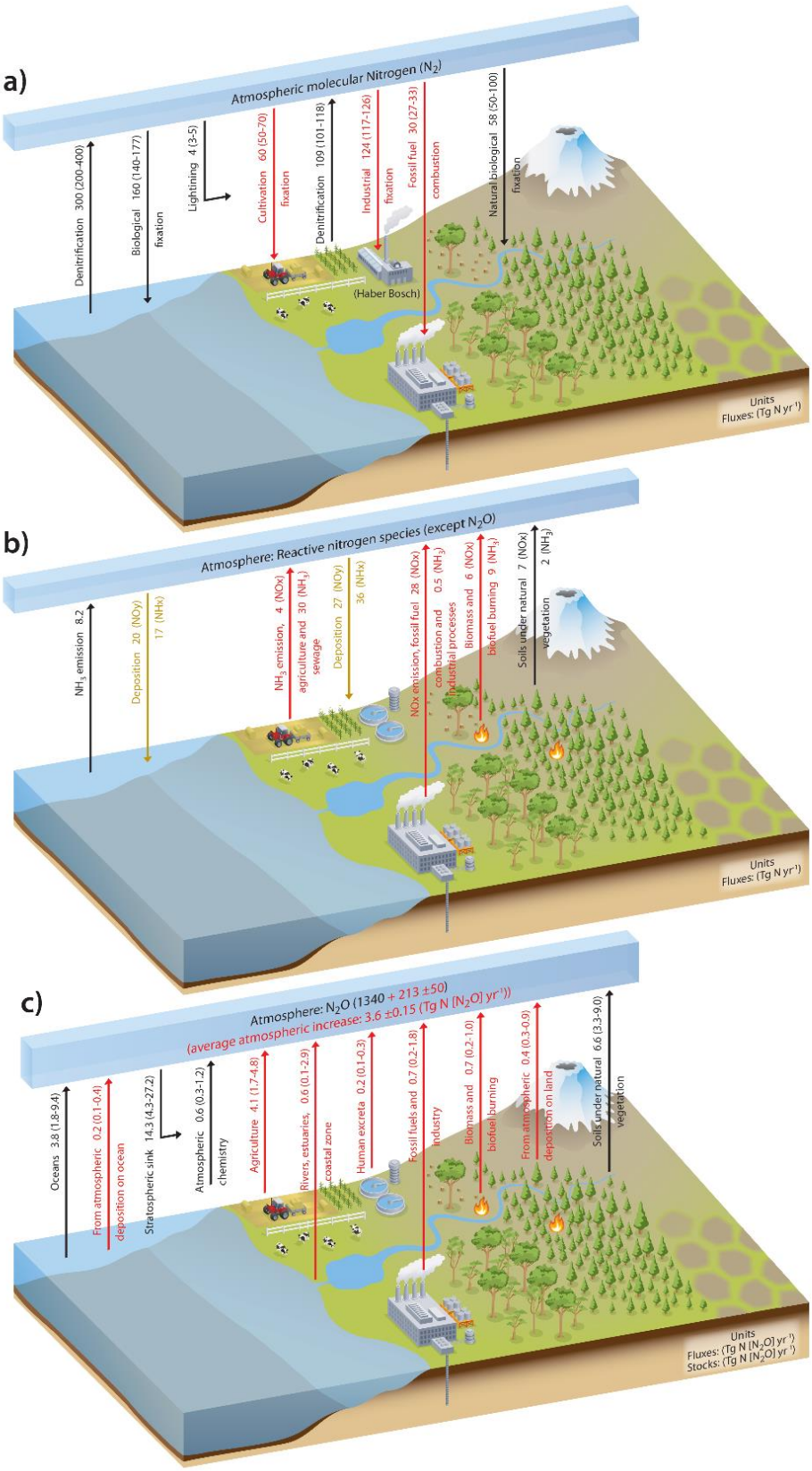

Figure 2.1. Nitrogen exchange between the Earth's surface and the atmosphere. Black arrows indicate natural flows, Red arrows – anthropogenic, and yellow – of mixed origin. (a) The natural and anthropogenic processes that create reactive nitrogen and the corresponding rates of denitrification that convert reactive nitrogen back to N_2. (b) The flows of the reactive nitrogen species NO_y and NH_x. (c) The stratospheric sink of N_2O is the sum of losses via photolysis and reaction with O(1D) (oxygen radical in the 1D excited state). The global magnitude of this sink is adjusted here in order to be equal to the difference between the total sources and the observed growth rate. The atmospheric inventories have been calculated using a conversion factor of 4.79 Tg N (N_2O) per ppb (Prather et al., 2012). Source: IPCC (2013).

An overview of the exchange of nitrogen between the surface and the atmosphere is given in Figure 2.1. In the top (Figure 2.1.a), natural and anthropogenic nitrogen fixation processes have been denoted with the respective N-flow magnitudes (in Tg N yr^{-1}) and together with estimated denitrification fluxes. In the middle, main production and deposition pathways is presented for NO_x with NH_3 (Figure 2.1.b). Nitrous oxide fluxes are shown in the bottom figure (Figure 2.1.c) together with the atmospheric burden.

In the current chapter, a broad overview of the global processes of nitrogen circulation in the Earth System shall be given in order to provide the necessary background for the discussion of the role of N_2O in the environmental issues which motivated this PhD work.

The chapter is divided into four main sections. Section 1 provides an overview of the main physical and chemical characteristics of both nitrogen and nitrous oxide. Section 2 is focused on the terrestrial part of the nitrogen cycle with explanation of the "nitrogen cascade" concept, with emphasis on N_2O emission processes. The main natural and anthropogenic sources and sinks of N_2O are discussed in the third section. The last section reviews available knowledge on atmospheric N_2O distribution in the past and the present. It also gives a glimpse into the probable future trends of atmospheric N_2O burden.

2.1. Physico-chemical properties of nitrogen and nitrous oxide.

As the fifth most abundant element in our Solar System, nitrogen is critical to a variety of biogenic processes that take place in the environment. In particular, nitrogen is essential in sustaining all life forms as it forms nucleic acids and proteins – the building blocks of all organic matter on Earth. Despite its apparent abundant availability, nitrogen is often a limiting factor in both terrestrial and marine ecosystems (Vitousek and Howarth, 1991), as it mostly occurs in the form of inert N_2 molecule, unusable to all but the most specialised types of organisms due to its strong triple-electron bond.

Discovered by a Scottish physician, chemist and botanist Daniel Rutherford in 1772, nitrogen had been given many informal names by scientists who studied it, such as "noxious air", "burnt air", "phlogisticated air" or "mephitic air". The last of these was used by Antoine Lavoisier, who has also referred to N_2 as *azote*, named derived from Greek word *azotos*, meaning "lifeless", as it caused the living organisms subjected to its influence to suffocate. This name is nowadays used for nitrogen in many languages, including Polish (*azot*), French (*azote*) and Italian (*azoto*). The English version of the name comes from combination of Greek words *nitron* – "sodium carbonate" – and genes – "forming", proposed by French chemist Jean-Antoine Chaptal, and related to the close connection between gaseous nitrogen, nitric acid and potassium nitrate.

Nitrogen atoms can be a part of vast array of chemical compounds thanks to their ability to take on wide range of oxidation states, from +5 to -3. The most notable reduced forms of nitrogen are ammonium (NH_4^+) and ammonia (NH_3), while the oxidized forms are more diverse, with a multitude of N oxides (N_2O, NO, NO_2, N_2O_5) and acids (HNO_2, HNO_3) present in the atmosphere.

In its most stable, gaseous form, nitrogen (N_2) is a colourless and odourless gas (Table 2.1.). Naturally occurring in large amounts in the atmosphere (78% by volume), it can be produced in its clean form

Table 2.1. Comparison of the most important physical properties of N_2 and N_2O molecules.

	N_2	N_2O
Particle schematic	N≡N	N≡N-O or N=N=O
Molar mass [g/mol]	28	44
Appearance	Colourless, odourless gas	Colourless gas of sweet taste
Density	1.251 g/L	1.997 g/L
Atmospheric concentration	78%	327 nmol/mol
Melting point	-210.00 °C (63.15 K)	-90.86 °C (182.29 K)
Boiling point	-195.80 °C (77.36 K)	-88.48 °C (184.67 K)
Solubility in water (at 15 °C)	0.023 g/L	1.5 g/L
GWP*	0	298
ODP**	0	0.017

*GWP – global warming potential in 100-year horizon, defined as the ratio of the time-integrated radiative forcing from the instantaneous release of 1 kg of a trace substance relative to that of 1 kg of a reference gas (CO_2).
**ODP – ozone depletion potential, defined as the amount of stratospheric ozone destroyed by the release of a unit mass of a chemical at Earth's surface to the amount destroyed by the release of a unit mass of chlorofluorocarbon 11 (CFC-11 or $CFCl_3$).

through the industrial processes, for instance as a by-product of oxygen production in steel industry. At atmospheric pressure, molecular nitrogen undergoes condensation at 77 K (-196 °C) and freezes at 63 K (-210 °C). In its liquid form, it is often used as cryogen.

Two stable isotopes of nitrogen exist, namely ^{14}N and ^{15}N, with the former being the most widespread, with natural abundance as high as 99.634%. This overwhelming majority of ^{14}N isotope stems from the reaction of CNO (carbon-nitrogen-oxygen) cycle that occurs in the cores of the stars. It is also reflected in the isotopic composition of molecular nitrogen in the Earth's atmosphere, of which 92.7% is made of $^{14}N_2$ molecules and the majority of the rest being $^{14}N^{15}N$ molecules. The isotopic composition of nitrogen is important in process-based studies, where application of labelled nitrogen compounds provides information on intrinsic characteristics of the studied system through enrichment or depletion of the products in ^{15}N, relative to the substrates (see Pérez et al., 2006, Sutka et al., 2006, Bergstermann et al., 2011).

The nitrous oxide has been discovered in the same year as molecular nitrogen (1772) by an English philosopher and chemist Joseph Priestley, who named it a "nitrous air diminished" and published the method of producing this gas with the use of nitric acid (Priestley, 1776). Nitrous oxide has many common names that stem from its intended usage. Due to euphoric effects of its inhalation, it is commonly known as "laughing gas" and often used for anaesthetics in medicine. The automobile industry utilizes names "nitro" and "NOS" frequently – in this case N_2O is used as a potent oxidiser in high-temperature engine combustion processes, allowing higher power output of motor engines. It is also frequently used as a fuel in the rocket industry, with additional advantage of being non-toxic, stable at room temperature and relatively easy to store.

Under normal conditions, nitrous oxide is a colourless gas of sweet odour (Table 2.1.). Lots of similarities exists between N_2O and CO_2: they both have the same linear structure of the molecule, they share the same molar mass, they have the same number of electrons and similar, low chemical reactivity. CO_2 is slightly more soluble in water due to acid reaction with H_2O.

Low reactivity of N_2O is crucial from the climate change perspective, as N_2O strongly absorbs infrared radiation emitted by the Earth's surface in the mechanism of the greenhouse effect. Long atmospheric lifetime, between 118 to 131 years (Volk et al., 1997, Hsu and Prather, 2010, Fleming et al., 2011, IPCC, 2013) and higher overall Global Warming Potential (GWP) when compared to CO_2,

i.e. 298 GWP over 100 year time horizon, including the carbon-cycle feedback, makes the N_2O an important greenhouse gas (IPCC, 2013). The overall smaller net radiation effect of N_2O stems from its low atmospheric abundance, with global mean of approximately 327 nmol/mol (ppb) in 2015 (Elkins and Dutton, 2009, NOAA, 2015). Long atmospheric lifetime is connected with slow diffusion of N_2O molecules to the stratosphere, where they are destroyed by photolysis, releasing nitrogen oxide that regulates the dynamics of stratospheric ozone formation. A more detailed description of this process will be given in section 2.3.3.

2.2. Main pathways of nitrogen in the terrestrial environment.

While the global carbon cycle is essentially controlled by net primary production of terrestrial and marine systems, biogeochemical cycle of nitrogen is mainly driven by microbial processes that occur in the soils, water bodies and sediments (Seitzinger et al., 2006, Sutton et al., 2008, IPCC, 2013). Soils are particularly important in case of nitrogen cycle, as it has been shown by Batjes (1996) that they are the largest terrestrial reservoir of nitrogen, with 133-140 Pg of N in the upper 100 cm of the soil. The amount of N stored in plant and microbial biomass is much smaller, with 10 Pg and 2 Pg of N, respectively.

Before the XIX century industrialization, the main input of N_r in the terrestrial ecosystems was provided through the biological nitrogen fixation (BNF) process, which can be summarized by the same chemical formula as the Haber-Bosch process:

$$\mathrm{N_2 + 3\,H_2 \rightarrow 2\,NH_3}. \qquad (2.1)$$

The energy required to break the triple bond of N_2 molecule is generated in oxidation of carbohydrates inside the nitrogen fixing organisms. Ability of BNF plants to produce N_r is strong enough to support whole ecosystems and even accumulate N over long time scales (Vitousek et al., 2002). The highest capability of BNF is associated with symbiotic plants, e.g. leguminous plants that rely on N_r produced by *Rhizobium* bacteria that infects their roots. The amount of N_r that is produced is significant, with up to 200 kg N ha^{-1} yr^{-1} achieved by certain leguminous plants (Sutton et al., 2011a), making them a desirable part of the rotational farming systems. On the global scale (Figure 2.1.a), BNF input by agricultural crops is estimated to be in the range of 30 – 70 Tg N yr^{-1} (see Galloway et al., 2008, Herridge et al., 2008, Sutton et al., 2011a, IPCC, 2013).

Other existing BNF organisms are not so well understood as leguminous crops. Direct fixation of N_2 occurs also in soils and sediments through heterotrophic bacteria that decompose plant litter. This N_2 sink usually does not exceed 5 kg N ha^{-1} yr^{-1} for terrestrial ecosystems, but can reach higher values in wetland soils. Less is known about the fixation rates of other microorganisms, like symbiotic cyanobacteria, which can significantly contribute to the N_r production in certain ecosystems (Sutton et al., 2011a).

Invention of the Haber-Bosch process led to a dramatic increase of N_r inputs into terrestrial ecosystems in the last century. Global annual mineral fertilizer usage has increased from 4 Mt in 1950 to more than 80 Mt in 1990 (Roy and Hammond, 2004). In Europe, mineral fertilizer and livestock manure are the main sources of anthropogenic N_r ecosystem inputs, with N application rate estimated at 123 kg N ha^{-1} yr^{-1} in 1990s (van Egmond et al., 2002, Sutton et al., 2011a). Today, the average N input in the agriculture has slightly decreased in some EU countries, e.g. Netherlands, where they have been reduced from 398 kg N ha^{-1} yr^{-1} in 2004 to 346 kg N ha^{-1} yr^{-1} in 2012. In other

countries however, the fertilizer application rates have increased, stabilizing EU average in the range of 128 to 135 kg N ha^{-1} yr^{-1} in the years 2004-2011. In Poland, the overall N application rates have increased from 102 to 132 kg N ha^{-1} yr^{-1} between 2004 and 2013, following the improving economic situation in the agricultural sector (Eurostat, 2015).

Another anthropogenic source of N_r is related to stationary combustion processes, mainly through emissions of nitrogen oxides (NO, NO_2) from the transport sector. On the global scale, it was estimated that this process is responsible for additional 25 Tg N entering the ecosystems every year (ENA, 2011).

Regardless of the source of reactive nitrogen, once it enters the system, it will inevitably undergo physical and chemical processes that will ultimately lead to its denitrification back to the most stable form – gaseous N_2. While the last step of that chain of reactions must always be denitrification, nitrogen can become a part of various nitrogen compounds. This phenomenon has been dubbed "the nitrogen cascade" (Figure 2.2.; see Galloway and Cowling, 2002, Galloway et al., 2003). For example, an N atom entering the system as part of mineral fertilizer molecule can, in the simplest path, be absorbed by the microbial community that lives in the soil and denitrified in the same spot, while nitrogen atom from the molecule just several micrometres away can have an altogether different fate: it can be absorbed by the crop that was fertilized, forming one of its many proteins. After harvest, it can become a part of animal forage in one of the nearby livestock farms, to be excreted, volatilised and transported away as ammonia molecule, be wet-deposited in the natural forest somewhere downwind, be washed away by rainwater into the riverine system and ultimately denitrified hundreds or thousands kilometres in the shallow sea beyond the river estuary. At any given step this N atom may contribute to a series of environmental issues, including air quality,

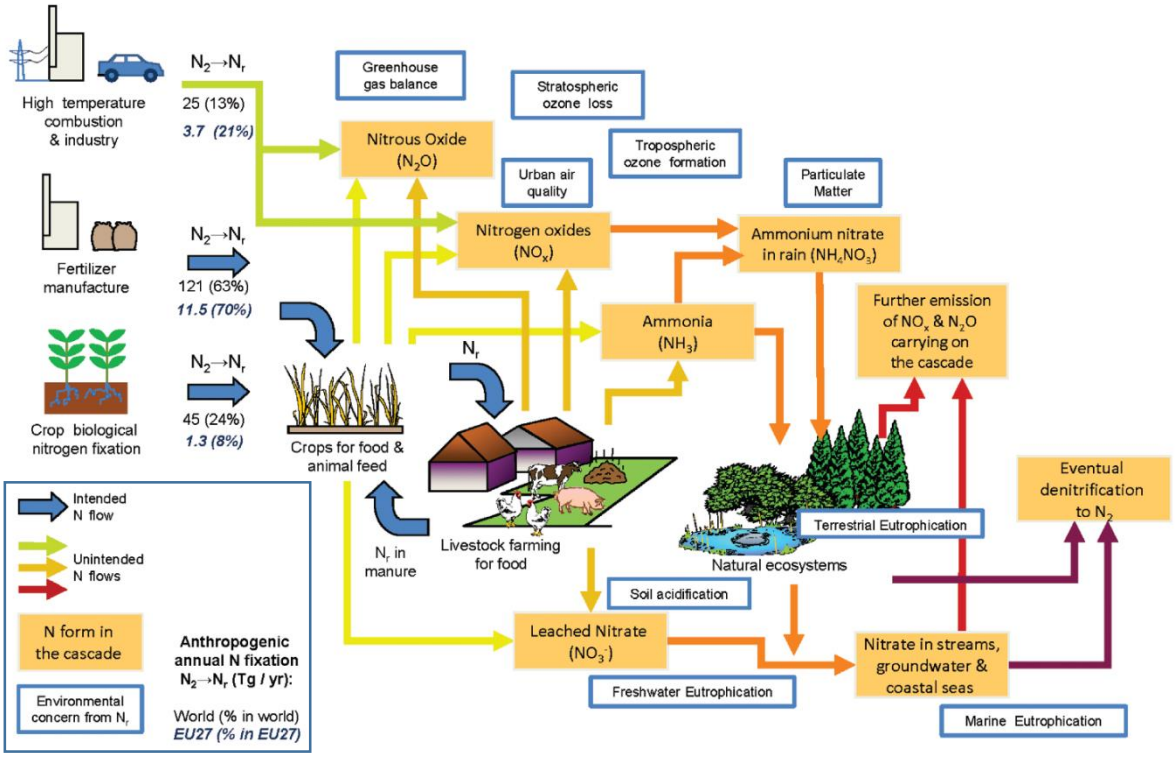

Figure 2.2. Simplified view of the nitrogen cascade, highlighting the major anthropogenic sources of reactive nitrogen (N_r) from atmospheric nitrogen (N_2), the main pollutant form of N_r (orange boxes) and nine main environmental concerns (boxes outlined with blue). Estimates of N fixation for the world (Tg/yr for 2005, in black) (Galloway et al., 2008) are compared with estimates for Europe (Tg/yr for 2000, in blue italic; Leip et al., 2011, Sutton et al., 2011a) . Energy is needed to fix N_2 to N_r, which is gradually dissipated through the cascade with eventual denitrification back to N_2. Blue arrows represent intended anthropogenic N_r flows; all the other arrows are unintended flows. Source: Sutton et al. (2011a).

particulate matter formation and its effect on weather patterns, terrestrial and marine eutrophication and others.

The resulting emissions of N_2O into the atmosphere (cf. Figure 2.1.c) represent only one of many negative effects of increased N_r inputs associated with human activities. In the European Nitrogen Assessment (Sutton et al., 2011a, see also Sutton et al., 2011b) the monetary cost of fighting these negative effects (i.e. human health, ecosystem degradation and climate change) in the European Union was estimated based on a "willingness to pay" methodology. The overall societal cost was estimated to be between 70-320 billion Euros for the year 2000, with 5-10 billion euro attributed to the cost of climate-change issues caused by N_2O emissions to the atmosphere. Such cost-benefit assessments are subject to large uncertainties, but can hint at most cost-beneficial methods of mitigation for undesired effects. On the other hand, they do not take into account all of the long-term effects of N_2O emissions on climate change, as these can be complex.

2.3. Sources and sinks of N_2O.

While the main mechanisms of N_2O production and destruction have been known for some years now, the detailed budget of this gas is still characterised by large uncertainties. The reason behind this are the intrinsic characteristics of sources and sinks, as well as gaps in detailed knowledge concerning the factors controlling the dynamics of N_2O in the atmosphere. The following sections will provide an overview of the current state of knowledge on main sources and sinks of N_2O, both natural related to human activities, as well as on its main destruction processes.

Prior to the industrial era, almost all molecules of N_2O present in the atmosphere were of the microbial origin, formed either as a by-product in, or as an obligatory intermediate of one of a multitude of known metabolic processes of nitrogen-transforming bacteria. Of these, the most significant sources of N_2O are nitrification and denitrification processes (Figure 2.3.), which can occur in a wide range of terrestrial, aquatic and marine ecosystems as long as sufficient supply of needed nitrogen compounds is available.

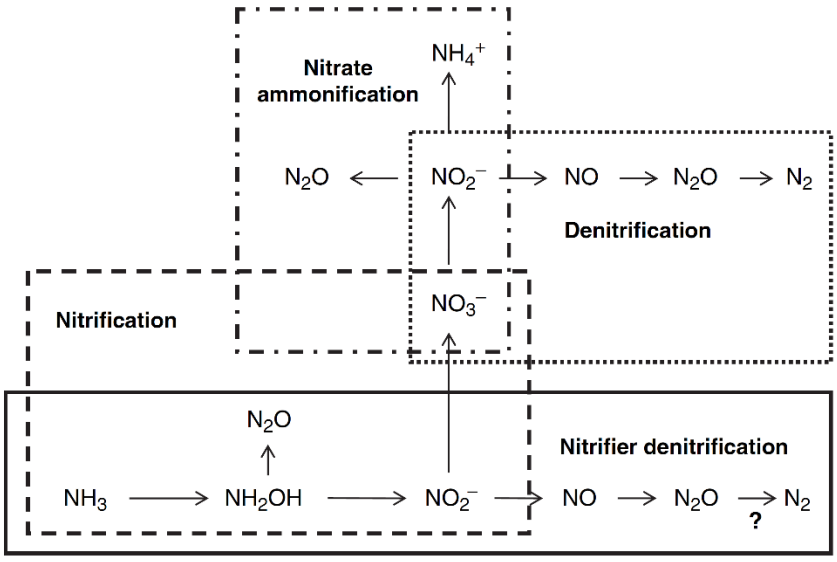

Figure 2.3. Microbial sources of N_2O in soils (Baggs, 2008). Source: (IPCC, 2013).

Nitrification is a microbial process that converts ammonium (NH_4^+) or ammonia (NH_3) to nitrite (NO_2^-) or nitrate (NO_3^-), with hydroxylamine (NH_2OH) is an intermediate product. It is during the formation of this compound that N_2O is produced, with 0.1 to 10‰ of N mass being converted to N_2O (Sutton et al., 2011a, and references therein), and subsequently released to the atmosphere. Nitrification is generally an anaerobic process, with optimum value of the soil water content between approximately 30%-60% (Bouwman, 1998), and pH and temperature exerting smaller control on the process dynamics.

Denitrification is the process of dissimilatory reduction of nitrite, nitrate and nitric oxide to nitrous oxide and N_2, usually attributed to certain species of microbes. Ability to denitrify nitrogen compounds is not limited to bacteria, however, as it was demonstrated to be mediated also by certain species of fungi and archaea (Sutton et al., 2011a). It generally occurs under anaerobic conditions and is considered to be the main mechanism of N_r destruction in terrestrial ecosystems.

The global budget of nitrous oxide is difficult to quantify, given a multitude of environments and processes that need to be included to gain detailed information. The currently available estimates (Table 2.2) point to the global N_2O source of 17.9 Tg N-N_2O yr^{-1} and the global N_2O sink (stratosphere) 14.3 Tg N-N_2O yr^{-1}, the difference driving the continuous growth of N_2O mixing ratio in the atmosphere. These numbers, however, are associated with very large uncertainty ranges.

The single largest source of atmospheric N_2O releases is attributed to microbial activity in soils under natural vegetation, responsible for approximately 6.6 Tg N-N_2O yr^{-1}. The mechanisms of emissions in natural soils are the same as in case of agricultural soils, albeit with smaller N_r inputs available.

Table 2.2. The N_2O budget for the years 2006/2011. Source: IPCC (2013) .

	Global annual N_2O emissions - AR5 [Tg N-N_2O]	Uncertainty range [Tg N-N_2O]
Anthropogenic sources		
Fossil fuel combustion and industrial processes	0.7	(0.2 - 1.8)
Agriculture	4.1	(1.7 - 4.8)
Biomass and biofuel burning	0.7	(0.2 - 1.0)
Human excreta	0.2	(0.1 - 0.3)
Rivers, estuaries, coastal zones	0.6	(0.1 - 2.9)
Atmospheric deposition on land	0.4	(0.3 - 0.9)
Atmospheric deposition on ocean	0.2	(0.1 - 0.4)
Surface sink	-0.01	(0.0 - -1.0)
Total anthropogenic sources	**6.9**	**(2.7 - 11.1)**
Natural sources		
Soils under natural vegetation	6.6	(3.3 - 9.0)
Oceans	3.8	(1.8 - 9.4)
Lightning		
Atmospheric chemistry	0.6	(0.3 - 1.2)
Total natural sources	**11.0**	**(5.4 - 19.6)**
Total natural + anthropogenic sources	**17.9**	**(8.1 - 30.7)**
Stratospheric sink	**14.3**	**(4.3 - 27.2)**
Observed growth rate	**3.6**	**(3.5 - 3.8)**
Global top-down estimate (year 2011) Based on Prather et al. (2012)		
Burden (Tg N)	1553.0	
Atmospheric loss	11.9	± 0.9
Atmospheric increase	4.0	± 0.5
Total source	15.8	± 1.0
Natural source	9.1	± 1.0
Anthropogenic source	6.7	± 1.3

Large uncertainty is related to the total emission value, however, as a limited amount of studies is available in some important ecosystems, e.g. in equator zones (IPCC, 2013).

Another significant natural source exist in a wide range of aquatic and marine ecosystems. (IPCC, 2013) has estimated the marine sources to be responsible for 3.8 Tg N-N_2O yr^{-1}, also with broad uncertainty range (1.8 – 9.4 Tg N-N_2O yr^{-1}; see Table 2.2. An earlier synthetic study by US Environmental Protection Agency (Anderson et al., 2010), attributed a total of 5.4 Tg N-N_2O yr^{-1} to marine and aquatic ecosystems, with 59% estimated to origin from the open ocean (3.2 Tg N-N_2O yr^{-1}), 28% from continental shelve waters (1.5 Tg N-N_2O yr^{-1}), 7% from upwelling zones (0.4 Tg N-N_2O yr^{-1}) and the rest from estuaries and rivers (4% and 2%, respectively). While these budgets agree in the range of provided uncertainties, further studies are necessary to better constrain the provided annual emissions. For example, in a very recent study by Arevalo-Martínez et al. (2015), a large N_2O emissions associated with the upwelling ecosystem off the coast of Peru are reported. The releases from that source alone are estimated to be in the range of 0.2 – 0.9 Tg N-N_2O yr^{-1}, which comprise from 5% to 23% of the total ocean emission provided by IPCC.

Many of the studies performed in the last decade focused on the anthropogenic sources of N_2O, following the influence of the human-related N_2O emissions on the global warming effect and stratospheric ozone depletion. Releases from N-additions in agriculture are of particular importance due to their estimated magnitude. N_2O emissions from combustion, industrial and waste management systems are also well-documented, due to their connection to mitigation measures applied in the framework of international conventions. These will be described in the following sections.

2.3.1. The role of agriculture in the total N_2O emissions.

The current growth rate of the globally averaged atmospheric concentration of N_2O (0.73 ± 0.03 ppb yr^{-1}) is commonly attributed to the increasing N_r inputs, mainly related to agricultural activities (IPCC, 2013). Dramatic increase in the N_r inputs into the Earth system that followed the industrial revolution of mid-XIX century has caused a significant increase in the N_2O production on the global scale, mainly related to the application of mineral fertilizer in agriculture, and to a lesser degree through direct emissions from chemical industry and fossil fuel combustion. Fifth Assessment Report of IPCC estimated that food production is likely responsible for 80% of the increase in atmospheric N_2O concentrations due to addition of nitrogen fertilizers. This conclusion is supported both by terrestrial biosphere models as well as stable isotopic composition of atmospheric N_2O (IPCC, 2013, see also Park et al., 2012).

Of the total amount of 6.9 Tg N-N_2O yr^{-1} attributed to human activities, over 4 Tg are connected to direct emissions from agriculture, and at least another 1 Tg from the indirect emissions also associated with agricultural activities. The agricultural emissions have increased by approximately 0.4 Tg N-N_2O yr^{-1} between mid-1990s and the first decade of XXI century, following an increased demand for food (IPCC, 2013). This trend is expected to continue in the following decades, driven by continuous growth of human population and increased demand for biofuel crops. The possibility to predict the exact future emission scenarios of N_2O is difficult, however, as understanding of interactions between changes in climate and the nitrogen cycle is still limited, with some studies pointing to a positive feedback between N_2O emissions and the rise of temperatures over land (Khalil and Rasmussen, 1989, Zaehle and Dalmonech, 2011, Xu et al., 2012).

Although agriculture is a critical sector for constraining the N_2O emissions on global and regional scales, its exact contribution to the global N_2O budget is very uncertain. Bottom-up methodologies (e.g. IPCC, 2006) used for emission assessments rely mostly on the concept of *emission factors* (EF) – a set of constants that, when multiplied by a related, proxy quantity (e.g. population density or annual crop production), allows to obtain estimates of N_2O emissions. In most cases, the used EFs grossly simplify the intricate processes that they represent, which results in large relative uncertainties in the values of EFs, and, consequently, in the estimated releases of N_2O. Although the default IPCC emission factor for direct N_2O emissions is equal to 1% of the N_r input, more recent studies by Crutzen et al. (2008) and by Davidson (2009) indicate that when indirect emission of N_2O in the latter part of the nitrogen cascade are included, the EF increases to approximately 2.5% - 4.5%.

The top-down studies provide more precise constraints on the estimated total N_2O emission values. Prather et al. (2012) estimated total annual emission of N_2O to be 15.7 ± 1.1 Tg N-N_2O yr^{-1}, with anthropogenic and natural contribution of 6.5 ± 1.3 Tg N-N_2O yr^{-1} and 9.1 ± 1.3 Tg N-N_2O yr^{-1}, respectively. However, the ability to differentiate between agricultural and other anthropogenic sources is limited in top-down studies, and relies on the estimations of releases from other sectors which are easier to quantify (Crutzen et al., 2008).

2.3.2. Other anthropogenic sources of N_2O.

While N_2O releases from non-agricultural anthropogenic sources are far less important than those related to crop production on the global scale (Table 2.2.), these can still play a significant role for regional balances of this gas. The Emissions Database for Global Atmospheric Research (EDGAR) v.4.2 bottom-up inventory associates the largest releases of non-agricultural N_2O with large-scale biomass burning and industrial sources (EDGAR, 2011). Smaller releases occur in energy production, waste management and transportation sectors (Table 2.3.). Notable differences exist between EDGAR, IPCC and other available inventories of N_2O emissions, underlining the gaps still present in the current knowledge about N_2O release processes.

Industrial sources of nitrous oxide emissions are primarily related with nitric acid, adipic acid and caprolactam production chains. As the processes causing the emissions of N_2O are limited in number, appropriate mitigation measures are relatively easy to introduce. Such measures have already been successfully implemented within the EU with respect to adipic acid production facilities, where emissions of N_2O were reduced from approximately 60 Tg CO_2-equivalent in 1990 to 9 Tg CO_2-equivalent at the beginning of XXI century (Sutton et al., 2011a).

As N_2O is a greenhouse gas, its emissions sources are required to be estimated and reported under UNFCCC (United Nations Framework Convention on Climate Change), of which Poland is an Annex I Party as an independent signatory, as well as through membership in European Union. This means that Poland is required to adopt national mitigation policies on greenhouse gas emissions. As another requirement of the convention, the emissions of the agreed pollutants need to be annually reported to the UNFCCC database, in accordance with the methodologies previously agreed upon. In order to do that, national budgeting agencies have been established with the task to gather the necessary information. In Poland, such data is gathered by KOBIZE (National Centre for Budgeting and Emissions Management, (*Krajowy Ośrodek Bilansowania i Zarządzania Emisjami*), which is a part of the Institute of Environmental Protection - National Research Institute in Warsaw. The emission

Table 2.3. Global N_2O emissions from IPCC (2006) sectors according to EDGAR v4.2 database (EDGAR, 2011). Sectors not directly associated with N_2O releases due to agricultural N_r input are shaded.

	Global N_2O emissions in 2008	Percentage of total
Process Group (code)	[Gg]	[%]
Agricultural soils (AGS)	2970.9	44.1
Manure management (livestock) (MNM)	213.7	3.2
Agricultural waste burning (AWB)	26.0	0.4
Large-scale biomass burning (BMB)	887.1	13.2
Industrial processes and product use (IPU)	846.7	12.6
Energy manufacturing transformation (EMT)	206.2	3.1
Fossil fuel fires (FFF)	0.5	0.0
Indirect emissions from NO_x & NH_3 (IDE)	458.1	6.8
Indirect N_2O emissions from agriculture (N2O)	569.1	8.4
Oil production & refineries (OPR)	4.1	0.1
Buildings (residential & others) (RCO)	181.5	2.7
Waste (solid & wastewater) (WST)	233.2	3.5
Non-road transportation (TNR)	49.6	0.7
Road transportation (TRO)	142.2	2.1
Total	**6743.0**	**100.0**
Total without large-scale biomass burning	**5855.9**	**86.8**

reports are submitted annually (with a two-year delay of the reporting period), and are freely available to the public. The last available report was published in 2014 and covers the period between 1988 and 2012 (UNFCCC, 2014).

Another pathway of obtaining information on the releases of N_2O from industrial plants located in Europe is through E-PRTR (European Pollutant Release and Transfer Register), established by the EU in 2006 in the framework of the UNECE (United Nations Economic Commission for Europe) Convention on Access to Information, Public Participation in Decision-making and Access to Justice in Environmental Matters, known as Aarhus Convention. The main role of the convention is to "*ensure a real participation of citizens in environmental matters by enhancing public access to environmental information*" (E-PRTR, 2015). As a signatory country, Poland requires selected industrial facilities to measure or estimate the emissions of 91 pollutants covered under E-PRTR. The data needs to be reported when: (i) the given facility falls under at least one of the 65 E-PRTR economic activities, (ii) the facility has a capacity exceeding at least one of the E-PRTR capacity thresholds, or (iii) the facility releases pollutants or transfers waste off-site which exceed specific thresholds set out in Article 5 of the E-PRTR Regulation.

The databases mentioned above provide data on emissions from industrial N_2O sources. In particular, they show that nitric acid and caprolactam production chains remain significant sources of N_2O, mainly due to releases occurring during the process of ammonia oxidation on platinum catalysers. The European Nitrogen Assessment states that the emission from nitric acid production alone was close to one quarter of the direct N_2O soil emissions in 2007 (Sutton et al., 2011a). The importance of industrial sources is also reflected in EDGAR v4.2 emissions, where these are responsible for approximately 12.6% of the total anthropogenic N_2O releases in 2008 (Table 2.3.).

Other significant anthropogenic sources of N_2O are related to transportation and waste management. N_2O emissions from transportation sector originate from two major pathways: (i) N_2O

is formed in the combustion process together with other nitrogen oxides (NO_x), and (ii) N_2O is formed in the process of non-selective catalytic reduction of NO_x, used as an abatement measure that reduces NO_x emissions. The latter is an example how a solution to tackle one environmental issue can be harmful in another area (Sutton et al., 2011a). Transportation sector is only a small source of N_2O compared to the emissions of this gas from agricultural activities, however. As seen in Table 2.3, both road and non-road transportation account for only 2.8% of the global total N_2O emissions.

Sewage treatment and waste incineration plants constitute another anthropogenic N_2O source that can have large influence on the local budgets of this gas. N_2O is formed in both heterotrophic denitrification and nitrification (or more specifically, nitrifier denitrification; see Sutton et al., 2011a) during wastewater treatment under anoxic conditions and during the incineration of the solid waste. On a global scale, such facilities release similar amounts of N_2O to those from transportation sector, i.e. approximately 230 Tg N-N_2O annually (3.5% of the total N_2O emissions, c.f. Table 2.3). In Europe, their relative importance is larger, with approximately 6% of total EU-27 emissions coming from this sector (Sutton et al., 2011a).

2.3.3. Stratospheric and other potential sinks.

The predominant sink of nitrous oxide exists in the stratosphere, to which N_2O molecules slowly diffuse on decadal time-scales. There, they can be destroyed via two possible chains of reactions, both stimulated by the UV radiation coming from the Sun. The first reaction is a direct photolysis of N_2O molecules that produces the stable, non-reactive N_2 molecule and an excited oxygen atom:

$$\mathrm{N_2O} + \mathrm{h\nu} \rightarrow \mathrm{N_2} + \mathrm{O(^1D)}. \qquad (2.2)$$

The second reaction chain occurs when N_2O molecules interact with the excited oxygen atoms, yielding either a pair of N_2 and O_2 molecules (in 40% cases) or two nitric oxide molecules (in 60% cases):

$$\mathrm{N_2O} + \mathrm{O(^1D\ )} \rightarrow \mathrm{N_2} + \mathrm{O_2}, \quad (40\%) \qquad (2.3)$$

$$\mathrm{N_2O} + \mathrm{O(^1D)} \rightarrow 2\ \mathrm{NO}, \quad (60\%). \qquad (2.4)$$

Other oxygenated nitrogen compounds can also be formed (e.g. HNO_3, N_2O_5), however in smaller amounts (Prather, 2007, Smith, 2010).

On average, about 90% of the N_2O mass entering the stratosphere is destroyed following the direct photolysis chain, with the remaining 10% undergoing reactions with excited oxygen atoms (Smith, 2010). While the destruction of N_2O has a positive impact on the overall greenhouse gas balance, the NO molecules formed in the second reaction chain cause decomposition of stratospheric ozone following the overall scheme (Ravishankara et al., 2009, and references therein):

$$\mathrm{NO} + \mathrm{O_3} \rightarrow \mathrm{NO_2} + \mathrm{O_2},$$

$$\mathrm{NO_2} + \mathrm{O} \rightarrow \mathrm{NO} + \mathrm{O_2},$$

$$\text{net outcome: } \mathrm{O} + \mathrm{O_3} \rightarrow 2\ \mathrm{O_2}. \qquad (2.5)$$

Following the implementation of the Montreal Protocol, most of other potent ozone depleting substances (ODS), such as CFC-11, CFC-12, CFC-113, CCl_4, CH_3Br and others, have been gradually

removed from the stratosphere. N_2O was not included in that agreement, and nowadays it became the most significant ODS (Ravishankara et al., 2009), even though it has relatively low ozone depleting potential (ODP, see Table 2.1.). As future predictions of N_2O releases are strictly related to the food production and, in turn, to the human population, significant reduction of the influence of N_2O on stratospheric chemistry is not to be expected without the application of emission mitigation measures.

The intensity of N_2O photolysis in the stratosphere varies on both spatial and temporal scales. The highest efficiency of N_2O destruction is observed at 30 to 35 km altitude range, over the equator, during the midday hours. The concentration of N_2O in the troposphere changes to a very small degree (usually in the range of 325-335 ppb), except for the local areas under strong influence of the N_2O sources. The vertical gradient becomes steeper only above the tropopause, with mixing ratios of approximately 120 ppb at 30 km altitude (see Smith, 2010, and references therein).

Knowledge of atmospheric loads and average lifetimes of N_2O allows to assess the magnitude of stratospheric sink. Smith (2010) describes the procedure that used the IPCC AR4 values of global N_2O atmospheric burden (1534 Tg N, at globally averaged concentration of 319 ppb), divided by the atmospheric lifetime of N_2O recommended by Montzka et al. (2003). The result was the annual stratospheric sink of 13.5 Tg N yr^{-1}. When updated values are used, i.e. the current average concentration of 327 ppb (NOAA, 2015) and atmospheric lifetime of 124.5 years (IPCC, 2013), the stratospheric sink becomes smaller: 12.7 Tg N yr^{-1}. However, in order for the sink to balance the globally observed atmospheric concentration increase, IPCC has estimated it to be equal to 14.3 Tg N yr^{-1}, albeit with a very large confidence interval (4.3 – 27.2 Tg N yr^{-1}).

An additional, small surface sink of N_2O, possibly existing in terrestrial ecosystems under limited N_r inputs, has been discussed for some time now. Tentative results of relevant process studies show that while on the local scales the surface uptake of N_2O might be observed, it should not have any discernible impact on the global balance of N_2O (IPCC, 2013, and references therein).

2.4. N_2O in the global atmosphere.

Regular observations of atmospheric mixing ratios of N_2O have been performed since 1975 (NOAA, 2015) and are currently performed in the framework of global atmosphere monitoring networks, such as the Global Atmosphere Watch (GAW, coordinated by the World Meteorological Organization – WMO), NOAA/ESRL's Global Monitoring Division programme or InGOS (Integrated non-CO_2 Greenhouse Gas Observing System). The data produced by these networks allow to quantify spatial and temporal changes of atmospheric N_2O concentrations and provide the basis for top-down estimates of global sources and sinks of this gas.

The time series of N_2O concentrations measured at background stations display seasonal variations of about 1 ppb peak-to-peak amplitude in the northern hemisphere and smaller, 0.4 ppb variations in the tropics and southern hemisphere (Figure 2.4.). It has been speculated that dominant driver behind the observed interannual variability of N_2O is caused not by the seasonality of emissions, but rather by the exchange of N_2O depleted air masses with the stratosphere (Nevison et al., 2011, IPCC, 2013).

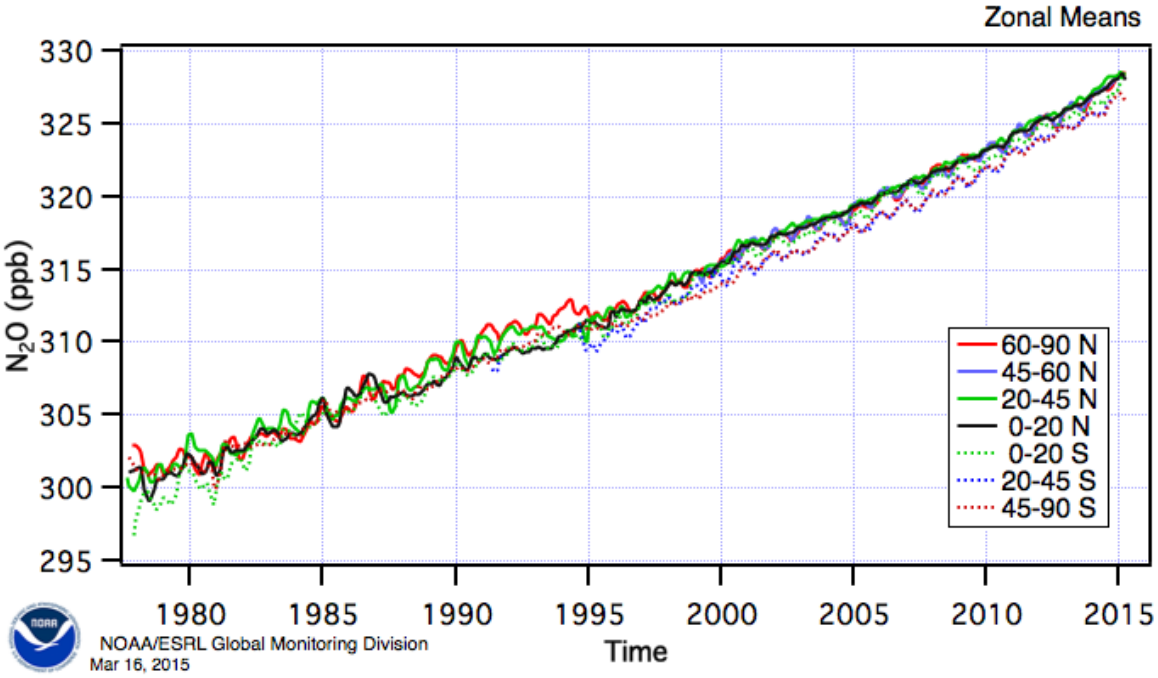

Figure 2.4. Zonal means of N_2O concentrations calculated by binning the stations of NOAA/ESRL measurement programs and calculating weighted averages. Source: NOAA (2015). Measurements after 1995 are of higher quality thanks to advancements in instrumentation and measurement methodologies.

A distinct latitudinal gradient is present in the monthly averaged N_2O concentrations, reflecting the relative distribution of the strongest sources of this gas. Maximum N_2O concentrations occur in the northern hemisphere, correlating with natural emissions from soils and ocean upwelling in the tropics, superimposed on anthropogenic agricultural sources concentrated at northern-tropical to mid-latitudes.

The ice-core data demonstrate that atmospheric concentrations of nitrous oxide oscillated between 200 ppb during glacial periods and 270 ppb during interglacials (Flückiger et al., 2004, Wolff and Spahni, 2007, IPCC, 2013). During the Holocene, the N_2O mixing ratios fluctuated between 260 and 270 ppb (Figure 2.5.), which means that the sources and sinks of this gas were approximately in balance. Since mid of the XIX century the atmospheric concentrations of N_2O started to rise, reaching 327 ppb in 2015 (NOAA, 2015). The rate of this growth was not constant; it increased from ca. 0.15 ppb yr^{-1} between 1900 and 1955, to the current value of 0.73 ppb yr^{-1} (IPCC, 2013). While the long-term changes in N_2O concentrations during the last ten thousand years do not have a clear explanation, the growth observed since the industrial age is unprecedented and is attributed to the additional releases of N_2O due to anthropogenic activities (IPCC, 2013). Isotopic composition of N_2O the air bubbles entrapped in ice cores suggests that the increase observed in the second half of the XX century is caused primarily by N_2O releases from fertilized soils (Röckmann and Levin, 2005, Ishijima et al., 2007, Davidson, 2009, Syakila and Kroeze, 2011, IPCC, 2013). The observed global average N_2O concentration of approximately 327 ppb in 2015 (cf. Figure 2.4.) is over 20% higher than the estimate for pre-industrial times.

Future concentration levels of N_2O in the atmosphere are strictly linked to effectiveness of the mitigation strategies adopted for all greenhouse gases. Whereas the industrial emissions have already been significantly reduced in some sectors (e.g. adipic acid production plants in Germany applied mitigation strategies that allowed to reduce national N_2O emissions by 9%), the mitigation options in agriculture are far more difficult to implement in societally acceptable manner. With the human population on Earth expected to grow to the value between 9.6 and 12.3 billion by 2100

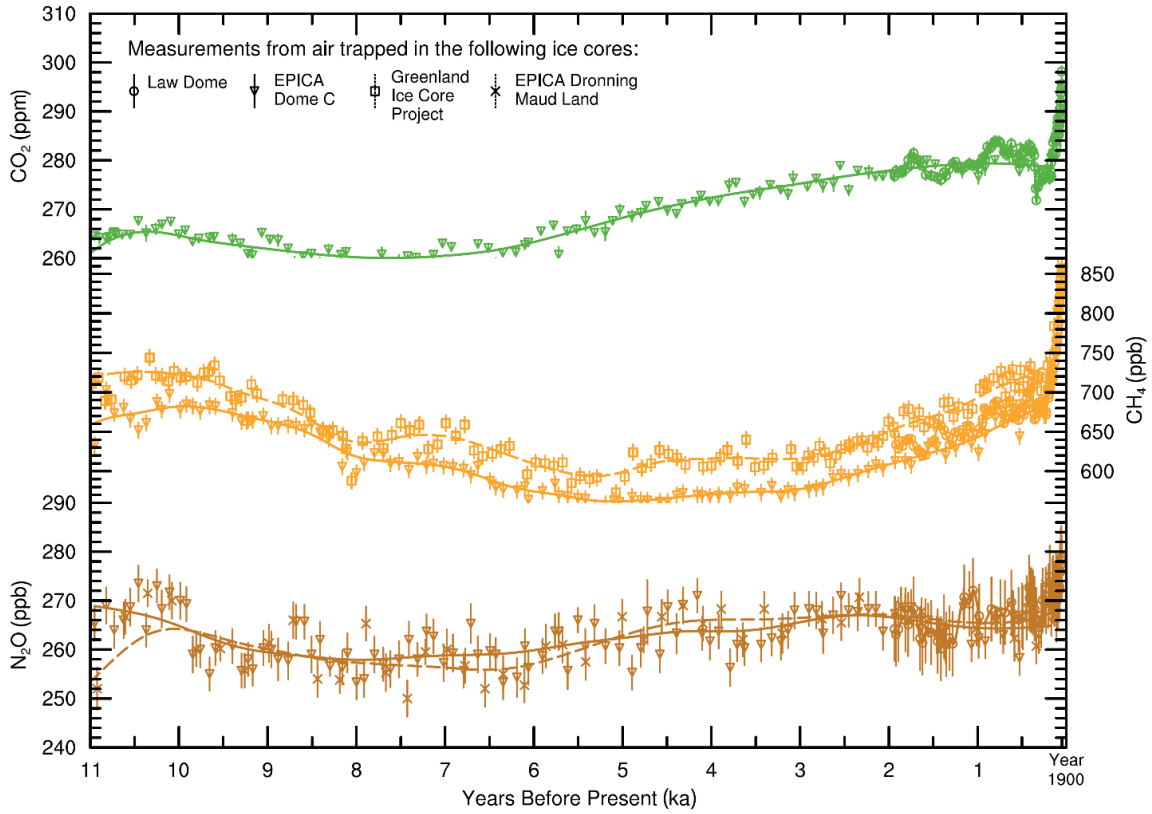

Figure 2.5. Variations of CO_2, CH_4 and N_2O concentrations during the Holocene. The data are for Antarctic ice cores: European Programme for Ice Coring in Antarctica EPICA Dome C – triangles; EPICA Dronning Maud Land – crosses; Law Dome – circles; and for Greenland Ice Core Project (GRIP) – squares. Lines correspond to spline fits. Source: IPCC (2013).

(Gerland et al., 2014), the demand for food is expected to follow, together with increased usage of nitrogen fertilizers. Without changes in the management of the anthropogenic N_r releases to the environment, N_2O emissions will also rise, resulting in sustained growth of atmospheric N_2O concentrations.

The current trend in the mitigation policies targeting N_2O emission assumes holistic approaches to reduce a multitude of negative effects related to N_r releases by anthropogenic activities. Among the most promising is the increase in nitrogen efficiency, defined as the amount of nitrogen mass included in the final product of the agriculture (e.g. cereals or dairy products) as compared to the N inputs to the farming system. While for cereals this efficiency was estimated to be as high as 80% in the 1960s, it has since dropped to approximately 30% in 2000 (Erisman et al., 2008). The main reason behind that drop is excessive use of mineral fertilizer in some areas of the world. Erisman et al. argue that additional food can be produced without increasing significantly the usage of N_r, and that the achievement of 50% N efficiency is feasible without significant investments.

Experience with the Kyoto and Montreal Protocol suggests that significant N_2O emission reduction efforts need to be coordinated through international agreements, since at present there is no economic incentive to implement mitigation measures, either on national nor on the smaller, company scales. Until now, however, agricultural N_2O emissions have not been a part of such agreements.

3. MEASUREMENTS OF ATMOSPHERIC N_2O MIXING RATIOS

The focus of this chapter is to present the results of regular measurements of ambient concentrations of atmospheric nitrous oxide (N_2O) in the atmosphere over Lesser Poland region (Małopolska), which were performed in the scope of this thesis. The outline of the chapter is as follows: first, the role of atmospheric trace gas measurements in the contemporary atmospheric research will be briefly explained, followed by a short overview of the available measurement techniques of N_2O. Next section will present technical aspects of setting-up analytical system for quasi-continuous measurements of atmospheric mixing ratios of N_2O, followed by the results of approximately 2 years of regular measurements of nitrous oxide concentrations at 2 stations of contrasting characteristics. These datasets provide the basis for the detailed description of temporal and spatial variability of atmospheric nitrous oxide loads in the atmosphere over southern Poland.

3.1. Rationale for regular observations of atmospheric trace gas composition.

Throughout the history, the Earth's atmosphere was subjected to influence of humans (and vice versa). It is clear that various meteorological phenomena occurring in the atmosphere were influencing the behaviour of humans on various spatial and temporal time scales since the dawn of civilization. In the last 50 years however, it has become clear that there also exists a causal relationship pointing in the opposite direction as well. Certain human activities interfere with the atmospheric system, changing its important parameters, and ultimately, the global climate (IPCC, 2013). The most important among those interactions are the emissions of primary and secondary greenhouse gases, such as carbon dioxide, methane and nitrous oxide, whose concentrations have increased significantly since the mid XIX century. Other purely anthropogenic trace compounds of the atmosphere, such as freons, HFCs and SF_6, not only add to the atmospheric greenhouse effect but are also transported to the stratosphere, where they influence the concentrations of stratospheric ozone, a crucial substance regulating the amount of UV radiation reaching the Earth's surface from the Sun. Finally, there is a group of both gaseous and non-gaseous anthropogenic compounds, of which elevated atmospheric concentration can cause harmful effects on human health, e.g. when inhaled. Of these, the most important are nitrogen oxides (NO_x), sulphur dioxide, tropospheric ozone and a multitude of non-gaseous chemical compounds that form particulate matter suspended in the atmosphere (PM).

In recognition of the importance and the complicated nature of all of these effects, massive scientific efforts are underway in order to better understand the dynamics and the composition of the atmosphere on various time scales, together with their interactions with other components of the Earth’s system. The main aim of these efforts is to provide quantitative understanding of anthropogenic impact on the atmosphere, with all complexity of the Earth's system in mind, and especially to assess the usefulness of potential mitigation measures aimed at reducing negative effects of human activities, e.g. through implementation of policies aimed at reduction of emissions of harmful substances to the atmosphere.

Both the multitude and complexity of the processes governing the behaviour of the atmosphere makes it impossible to describe it through physical equations that can be solved analytically. In many areas, scientific understating of parts of the atmospheric system comes from empirical or semi-empirical descriptions based either on some fundamental laws of physics, observations, or both. These descriptions frequently rely on a set of assumptions about the system that are made *a-priori* and are often valid only on specific spatial and temporal scales. For each of these many areas of scientific interest, observations of the atmosphere serve as a foundation, providing data necessary for developing new theories and testing the existing ones, thus advancing our knowledge of the system and helping to resolve present-day and future day issues related to Earth's system functioning.

Historically, observations of atmospheric composition relied either on a limited number of remote sites where air samples have been collected for subsequent laboratory analyses, or on even more limited number of *in-situ* measurement sites (e.g. Mauna Loa station, Hawaii, USA, established in 1956). The atmospheric observations at these remote locations were used in simple box-type models to derive estimates of atmospheric budgets of greenhouse gases or ozone-depleting substances on a global scale. The rapid growth of scientific understanding and computational power allowed expansion of these simple models and inclusion of more sophisticated process representations. This has provided an even more detailed picture of the present-day atmosphere, its behaviour and composition, on high temporal and spatial resolution (see selection of relevant literature related to nitrous oxide - Bergamaschi et al., 2005, Bergamaschi et al., 2009, Schulze et al., 2009, Stohl et al., 2009, Corazza et al., 2011, Manning et al., 2011, Thompson et al., 2014).

These advanced numerical tools (atmospheric models) rely heavily on atmospheric observations. With increasing complexity of the processes description, there is a growing need for observational data. However, if regional analyses of greenhouse gas budgets are considered, there are strict requirements, concerning temporal resolution, spatial extent, precision and the accuracy of the data.

First, the required temporal resolution of measurements will depend on the processes involved in atmospheric circulation on the spatial scale that is relevant for the model. For instance, in atmospheric pollutant transport, the main driving factors are usually horizontal and vertical wind speeds, which fluctuations depend mostly (but not solely) on synoptic scale phenomena. In regional analysis, local variations can be omitted and the typical time scale that needs to be considered is hourly. In order to represent these hourly changes in the atmospheric composition, measurements of at least the same frequency (preferably higher) are needed. This means that flask data with 1- or 2-week sampling frequency cannot sufficiently represent the processes that are involved in atmospheric circulation on these scales.

Second, in order to obtain fine-scale information on the emission and transport of atmospheric constituents, high spatial resolution of the available data is necessary, as the role of local (or *near-field*) sources increases. In order to capture these local effects, observational data from locations close to emission sources are needed. This can be achieved simply through the increase of the number of observational sites so that every emission source is closely monitored. This approach, however, is not optimal in respect of neither costs nor labour required to operate the stations. To solve that issue, a Bayesian inversion approach has been utilized, which allows to extract emission information on a relatively high spatial resolution using a limited amount of observational data, together with some additional *a-priori* information (Bergamaschi et al., 2009). While the requirements for the number of observations are reduced with the Bayesian approach, it still requires a significant amount of data originating from distributed sampling sites, typically operating

as networks. Examples of such networks of global extend include WMO GAW programme (WMO, 2015), NOAA ESRL Global Monitoring Division (NOAA, 2015), AGAGE (2015) and others. Nowadays, there is an on-going effort in the scientific communities to develop denser, smaller-scale networks that are focused on robust regional analyses, e.g. ICOS (2015), NEON (2015) or InGOS (2015).

Most of the atmospheric greenhouse gas measurement networks have started as international collaborations between scientific groups. In many cases, it was not feasible to unify measurement methodologies and techniques that were in use at the time. This has led to a series of efforts towards unification of measurement scales and inter-laboratory reproducibility, in order to ensure that internal network bias is as low as possible. Such efforts were undertaken in the framework of several projects, e.g. GAW, CarboEurope and InGOS. The problem of network bias is of critical importance, as such bias will always lead to a false distribution of sources and their strengths, whether in Bayesian inversion approach or when simplified analyses are performed. One of important outcomes of these efforts is a series of recommendations that concern the quality of observations performed at any measurement site included in the network. Among these recommendations, the goals for precision and accuracy of the measurement results are often set (WMO, 2013).

Using ground-based, stationary networks is not the only possibility of measuring greenhouse gas concentrations. Another option is to use remote sensing (i.e. satellite-based) measurements. One of the advantages of using satellite observations is very large spatial extent of the data coverage, combined with a possibility to provide information on vertical profiles of the measured atmospheric constituents. Disadvantages of remote sensing include lower measurement precision, lower temporal resolution, uneven temporal coverage (e.g. due to orbit dependence, cloud coverage sensitivity), backscattering on aerosol particles and others (Bergamaschi et al., 2009, and references therein). Currently, the usage of remote sensing in greenhouse gas analyses for lower troposphere is limited to carbon dioxide and methane, although the release of new generation of satellites may also make it possible to retrieve information about other atmospheric constituents, including N_2O.

3.2. Analytical methods for measurements of atmospheric nitrous oxide mixing ratios.

There are currently two main methods of measuring ambient concentrations of nitrous oxide in the atmosphere. The most popular of these is gas chromatography (GC), which generates high-quality measurement data but often requires high level of technical expertise to maintain quality of measurements over longer periods of time. The other method is utilizing state-of-the-art instruments based on mid-infrared light absorption techniques. These allow not only the highest currently available precision of a single measurement, but also offer very high frequency of the analyses, at least an order of magnitude higher than the GC technique, together with significantly smaller efforts required to implement proper calibration procedures.

In atmospheric nitrous oxide measurements, gas chromatography has been a most wide-spread technique thanks to its relatively low set-up cost and adaptability; GC instruments can be reconfigured to fit the specific needs, with a possibility to measure a number of chemical compounds simultaneously. For instance, in case of the equipment used for measurements of atmospheric N_2O mixing ratios performed in the scope of this work, the GC was equipped with both ECD (*electron capture detector*) and FID (*flame ionization detector*) detectors and it could

simultaneously measure N_2O, CO_2, CH_4 and SF_6 mixing ratios with both high precision and accuracy. Another advantage of this technique is a possibility to combine GC with an Isotope-Ratio Mass Spectrometer (IRMS) in order to obtain information on the isotopic composition of the measured compounds (e.g. nitrous oxide). With additional effort, IRMS also allows to obtain site-preference information on N_2O molecules (Rapson and Dacres, 2014, and references therein).

The main disadvantage of using GC-ECD method for atmospheric trace gas concentration measurements is difficulty in maintaining long-term precision and stability of the measurements. This has its roots in high sensitivity of GC system to changes of ambient temperature and pressure and inherent non-linearity of the ECD detector response. In addition, special care and expertise is needed in maintaining appropriate calibration scale, including its linkage to the primary scales as well as preparation of the working standards.

The optical spectroscopy techniques include a variety of different measurement methods, including Fourier Transform Infrared Spectroscopy (FTIR), Cavity Ring-Down Spectroscopy (CRDS), Quantum Cascade Laser Spectroscopy (QCL) or Off-Axis Integrated Cavity Output Spectroscopy (OA-ICOS). Although the specific construction of these instruments differ, all utilize the infrared absorption of the specific parts of EM spectrum by nitrous oxide molecules, usually in the mid-infrared range of 4000 cm^{-1} – 400 cm^{-1} wavenumber (2.5 to 25 μm wavelength). These instruments have the ability to measure ambient air concentrations of N_2O at very high precision, up to 0.02 ppb (20 ppt), at a very high frequency (as high as 10 Hz), though highest precision can only be obtained through averaging,

Table 3.1. Summary of advantages and disadvantages of different techniques of ambient N_2O analyses (Rapson and Dacres, 2014).

Technique	Sensitivity	Advantages	Disadvantages
GC-ECD	LOD*: 30 ppb, Precision: 0.18-0.4 ppb	Low cost of set-up, medium cost to run If linked to IRMS, isotope analyses can be performed	Lower measurement frequency than with optical instruments (5-10 minutes per sample) Frequent calibration required (at least several days) Necessary to use working tanks for drift correction
FTIR	Precision: 0.1 ppb (1 min avg.) or 0.03 ppb (10 min avg.)	Fast and precise measurements Continuous Lower calibration requirements (compared with GC) Broadband spectrum allows for multi-component analyses, and storage of spectrums allows to produce a digital archive that can be used afterwards Ability to analyse isotopic composition including isotopomers Mid IR used at atmospheric pressure Portable	High cost of instrument Low brightness of light source Lower measurement frequency than with other optical instruments Complicated analysis of data Difficult maintenance
Lasers (QCL, CRDS, IA-ICOS)	Precision: up to 0.03 ppb (1 s) or up to 0.01 ppb (1 min avg.)	No cryogenic cooling needed in the modern versions Fast and precise measurements Possible to perform isotopic composition analyses without preconcentration, including site-preference	Expensive Low pressure necessary Narrowband - limited amount of compounds can be measured Difficult maintenance

*LOD – Limit of Detection

usually of the order of 1 min. These instruments are also more stable and do not require frequent calibrations.

Another advantage of optical instruments is their portability. Most of currently available instruments can operate at room temperatures without the need of using cryogenic cooling. Consequently, they can be easily transported and quickly set-up at any desired measurement location or even installed on mobile platforms – both surface and aerial – designed for in-situ flux measurement campaigns, as well as plume hunting surveys. Some types of the optical instruments can simultaneously measure the isotopic composition of N_2O, including the site preference, allowing for on-the-fly source apportionment, e.g. through Keeling plot approach (Wolf et al., 2015).

All these features make the optical instruments an equipment of choice for both long- and short-term measurement campaigns. Currently, however, their main disadvantage is high purchase cost. Another one is a limited ability of the owner to perform on-site maintenance, which means that in case of any critical malfunction, the instrument needs to be shipped back to the manufacturer, potentially resulting in long downtime periods. Main advantages and disadvantages of GC and optical techniques for atmospheric N_2O measurements are summarized in Table 3.1.

Remote sensing presents an altogether different approach to measuring nitrous oxide. Due to its physical properties and the limitations of the instrumentation available, N_2O retrievals were first used for providing information on its stratospheric abundances. During the last 15 years, observations using Thermal Infrared (TIR) sounders made it possible to measure N_2O concentrations in the middle and upper troposphere. Instruments like IASI (Infrared Atmospheric Sounding Interferometer) or AIRS (Atmospheric Infrared Sounder) provide maximum vertical sensitivities between 750 and 200 hPa (approximately 3 – 12 km) (see Xiong et al., 2014 and references therein), complementing the surface measurements performed with previously described techniques. However, the precision of satellite measurements is lower than in case of surface observations, and global inversions using the remote sensing data have yet to be performed for N_2O. Therefore, regional analyses are still based on ground-based networks.

3.3. Atmospheric N_2O monitoring stations discussed in the thesis

Every station measuring ambient air concentrations of atmospheric trace constituents is different in regards to main purpose of the performed measurements. While some sites are established to represent conditions typical for the region, country or even a part of a continent, others are chosen to represent more specific local conditions, e.g. to investigate atmospheric transport in a typical rural setting or to assess the influence of local sources on the urban atmosphere. On the other hand, the data originating from a single station are often not sufficient to address large-scale phenomena in the atmosphere. In such cases, the work of numerous stations can be coordinated through a measurement network. Such networks can comprise of varying number of stations, depending on the goal of the project, with numbers ranging from several (AGAGE), through tens (InGOS, ICOS) to hundreds (NOAA Cooperative Sampling Network[2]).

[2] http://www.esrl.noaa.gov/gmd/ccgg/flask.php

Due to the above-mentioned diverging purposes associated with location of a given monitoring station, it is crucial to have a detailed knowledge of station characteristics before considering its inclusion in any type of network. Failure in obtaining this information could lead to the possibility of including a measurement site that does not provide useful scientific information about the tackled problem or possibly worse, e.g. when misinterpretation of the spatial representativeness of the given site produces errors and/or biases in the final results. An example of such a case would be to use the data from an urban station in the global inversion study of CO_2. Necessity of having detailed information also holds when the measurement results from a single station are being compared with the analogous results from another one. If the intended research is focused on investigating pollutant emission and transport patterns, by far the most important characteristic of the site is the distribution of sources and sinks of the measured compound(s) in the surroundings of the station, sometimes called *near-field*.

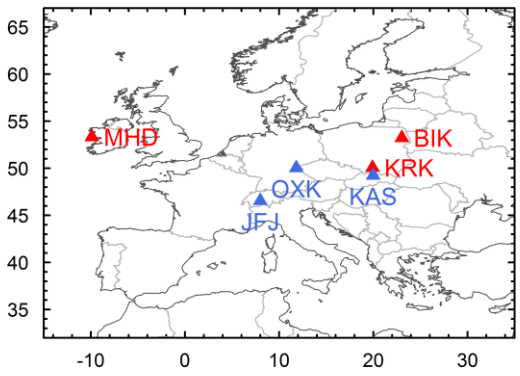

Figure 3.1. Overview of N_2O monitoring sites discussed in the current work. Stations measuring in lower troposphere in relatively flat terrain are marked in red. Mountain stations marked with blue.

As the number of stations in a given network grow, it is increasingly difficult for all interested parties (experimentalists, modellers and other data users) to keep detailed information about the sites in mind. Therefore, in order to systemize the information on the stations location and their near-field characteristics, a common spatial scale of influence (footprints) can be proposed, consisting of four different spatial scale ranges:

a) local (tens or hundreds of meters, building scale) – sources located in this area are capable of generating very strong, rapid, short-term changes in the measured concentrations,
b) short-range (1 km to several km) – usually responsible for most peaks in the record,
c) long-range (from tens up to several hundreds of km) – responsible for synoptic-scale variability,
d) regional (continental scale) – responsible for changes in background concentrations.

For each of the measurement sites discussed in this chapter (Figure 3.1.), the above-outlined classification will be used to establish a common frame of reference and to estimate the range for which the conclusions drawn from the analyses of the measurement records holds true.

3.3.1. Kasprowy Wierch (KAS) mountain station.

The Kasprowy Wierch station (KAS, 49.232° N, 19.982° E, 1989 m a.s.l.) was established in 1994 by a joint effort of the Faculty of Physics and Applied Computer Science[3] of the AGH University of Science and Technology in Kraków and of the Institute of Environmental Physics, University of Heidelberg, Germany. The main task of the site is to monitor concentrations and isotopic composition of main atmospheric greenhouse gases such as CO_2, CH_4, SF_6 and N_2O, in order to

[3] At that time: Faculty of Physics and Nuclear Techniques..

Figure 3.2. Kasprowy Wierch station from Kopa Kondracka peak (W to E). Author: Jerzy Opioła. Photo used under Creative Commons GNU Free Documentation license 2.5.

characterize their emission and transport patterns in the region of Central and Eastern Europe. The station is located on top of Kasprowy Wierch mountain peak in the High Tatras, at the border between Poland and Slovakia (Figure 3.2.). The laboratory is located in the building of meteorological observatory operated by the Polish Institute of Meteorology and Water Management (IMiGW – *Instytut Meteorologii i Gospodarki Wodnej*). The air inlet is located on the roof of the building, approximately two meters above the local ground (1987 m a.s.l.).

In 1996, an automated gas chromatograph (Agilent HP5890) equipped with FID (Flame Ionization Detector) and ECD (Electron Capture Detector) detectors was installed and quasi-continuous analyses have been carried out ever since (Necki et al., 2003, 2013, Chmura et al., 2008, Różański et al., 2014). Currently, in-situ analyses of ambient concentrations of CO_2, CH_4, N_2O, SF_6 (GC), H_2 and CO (Peak Performer, PP1) are performed approximately every 20 minutes. All results are calibrated and are traceable to the international primary scales, e.g. WMO CH4 X2004 for methane and WMO N2O X2006A for nitrous oxide, with inter-comparison programs conducted in the framework of several EU Projects a part of quality control procedures at the station. KAS station is currently

Table 3.2. Important near-field sources of N_2O emissions for KAS (Kasprowy Wierch) measurement site, classified according to distance.

Scale	Distance	Known sources of N_2O	
		Distributed	Point emissions
Local	up to 1 km	none	none
Short-range	up to 10 km	agricultural activities in the area are limited due to hilly terrain; occasional peaks from traffic and stationary combustion (e.g. heat ovens) are possible	none
Long-range	up to 300 km	agricultural activities in southern Poland and northern Slovakia	emissions from traffic, heating and waste, mainly in the cities of the region; nitrogen fertilizer production plant approximately 130km to the NE (ZAT Tarnów)
Regional	above	agriculture in Central and Eastern Europe	cities and fertilizer production plants

delivering near real-time data (NRT) in the framework of the InGOS project (http://ingos-atm.lsce.ipsl.fr/NRT).

The KAS station participated in many international collaborations focused on monitoring and research of greenhouse gases, providing long-term measurement records of CO_2 and CH_4 to scientific databases (e.g. CarboEurope-IP, GHG-Europe). However, while the possibility of N_2O measurements existed at the site since the beginning of its operation, no consistent, long-term, quality-controlled record of nitrous oxide concentrations became available for this station. As a part of this PhD thesis, the existing analytical system was modified and appropriate measurement methodology was introduced on the site in order to provide such high-quality data record of ambient nitrous oxide concentrations.

The KAS station, thanks to its high altitude and lack of significant N_2O sources nearby, is a good location for performing observations of a continental background of this gas. Detailed information on near-field N_2O sources that could be influencing measured concentrations can be found in Table 3.2.

3.3.2. Kraków (KRK) urban station.

Similar to KAS station, the measurement site in Kraków (KRK, 50.067° N, 19.913° E, 221 m a.s.l.) has been performing regular monitoring of greenhouse gases and other pollutants for a number of years. However, up to now no long-term, consistent record of nitrous oxide has been made available to scientific community. The KRK station is located approximately 2 km east of the city centre of Kraków, the capital of Małopolska (Lesser Poland) voivodoship. According to some estimates, the population of Kraków agglomeration reaches approximately 1 million inhabitants. The station is located in the building of the Faculty of Physics and Applied Computer Science of AGH University of Science and Technology, and its air inlet is located ca. 20 m above the local ground (Figure 3.3.). KRK is a typical urban station, characterized by distinctive features, such as relatively high frequency of daytime atmospheric inversion occurrences during winter induced by specific local microclimate. Another is a specific composition of the mixture of local sources, e.g. car fleet being significantly older than in the cities of Western Europe, and a large amount of coal-powered heating stoves still

Figure 3.3. KRK measurement site. Air inlet is located on the roof of Faculty of Physics and Applied Computer Science (left, marked with arrow). Author: M. Zimnoch.

Table 3.3. Important near-field sources of N_2O emissions for KRK (Kraków) measurement site, classified according to distance.

Scale	Distance	Known sources of N_2O	
		Distributed	Point emissions
Local	up to 1km	several near-by roads that are heavily used especially during rush hours - mostly N and E	chimneys emitting exhaust gases from coal-stoves, mostly in the N and E sector
Short-range	up to 10km	agglomeration of Kraków; scattered agriculture outside of the city	large steel mill in the E part of the city; several waste-water treatment plants
Long-range	up to 300km	agricultural activities in southern Poland and northern Slovakia	emissions from traffic and heating in the cities of the region; nitrogen fertilizer production plant approximately 100 km to the E (ZAT Tarnów)
Regional	above	agriculture in Central and Eastern Europe	cities and fertilizer production plants

present in many households. Recently, the city council started a series of efforts to limit the amount of this type of devices, together a simultaneous detailed quantification of their number in the agglomeration.

A short overview of the most important sources of nitrous oxide in Kraków agglomeration is presented in Table 3.3. It can be expected that, due to relatively low elevation and close vicinity of the nitrous oxide emission sources, there is limited possibility to use the analyses of Kraków ambient air to draw conclusions on the behaviour of nitrous oxide on scales larger than dimensions of the city.

3.3.3. Białystok (BIK) and Ochsenkopf (OXK) tall towers.

Direct access to the data from BIK and OXK sites has been obtained thanks to bilateral agreement between the author of this PhD thesis and the Max-Planck Institute for Biogeochemistry in Jena, in the framework of NA2/NA3 package of the InGOS project. In this PhD thesis, the data from BIK were used as a basis for comparison between Kraków urban conditions and rural conditions typical for Poland, under the assumption that N_2O emissions-related parameters do not differ significantly between Małopolska and Podlasie (where BIK is located, approximately 600 km north), as variations

Table 3.4. Important near-field sources of N_2O emissions for BIK (Białystok) measurement site, classified according to distance.

Scale	Distance	Known sources of N_2O	
		Distributed	Point emissions
Local	up to 1km	agricultural activities, mostly small scale private farms; a national roadway approx. 1 km west	possible emissions from stationary combustion in nearby villages of Krynice (S, SE) and Obrubniki (N);
Short-range	up to 10km	agglomeration of Białystok (city centre approx. 15 km to SE); agricultural activities, lower intensity to the E and NE due to presence of a large forest	power plant in Białystok city limits, approx. 15 km SE of the measurement site
Long-range	up to 300km	agricultural activities in northeast Poland, southwest Lithuania and western Belarus; mostly fields mixed with scattered forests.	emissions from traffic and heating in the cities of the region; largest fertilizer production plant in Belarus (Grodno) is located approx. 80 km NE from the station.
Regional	above	agriculture in central and eastern Europe	cities, power production and chemical component production facilities

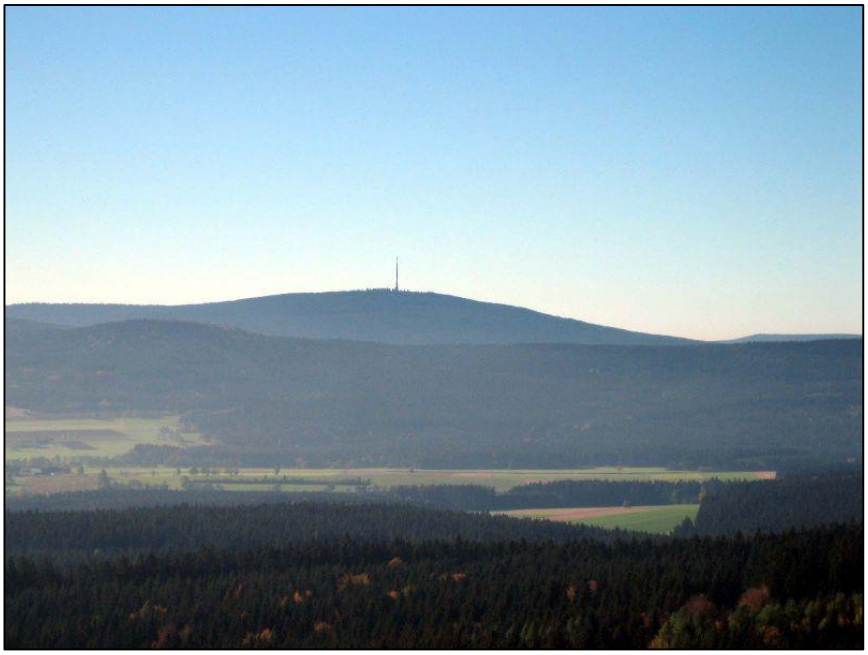

Figure 3.4. Left: Bialystok-Krynice (BIK) tall tower. Author: unknown. Right: Ochsenkopf, as seen from the Waldstein in 2006. Author: Adrian Michael. Used under CC GNU Free Documentation license 2.5.

usually occur on larger spatial scales (e.g. through country-specific fertilizer application recommendations). The data from OXK station was used as a reference point for characterisation of Kasprowy Wierch as a high-altitude background site, together with Jungfraujoch station (see below).

The Białystok-Krynice tall tower (BIK, 53.231° N, 23.026° E, 186 m a.s.l., 331 m high), is a site established in the framework of the CHIOTTO project (*Continuous High-precision Tall Tower Observations of Greenhouse Gases*, 5th EU Framework Programme) as a part of an European network designed to monitor main greenhouse gas components in Europe. It is located approximately 15 km NW of Białystok city centre, capital of Podlaskie voivodoship in northeast Poland, with population of approximately 300 thousands inhabitants. The main purpose of the station was to characterise rural background conditions of Central and Eastern Europe with regard to emissions and transport of atmospheric trace constituents such as CO_2, CO, CH_4, N_2O, SF_6 and others (Table 3.4.). The air inlets are located at five different heights, with the highest port located 300 m above the local ground (Figure 3.4.). A more detailed description of the site and the measurement methods can be found in Popa et al. (2010).

As in the case of BIK site, the Ochsenkopf tall tower (OXK, 50.031° N, 11.808° E, 1024 m a.s.l., 163 m high) is also a site established in the framework of the CHIOTTO project and now takes part in the InGOS 7th EU Framework Project. Its main purpose is to characterize the higher parts of the lower

Table 3.5. Important near-field sources of N_2O emissions for OXK (Ochsenkopf) measurement site, classified according to distance.

Scale	Distance	Known sources of N_2O	
		Distributed	Point emissions
Local	up to 1km	none	None
Short-range	up to 10km	several small villages in the vicinity	None
Long-range	up to 300km	agricultural activities in central Germany and western part Czech Republic	waste water treatment plants (closest in Bayreuth and Hof)
Regional	above	agriculture in Central and Eastern Europe	power production and chemical component production facilities; cities

troposphere in the hilly region of East Germany. Located approximately 30 km NE of Bayreuth (Northern Franconia, Bavaria, Germany) in the Fichtel Mountains, the station is set on a 163m high television and radio transmission mast, located on top of Ochsenkopf Mountain (1024 m a.s.l., Figure 3.4., Table 3.5.). The measurement site is relatively secluded, with landscape covered by the mixed forest typical for Central Europe. The air is sampled from three vertical levels (with the highest one at the very top of the tower) and subsequently analysed for concentrations of various greenhouse and other compounds, including N_2O. Detailed description of the OXK station can be found in Thompson et al. (2009).

3.3.4. Mace Head (MHD) and Jungfraujoch (JFJ).

Nitrous oxide records from two global background stations of different characteristics were chosen to compare with the N_2O concentrations measured at KRK and KAS, in order to put the obtained results in a proper context, especially with regard to long term trends and N_2O annual cycle. As both of these stations can be characterized by a lack important local sources of N_2O, classifications of near-field emissions was not performed.

Mace Head Atmospheric Research Station (MHD, 53.327° N, 9.905° W, 5 m a.s.l., Figure 3.5., left) is a "global" WMO GAW monitoring site as well as a supersite of European Monitoring and Evaluation Programme (EMEP). Operated by the National University of Ireland Galway's School of Physics and the University's Ryan Institute Centre for Climate and Air Pollution Studies, the site takes part in a multitude of research networks focused on atmospheric chemistry. Thanks to its location on the western coast of Ireland, MHD measures a multitude of atmospheric components under prevailing Northern Hemispheric background conditions, with occasional influences from the continental Europe. Nitrous oxide is measured in the framework of Advanced Global Atmospheric Gases Experiment (AGAGE), using a well-established GC-ECD technique. A detailed description of the equipment in use at MHD can be found at the AGAGE website[4], as well as in dedicated publications (Prinn et al., 1990, 2000, Nevison et al., 2011).

A high mountain station measuring continental background values of many atmospheric species was also chosen in order to compare with the measurements performed at Kasprowy Wierch. Alpine Research Station Jungfraujoch (JFJ, 7.984° E, 46.548° N, 3580 m a.s.l., Figure 3.5., right), located in

Figure 3.5. Left: Mace Head (MHD) station, Ireland. Right: Jungfraujoch station, Switzerland. Source: InGOS 7th Framework Project's website.

[4] https://agage.mit.edu/instruments/gas-chromatography-multidetector-gc-md

Switzerland, continuously monitors the concentrations of atmospheric N_2O in the framework of NABEL (Swiss National Air Pollution Monitoring Network) since 2005 (Leuenberger and Flückiger, 2008). The station is currently using GC-ECD techniques, with optical instruments (Quantum Cascade Lasers) for monitoring N_2O soon to be added. Reimann et al. (2008) have investigated the emission sources that have a measurable influence on the observed atmospheric concentrations of different gases observed at Jungfraujoch station. They have found that the station is most sensitive to the emissions from Switzerland, northern Italy, France, southern Germany, and to a lesser degree from northeastern Spain and Benelux countries.

Both MHD and Jungfraujoch participate in the InGOS NA2/NA3 workpackages, together with KAS, BIK and OXK stations. In particular, the datasets obtained by all these sites undergo the same quality-control and quality assurance procedures, assuring adequate data comparability between the sites.

3.4. Analytical set-up and methodology of N_2O measurements.

Both KAS and KRK stations rely on well-established gas chromatography techniques for measuring atmospheric N_2O mixing ratios. A detailed description of the analytical set-up, calibration methodology and the uncertainty estimation procedures is given in Annex A, with only a general overview provided below.

All N_2O results from KRK and KAS stations presented here were obtained using the Electron Capture Detector (ECD) coupled to the GC system in the back-flush mode. A direct link between the measured ambient concentrations of N_2O and a common scale of reference (WMO N_2O X2006A) (WMO, 2013), necessary to make the results comparable to the datasets from other measurement sites, was established through the usage of sets of primary and secondary laboratory standards (cf. Annex A). A 2-point calibration methodology was thoroughly tested and implemented to take into account non-linear response curve of the ECD detector, and thus provide high precision and accuracy of the measurements. A robust uncertainty estimation and monitoring procedure was established for Kasprowy Wierch and other measurement stations involved in the InGOS NA2/NA3 workpackages in the framework of that project. Thanks to these efforts, it was possible to obtain N_2O data records characterised by high precision, good accuracy and state-of-the-art uncertainty estimates. While the extent of this study is limited to N_2O, other compounds measured at KAS and KRK stations were also taken into consideration when testing and establishing measurement methodology, so that the obtained results can be used by scientific community for most demanding research purposes, e.g. numerical inversion modelling of greenhouse gas emissions.

3.5. An overview of N_2O records available for KAS and KRK stations.

Nitrous oxide ambient concentrations presented in this section span the period from 01.04.2013 to 30.09.2014. These dates reflect the periods when 2-point calibration methodology was implemented at both stations, as a direct result of this PhD work. Figure 3.6. presents an example of N_2O analyses performed over a period of 3 weeks at KRK and KAS stations, with one analysis performed every 22 minutes. The N_2O mixing ratios are reported in ppb (mole fraction), where 1 ppb is equal to 1 nmol of N_2O per 1 mol of dry air.

The measurements were monitored online with the use of custom-designed software *Panda*, developed by J. Bartyzel in close cooperation with the author specifically for that purpose. In the framework of this thesis, the raw datasets were reanalysed using a set of routines developed by the author in the R environment. Raw measurement results underwent a several-stage filtration procedure. The raw data extracted from each chromatogram were used to calculate the calibration curves, measured concentrations and appropriate uncertainty estimates, with respective filtrations following each step of

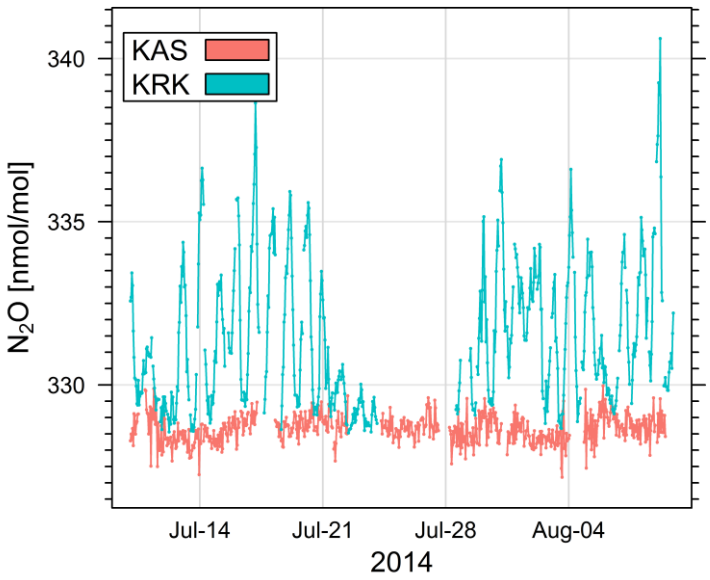

Figure 3.6. An example of N_2O measurements performed at KAS and KRK stations between July 10th and August 09th, 2014. Shown are individual data points after filtration procedure.

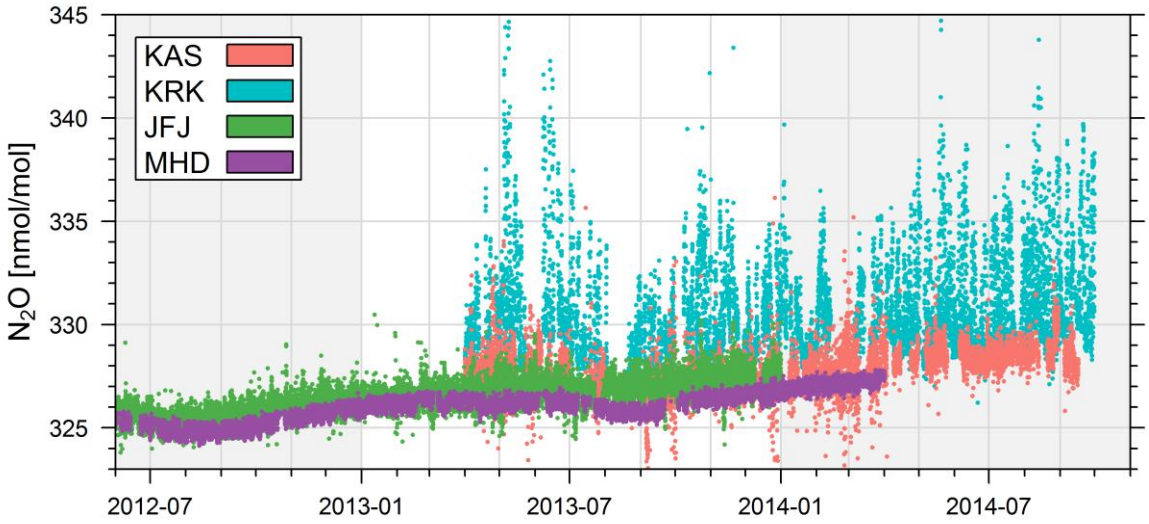

Figure 3.7. An overview of the atmospheric N_2O concentrations measured at the KAS and KRK stations, superimposed on atmospheric background measurements at JFJ and MHD stations. MHD data are wind-sector filtered to be representative of marine background. Hourly means after filtration of the data are shown.

the calculation procedure. The filtrations included both manual exclusions of measurements flagged as questionable in the stations log files, as well as automatic outlier filtrations (cf. Annex A).

In all subsequent analyses performed in the current study, hourly averages were used, calculated as an arithmetic average of all individual measurements performed during the given hour. This procedure is in accordance with internal recommendations of the InGOS project.

Figure 3.7. presents an overview of the records of atmospheric nitrous oxide concentrations (hourly means, filtered data) for KAS and KRK stations. For comparison, time series of N_2O for JFJ and MHD stations are also shown, representing continental high-altitude background and clean marine background, respectively. Presented data supports the choice of KAS station as a reference site for comparison with heavily polluted urban atmosphere of KRK station. The lower envelopes of all datasets are similar, with higher variability present in KRK nitrous oxide record caused by close proximity to N_2O sources and frequent events of stable inversion layer occurring in the lower troposphere (see below).

3.5.1. Quality of the data

A robust QA/QC analysis has been performed for the acquired data, based on the calculations of diagnostic parameters that are described in detail in Annex A. These parameters, named repeatability and reproducibility, allow quantitative estimation of the analytical uncertainty for both short and long time intervals, respectively. While repeatability can be calculated using only the results of working standard analyses, reproducibility quantification requires regular measurements of a non-calibration air mixture of known concentrations of the analysed species – a “target”. It is important to note that to date the repeatability values are not directly related to the WMO compatibility goals (see GAW Report no. 213: WMO, 2013), as the concept of repeatability is not widely used in the community. The results of target measurements and uncertainty parameters calculated for the N_2O record from KAS and KRK stations are presented in Figure 3.8.

Overall, short-term quality of the measurements at the KAS station is highly variable and generally lower than at KRK station (Figure 3.8., middle). This effect is more pronounced before 04.2014, with the mean value of 0.88 ppb before and 0.48 ppb afterwards. For KRK site, respective values are 0.27 ppb and 0.31 ppb. Certain events occur, however, during which repeatability values can reach up to 3 ppb, corresponding to very high noise in the record of N_2O mixing ratios, with over- or under-estimations of the ambient air concentrations.

Observed elevated N_2O repeatability values can in most cases be associated with suboptimal operating parameters of one of many system components, e.g. low ECD make-up gas flow or low pressure of the carrier gas. At KAS station, high values are also observed during windy conditions, which most probably cause rapid pressure and temperature changes in the laboratory to which the measuring system is highly sensitive. In general, repeatability could be used as a diagnostic quantity for the filtration procedure applied to NRT data. In the presented study, however, it was only used to indicate periods of high variability (i.e. repeatability values higher than 10 ppb), which were excluded from further analyses..

Regular analyses of a target gas has also been performed on both stations, with the goal of monitoring possible drift occurrences (Figure 3.8., top). At both KRK and KAS, two target mixtures

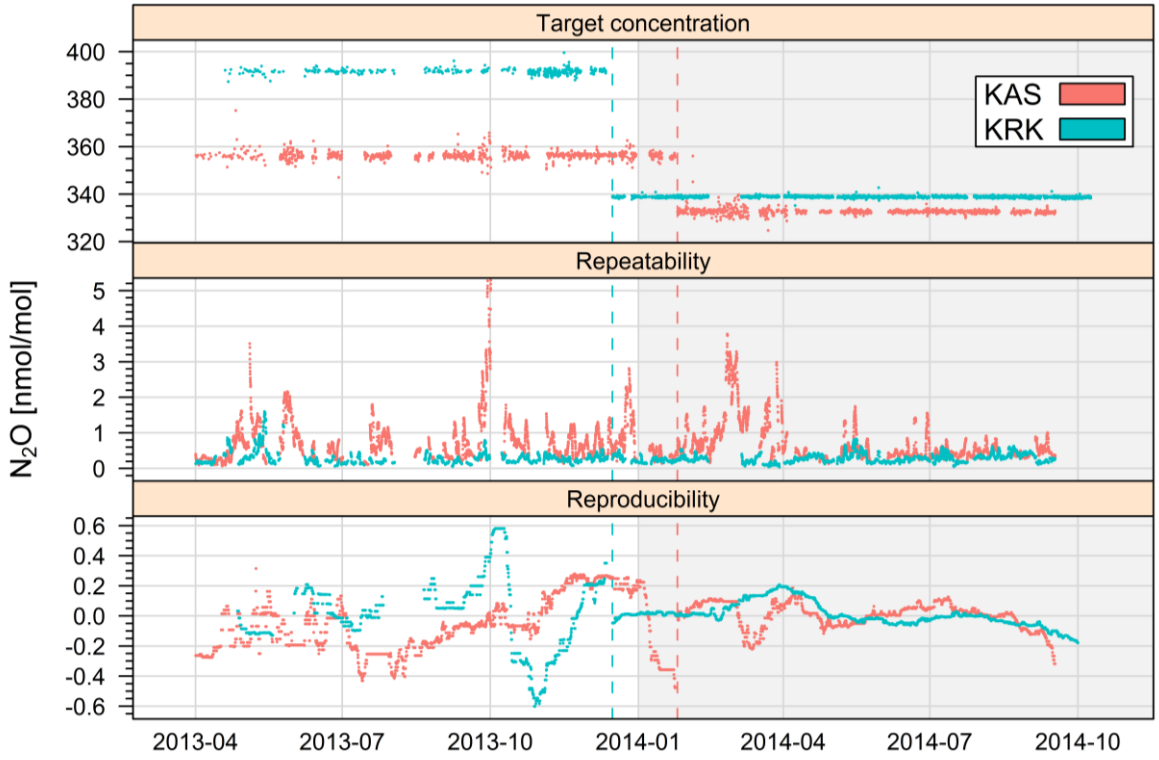

Figure 3.8. QA/QC parameters calculated for KRK and KAS stations. Top: Target gas measurements from 2013.04 to 2014.09, with respective repeatability (middle) and reproducibility (bottom) values – for calculation procedures, see Annex A. Dashed vertical lines denote target cylinder exchange.

have been measured between 2013 and 2014. Coincidentally, at both stations first of the used tanks was filled with air mixture containing higher than recommended N_2O concentrations (356.57 ppb KAS, 391.70 ppb KRK), i.e. well above ambient values. In these first periods, the calculated reproducibility values oscillate between -0.5 ppb to 0.5 ppb (Figure 3.8., bottom), which can be attributed to large deviation of the target mixture concentrations from the range covered by the SLS (*Secondary Lab Standards*) calibration mixtures. Measurements performed with the second set of target mixtures (332.83 ppb KAS, 338.83 ppb KRK) show much smaller deviations. The reproducibility data suggests that there are no drifts in the presented record significant from the perspective of the analyses presented in this study.

Generally, occurrences of high noise values and drifts were more frequent at KAS station, which can be attributed to lower accessibility of the station and much higher equipment and infrastructure age, causing a significant amount of malfunctions, especially in the first year of the presented record. A significant effort was put into improvement of the instrument performance throughout this PhD work. Apart from changes in measurement methodology and application of QA/QC procedures outlined in the previous sections and presented in Annex 1, a multitude of smaller improvements to both the measuring equipment and supporting infrastructure have been made, including a major laboratory refurbishment in October 2013. These changes have resulted in significant increase of the quality of measurements in the second half of 2014.

In Kraków, the task of providing high quality data was less challenging and the largest issue was the presence of periods with lower data coverage, an effect that is more pronounced for the first several months of 2013. During this time, a software malfunction has caused the measurements to be spontaneously interrupted after random number of samples and a manual intervention from the operator was required. After mid-2013, most of the interruptions in the analyses were related either

to periodic calibration procedures (up to 2 weeks long) or to measurements of other samples, e.g. related to soil-flux measurement campaign in March 2014 (approximately 1 month).

3.5.2. Data detrending and deseasonalization procedure.

The N_2O signals measured at KAS and KRK stations are a complex result of transport and emissions occurring on local, regional and global scales. Locally influenced N_2O concentration changes are superimposed on a global trend in atmospheric N_2O and its seasonal variability. To extract information on seasonal, weekly and diurnal patterns occurring the datasets due to local and regional influences, a detrending and deseasonalization (D&D) of KRK and KAS datasets was necessary.

D&D was performed by subtracting the mid-latitudes background values from N_2O concentration records measured at KRK and KAS stations. As there are no known significant N_2O sources in the open oceans, N_2O mixing ratios in marine air can be treated as representative of such background for a given latitude. For analyses in the presented study, a N_2O record from Mace Head station, subset for data flagged as measuring air masses originating from over the Atlantic Ocean, was chosen as a basis of the detrending and deseasonalization.

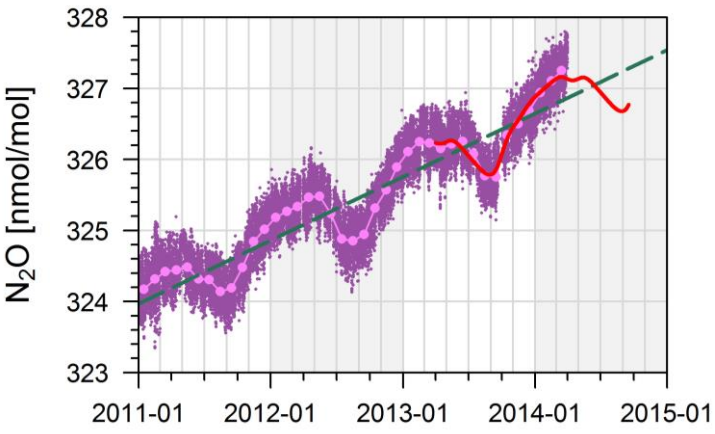

Figure 3.9. Background values used for detrending and deseasonalization (D&D) procedure. Purple: MHD N_2O concentrations with monthly averages. Green dashed line: linear trend. Red: extended background signal used for D&D.

Because the available MHD N_2O concentrations were only available until early 2014, the detrending of KAS and KRK datasets was not possible without the extrapolation of the dataset until 01.10.2014 (Figure 3.9.). In order to do that, N_2O background record, represented by monthly averages of MHD marine concentrations (2011.01-2014.03), was first divided into a 3 components: long-term, seasonal and residual, by a STL procedure (*Seasonal Decomposition of Time Series by LOESS*[5]) available in R software (RCT, 2014) via *stl* routine (Cleveland et al., 1990). Annual cycle of the marine background was assumed constant.

A linear function was fitted to the resulting trend component (R^2 = 0.9993, $p < 2.2 * 10^{-16}$) and extrapolated until January 2015, thus producing a long-term trend. Seasonal component was then added to the extrapolated data. A smooth curve was obtained from thus obtained monthly dataset, calculated by a *smooth.spline* routine available in R software. The final step of the procedure was a subtraction of the calculated smooth curve, thus obtaining the detrended and deseasonalised KRK and KAS N_2O records.

[5] LOESS - locally weighted scatterplot smoothing

3.6. Long-term trends of atmospheric nitrous oxide concentrations over Europe

Although the available nitrous oxide concentration record for Kasprowy Wierch is relatively short, it is already sufficient to gain a general information on the characteristics of the continental N_2O background on diurnal, weekly and monthly time-scales. Estimating long-term trend proves difficult, however, as interannual variability is superimposed on the underlying global increase of the N_2O signal. However, by comparing the N_2O mixing ratios available for Kasprowy Wierch with other continental stations of a similar nature one can see that two years of N_2O measurements at KAS station presented here show promise in estimating long term changes in nitrous oxide that are occurring at mid-latitudes of the northern hemisphere.

Figure 3.10., top, presents the monthly means of atmospheric nitrous oxide concentrations measured at four locations: MHD – representing marine background, JFJ – representative of continental background, OXK and KAS. To ensure that each of the stations is representative of the

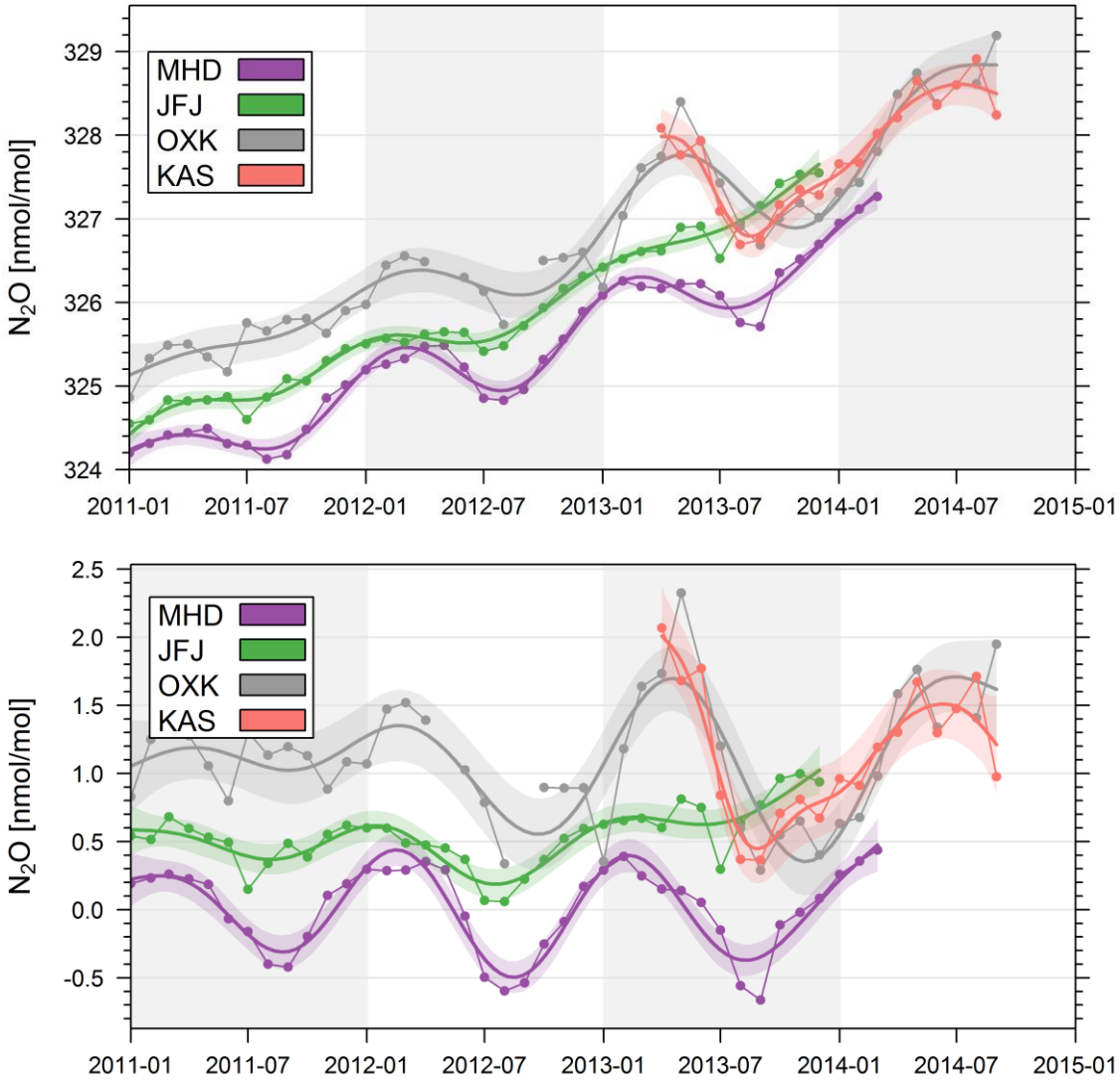

Figure 3.10. Top: Comparison of long-term records of monthly mean N_2O concentration changes calculated from selected data (see text) of four background stations, representing marine background (MHD – Mace Head) and continental background (JFJ – Jungrfaujoch; OXK – Ochsenkopf, KAS – Kasprowy Wierch). Lines and shaded areas represent respective trends with 95% confidence intervals calculated with smoothTrend function available in the openair package for R software.

clean background conditions pertaining to that station, the analyses were performed with selected, night-time data (from 23:00 to 03:00) in case of mountain stations and daytime data (11:00-16:00) for MHD. The rationale behind that choice is that during night-time, mountain stations are less affected by convective vertical mixing within the planetary boundary layer, contrary to low-altitude, where night-time concentrations of greenhouse gases are usually higher due to formation of stable nocturnal boundary layer and surface emissions. During daytime, vertical mixing is breaking that layer, and the concentrations observed around midday and in the early afternoon are usually closer to the respective background values.

From these subsets of N_2O records, monthly averages were calculated for each of the discussed stations, and a smooth spline was calculated using *smoothTrend* function available with the *opeanair* package (Carslaw, 2012, Carslaw and Ropkins, 2012) of the R software, together with a 95% confidence interval. Same type of smooth curves was applied to the detrended data, i.e. with linear trend subtracted (cf. section 3.5.2).

N_2O mixing ratios measured at all continental stations are consistently higher than marine background (approximately 0.5 ppb for JFJ station and 1 ppb at OXK and KAS sites). The most probable cause is the influence of the continental source that, as the air masses pass over Europe from west to east, elevates the N_2O concentrations in the upper troposphere through vertical pollutant transport via convection and turbulence. If this is the case, the overall longer distance that an air mass must travel from the Atlantic coast to the receptor point will result in higher difference in the mean N_2O load of marine air and the continental atmosphere at the given site. This could partly explain generally higher values observed at KAS and OXK stations when compared to MHD site.

Another important issue is the proximity to surface emissions located in the lower troposphere, both in horizontal and vertical planes. JFJ station is located on the high mountain pass that is surrounded by a system of ranges and valleys with very limited infrastructure and agriculture. The closest lowlands are located at least 50 km away (NW), which makes the probability of the emission plumes to reach the JFJ station very low. This probability is much higher for both OXK and KAS sites, which lie both lower and in close proximity to human settlements. This allows the transport of pollutants either through combination of convection and advection (summer) or through advection alone (mountain breezes), which could partly explain higher seasonality observed in KAS and OXK detrended records.

The data shown in Figure 3.10. (bottom) also indicate a phase shift in the seasonal cycles of N_2O for OXK and KAS sites, with N_2O maxima and minima occurring at KAS station approximately 1 – 2 months before respective maxima and minima at OXK. While the dataset is limited in its time span, this phenomenon could be explained through the mechanism of intrusions of stratospheric air depleted in N_2O into the troposphere. Nevison et al. (2011) have linked Brewer-Dobson circulation (by treating lower stratospheric air temperature in winter as a proxy) with the depth of summer N_2O minimum for northern hemispheric measurement sites (including MHD station) and found that there is a negative correlation between those two parameters. These results, as well as earlier studies (Liao et al., 2004, Nevison et al., 2004, 2007) support the idea of stratospheric influences as the main driving force behind the occurrences of N_2O of summer minimum. Slow subsidence of N_2O depleted air from higher to lower stratosphere that happens on monthly timescales causes its diffusion through the tropopause into the troposphere, where it can influence the air masses in the PBL.

The exact nature and mechanism of transport of N_2O depleted air through the tropopause and into PBL is not clear at the moment. However, one might speculate that faster occurrence of the

summertime minimum at KAS station could be caused by this slow subsidence. Observations from JFJ site seem to display the same pattern, with maxima and minima of N_2O occurring before their respective counterparts at OXK. On the other hand, minima of nitrous oxide at MHD station also occur faster than at OXK site, which underlines a necessity for an in-depth study of tropospheric and stratospheric transport patterns at mid northern latitudes in order to clarify the origin of N_2O seasonality at the stations discussed here.

3.7. Spatial and temporal patterns in atmospheric N_2O concentration over southern Poland.

Figure 3.11. shows monthly statistics of N_2O concentrations at KAS and KRK stations (calculated from data presented in Figure 3.7), displayed in the box-plot form. If the values in the interquartile range are considered (thick bars), N_2O concentrations at KAS station rarely exceed 330 ppb, pointing to clean background conditions at this measurement site. Maxima of medians were recorded in May-June period in both measurement years, which are summer months in southern Poland. The minima of N_2O concentrations (medians) occurred in August and September 2013. In 2014, no clear minimum could be distinguished before the measurement campaign has finished (end of September). The timing of the observed minima is roughly in line with other background stations located in mid-latitudes of the northern hemisphere. This effect is connected to the interannual variability of nitrous oxide concentrations and is attributed to the stratospheric intrusions of N_2O depleted air masses (cf. discussion above).

Variability of nitrous oxide concentrations in Kraków is much higher, with the signal being dominated by the diurnal cycle, and in particular, by night-time concentration increases which can

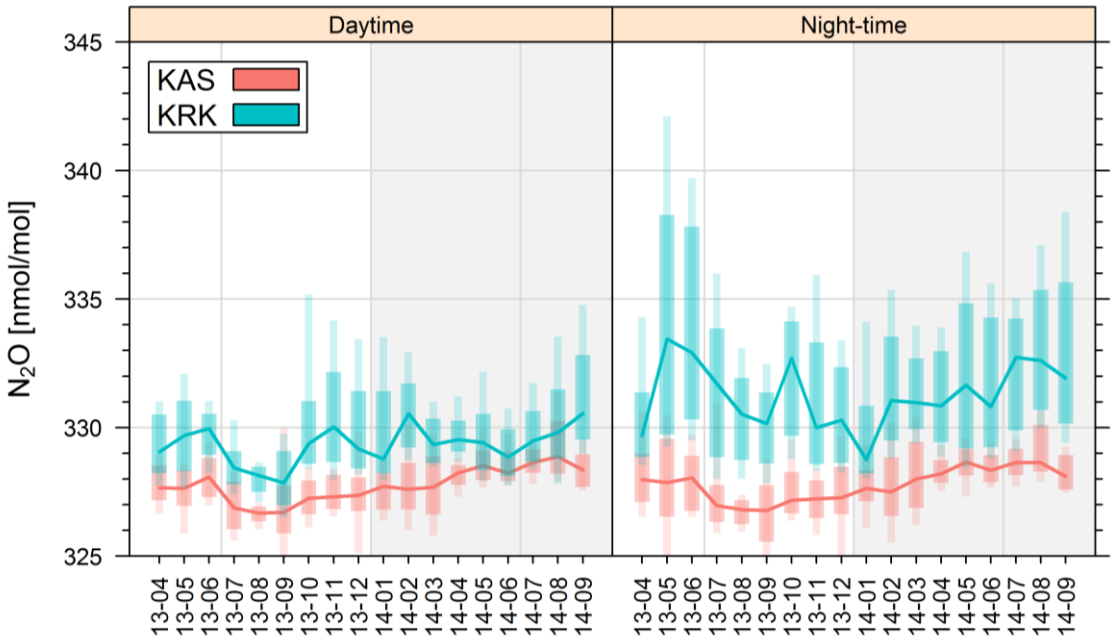

Figure 3.11. Box-plot of monthly distributions of atmospheric nitrous oxide concentrations observed at KAS and KRK stations. Heavy lines represent medians. Thick and thin rectangles represent 25/75 and 5/95 percentile of monthly statistics, respectively. Daytime concentrations were selected using the observations made between 11:00 to 14:00 LT. Respective period for night-time values spanned the period between 23:00 to 02:00 LT.

easily reach 335 ppb. They occur due to near-field surface emissions into the nocturnal inversion layer, which frequently develops in the city area. Such conditions are characterised by very low vertical mixing, which results in accumulation of nitrous oxide emitted from the surface in the lower troposphere, below the inversion layer. With the rise of the sun, temperature gradient in the lower troposphere is inverted, causing the disappearance of the inversion layer and reduction in concentrations of previously accumulated compounds. The effects of this phenomenon are visible in Figure 3.11., where the observed daytime N_2O concentrations are lower, with the mixing ratios often very close to those observed at KAS station.

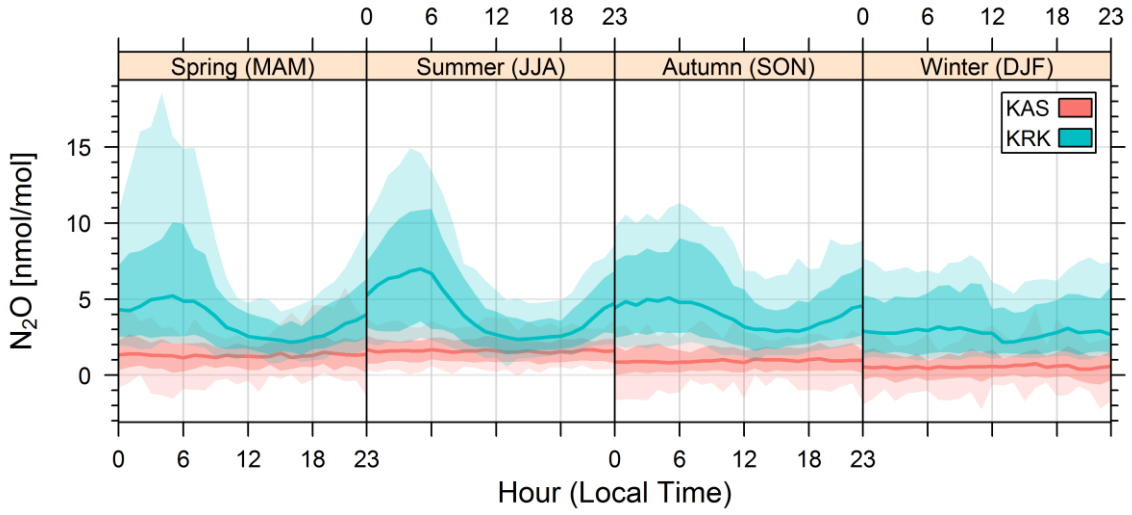

Figure 3.12. Mean diurnal variability of nitrous oxide detrended and deseasonalised concentrations at KAS and KRK stations for four seasons. Thick lines represent medians of hourly data. Dark and light coloured areas represent the 25/75 and 5/95 percentiles, respectively.

During autumn-winter period, the frequency of prolonged inversion episodes in Kraków increases. In such situations, elevated concentrations of nitrous oxide persist also during the day, which could partially explain higher interquantile values observed in September – February period. Another cause of elevated N_2O concentrations during this period might also be linked to the additional emissions of nitrous oxide from point stationary combustion sources such as coal and gas stoves.

The highest frequency of high night-time N_2O concentrations, exceeding in some cases 345 ppb, has been observed in Kraków during May – June 2013, October – November 2013, May 2014 and August-September 2014. While the main driver of night-time increases is usually the synoptic situation over the city, it is worth noting that these periods correspond to fertilizer application times in Southern Poland, usually between March and May for springtime application and September-October for autumn application. This may suggest a possibility of a direct influence of agricultural sources of N_2O located outside of the city limits on elevated atmospheric concentrations measured near the city centre. This could be explained by the excess of nitrogen in the soils which causes the enhancement in the emissions of N_2O from microbial sources for up to several weeks after fertilizer application (see chapter 4). However, no definite conclusions can be drawn at this moment, due to limited amount of information on the night-time pollutant transport patterns (see chapter 5).

The importance of biogenic N_2O sources for KRK station is clearly seen in Figure 3.12., showing statistics of mean hourly concentrations of this gas calculated for different seasons of the year from the detrended and deseasonalised data. The data shows no significant N_2O diurnal cycle for KAS station. For KRK, largest diurnal variations occur in spring and summer (March-May and June-August), with high night-time values observed more frequently during summer (highest median: 7.0

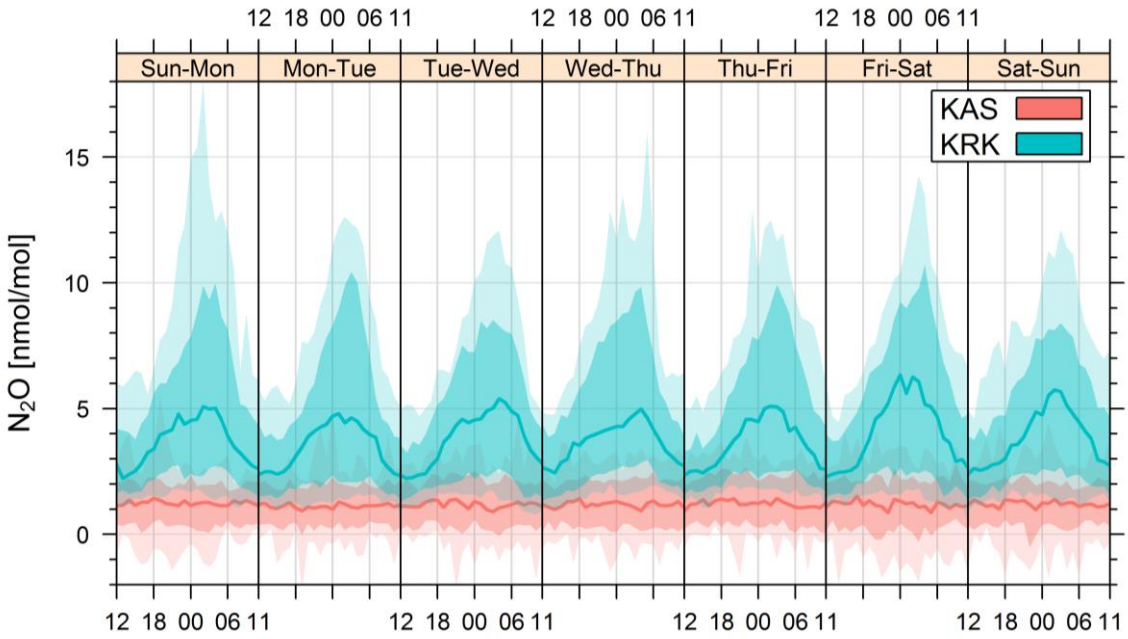

Figure 3.13. Diurnal cycle statistics for nitrous oxide mixing ratios (detrended and deseasonalised) measured at KAS and KRK stations, calculated for every weekday. Thick lines represent medians of hourly data. Shaded areas represent the 25/75 (darker) and 5/95 (lighter) percentiles, respectively.

ppb at 05:00), while smaller number of very high concentration events are visible in spring (highest daily median: 5.2 ppb, while highest 95th percentile: 18.6 ppb). Concentrations observed during autumn are similar to those in the spring, however with lower number of high-concentration events present in the record. Winter is characterised by smaller diurnal variability, which could be caused by reduced activity of microbial sources in the soil due to low temperatures and snow cover. While specific weather conditions during winter of 2013-2014 cannot be excluded at this moment, as the data for 2014-2015 winter was not yet analysed, albeit other available data also supports a significant role of biogenic emissions on diurnal cycle observed in KRK (see sections 3.8 - 3.10 in this chapter and chapter 5)

Possible differences in diurnal cycles for different weekdays was also investigated, to determine if it is feasible to distinguish influence of traffic emissions on the measured N_2O mixing ratios. Figure 3.13. shows the distributions of nitrous oxide concentrations throughout the measurement period, aggregated into seven 24-hour sets, each spanning from noon to 11:59 local time next day. No distinctive pattern is visible in the hourly data for either station. Daily averages calculated using selected night-time and daytime hours are shown in Figure 3.14. Again, no clear inter-weekly pattern is visible, with one feature of interest being the elevated mean N_2O concentrations observed in KRK during Friday-Saturday nights.

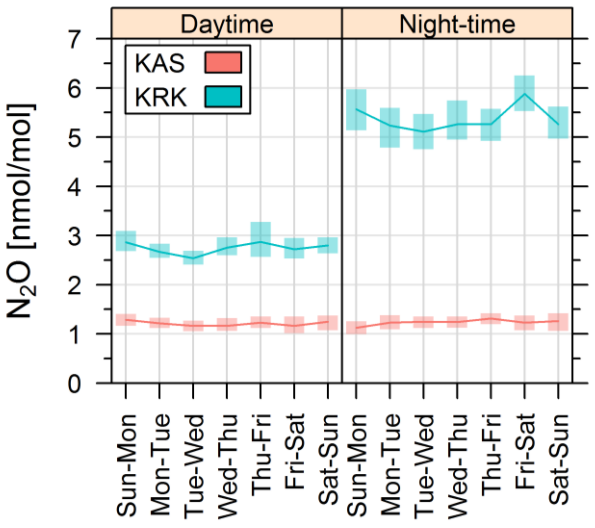

Figure 3.14. Weekday diurnal means of detrended and deseasonalised nitrous oxide concentrations observed at KAS and KRK stations. Thick lines represent means of hourly values selected for a given weekday. Rectangles represent 5/95 confidence intervals. Daytime and night-time concentrations were selected using the periods from 11:00 to 14:00 hours and from 23:00 to 02:00 hours, respectively.

3.8. Characterization of urban influence on atmospheric N_2O mixing ratios – comparison of KRK station with rural reference site (BIK).

In order to better characterize the way the urban environment influences the N_2O ratios in the lower troposphere, the N_2O data collected in Kraków in 2013-2014 were compared with the analogous record available for Białystok (BIK) tall tower in 2005-2014 period (Figure 3.15.). The data for BIK station have been available thanks to a bilateral cooperation with Max-Planck Institute for Biogeochemistry in Jena, which manages the BIK tall tower in the framework of the InGOS 7th EU Framework Project. As part of that cooperation, close to 8 years of atmospheric measurements performed at the rural background site BIK were reanalysed by the author of the thesis to provide high-quality atmospheric data for scientific community with a well described uncertainty estimation (cf. Annex A).

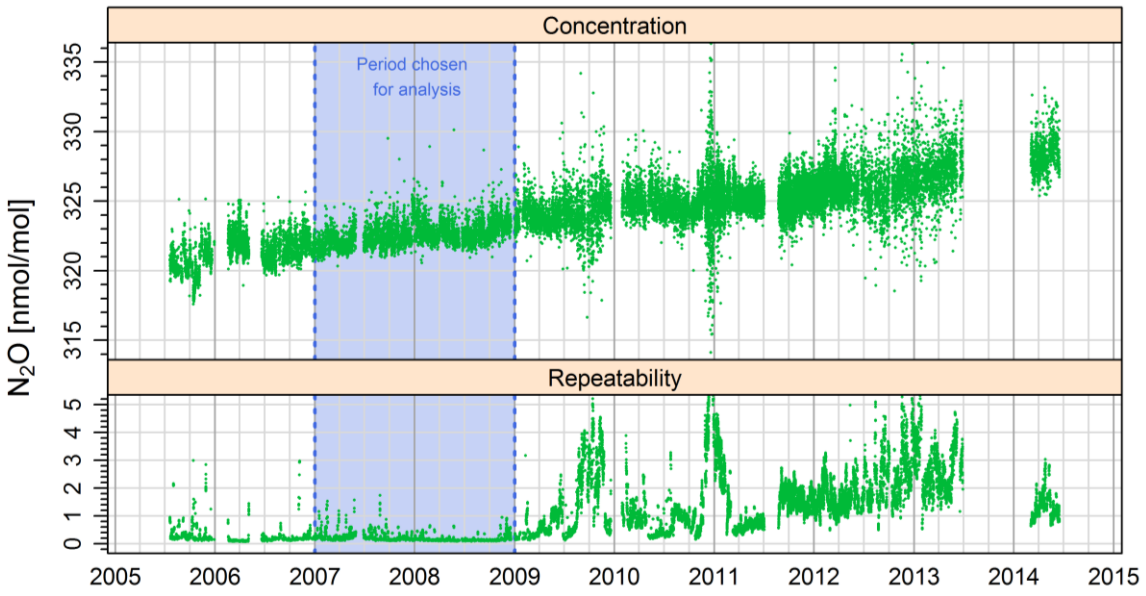

Figure 3.15. N_2O measurements at BIK station. Due to lower overall quality of the measurements since 2009, only the data from 2007-2008 were used for comparison against KRK station data. For detailed repeatability definition, see Annex A.

Figure 3.15. shows the results of the reanalysis. The data clearly show that since 2009, the quality of the dataset has significantly deteriorated, with repeatability values increasing to larger than 1 ppb. Another important issue is a presence of a large gap in the measurement record present in late 2013. Due to these circumstances, it has been decided to use only data from the years 2007 and 2008 for the purpose of this comparison, which are of generally higher quality. In order to do that, however, a previously described detrending and deseasonalization procedure (see section 3.5.2.) had to be applied to account for long-term growth of atmospheric nitrous oxide concentrations.

Figure 3.16. shows statistics of the diurnal cycle of nitrous oxide concentrations as measured at KRK and BIK stations, with data from the inlet located 30 m above the ground level, selected to be comparable with the elevation of inlet at KRK site (ca. 20 m). The result show a significantly higher amplitude of N_2O summer diurnal cycle in KRK (4.6 ppb, amplitude of medians) when compared to BIK, suggesting strong influence of local sources on the KRK N_2O record. A weak diurnal cycle is observed at BIK only during summer (1.1 ppb amplitude of medians), supporting the hypothesis of

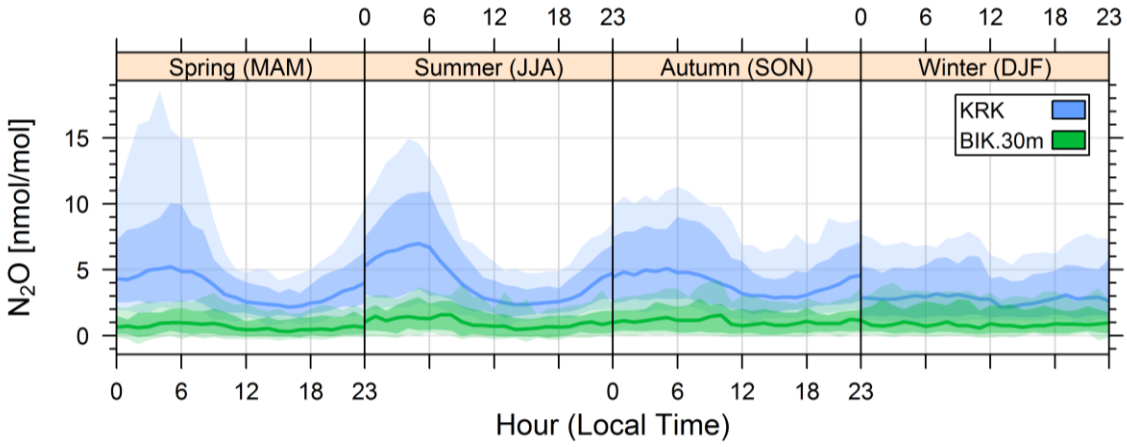

Figure 3.16. Diurnal variation of nitrous oxide (detrended and deseasonalised) concentrations at BIK and KRK stations during four seasons. Thick lines represent medians of hourly-binned data. Dark and light coloured areas represent the 25/75 and 5/95 percentiles, respectively.

the importance of biological activity in the KRK station's vicinity as the driver of diurnal N_2O variations.

Elevated 95th percentile ranges visible in BIK data during all seasons suggest a presence of high-concentration events in the record. These are occurring during daytime as well as night-time, pointing to the possibility of synoptic-scale transport as the source of these events. Per-weekday variability in diurnal cycle was not observed at BIK site (not shown).

3.9. Analysis of near-field emission sources with the use of meteorological data – Kasprowy Wierch.

Additional information about patterns of N_2O emissions and transport in the near-field of atmospheric pollutants can be obtained when meteorology is analysed together with chemical composition of the local atmosphere. Carslaw and Ropkins (2012) have recently developed a toolset designed for air quality analysis that has been implemented as a freely available R environment code package – *openair*. The functions provided in this package were used to provide information through several types of bivariate plots.

As described in the openair manual (Carslaw, 2012), a bivariate plot is constructed by first binning wind speed and wind direction data, with the number of bins depending on the plotted value range, with usual values of 30 wind speed intervals and 10° direction interval. Then, for each bin, statistics of concentrations (or other parameter) are calculated. Thus, a discrete set describing the concentrations function $C_i = f(u_i, v_i)$ becomes available. In order to diminish the influence of the noise present in the data, this discrete set can further be used to fit a smoothed surface function utilizing a General Additive Model (GAM; see references in Carslaw, 2012). This smoothed fit includes weighting of the bins with a small amount of data points, to reduce the influence of outliers on the results. For all of the subsequent bivariate plots, smoothing function was calculated excluding bins for which only one observation was available and applying 0.5 weight for bins with two observations, in order to reduce the influence of outliers on the resulting surface fit.

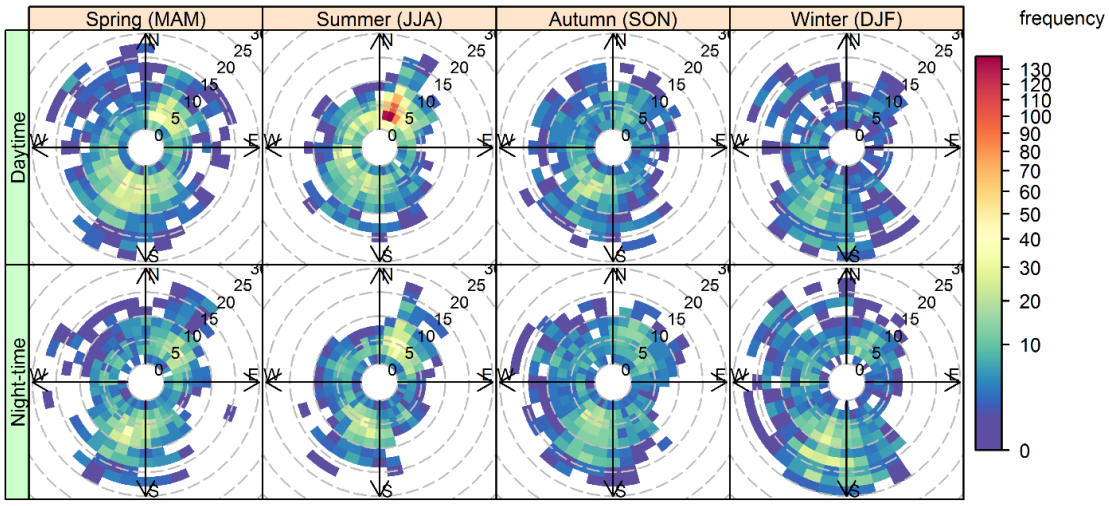

Figure 3.17. Basic statistics of wind speed and wind direction observed at KAS station in 2013-2014. Frequency of observed hourly means is conditioned for season and daytime (sunrise to sunset) and binned according to wind speed and wind direction values.

Hourly meteorological data for KAS station was obtained via *ftp* server of National Climatic Data Centre of National Oceanic and Atmospheric Administration, USA (NCDC). The NCDC collects the data from numerous meteorological land-based observation sites for climatological research purposes. The data was produced by Polish Institute of Meteorology and Water Management (IMGiW) at the rooftop of the observation building where inlet port of the atmospheric concentration measurement system is also located. Figure 3.17. presents the frequency of observations of a given set of wind speed and wind direction parameters, for the years 2013-2014, divided by season and the local time of the day (daytime, night-time). As can be seen, wind distribution is mostly isotropic, with a small preference of north-easterly and southern wind directions. The distribution does not vary significantly with season.

Detrended hourly N_2O concentrations measured at KAS have been plotted against wind speed and wind direction (Figure 3.18., left). Data representing calm wind conditions (wind speed smaller than

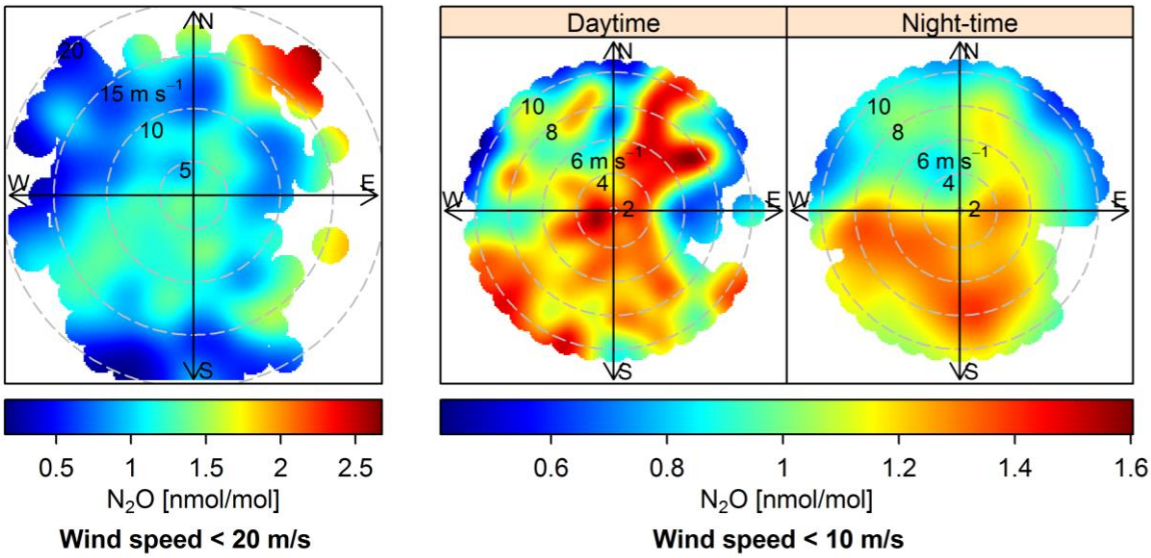

Figure 3.18. Left: Hourly N_2O concentrations (KAS, detrended, deseasonalised), plotted against simultaneous observations of wind speed and wind direction. Observations for wind speed exceeding 20 m/s were discarded (small sample). Right: Similar plot with the data conditioned according to the time of the day (daytime, night-time). Wind speed exceeding 10 m/s discarded to underline more local patterns of N_2O transport.

1 m/s) was excluded, as they represent calm conditions, which do not provide information on source spatial distribution. Measurements performed during very high wind speeds (greater than 20 m/s) were also excluded due to very small number of such events. As can be seen, interpretation of the source distribution can be difficult, as the plot is dominated by high values occuring during strong NE wind event, which occurred in 04.2014.

Binning the data according to daytime (sunrise – sundown), and limiting the data only to events with smaller windspeeds (less than 10 m/s) allows to extract more general information on the transport patterns of N_2O (Figure 3.18, right). Clear difference seen between the daytime and night-time observations is directly associated with a known effect of separation of atmospheric residual layer from PBL during night-time inversions, when convective vertical transport is inhibited. High-altitude sites like KAS station are effectively cut-off from local influences, so that the results can be interpreted as representative of free tropospheric background. During daytime, vertical temperature gradient is reversed, causing a development of both convective transport and mountain breeze effects that cause the lower troposhperic, polluted air to be transported to the high altitude and causing visible N_2O enrichment.

Elevated N_2O values occurring during the periods of southerly winds may be associated with the agricultural and traffic sources located in the Váh river valley (Slovakia), approximately 10-15 km south from KAS station, and possibly with emissions occurring in the industrial centres located near the cities of northern Slovakia (e.g. Žilina, Martin or Banská Bystrica), which lay in close proximity to Tatra mountains (up to 100 km). Higher values observed when the air is coming from the north is probably directly related to emissions from Kotlina Nowotarska, a densely populated flatland that stretches for approximately 30 km to the north of High Tatras, with emissions from agricultural, residential and traffic-related sources as the probable cause of the observed elevated N_2O values.

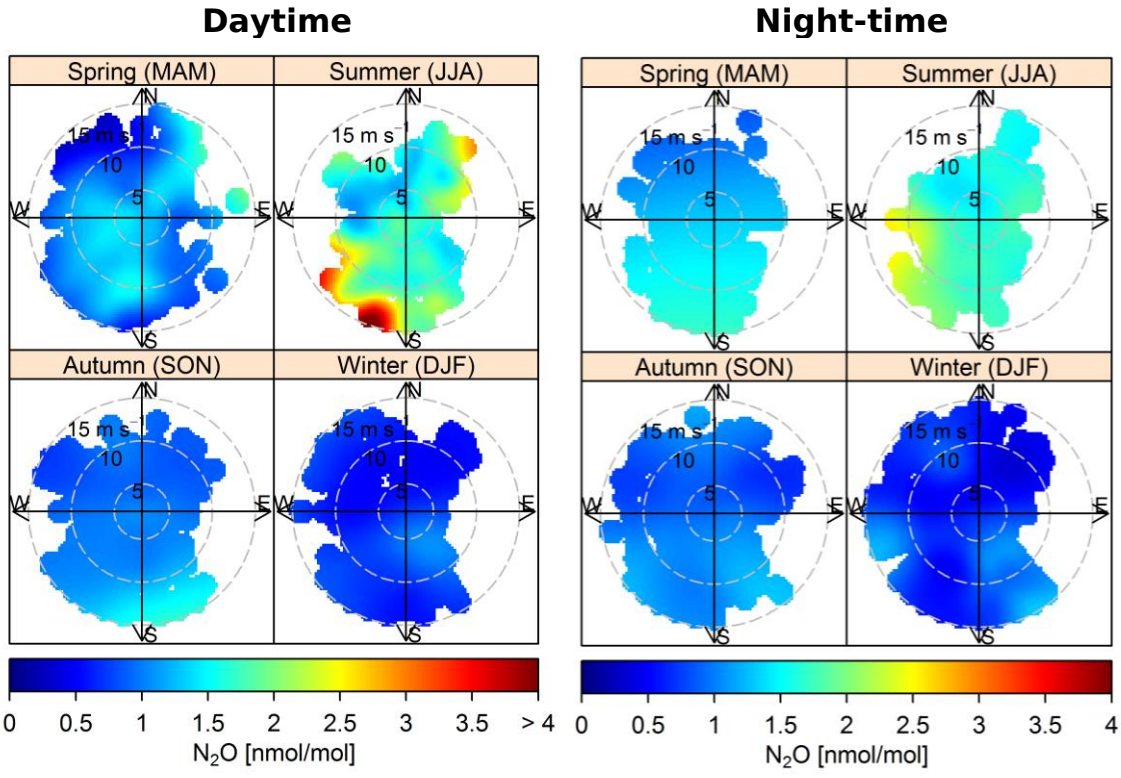

Figure 3.19. Nitrous oxide concentrations (hourly, detrended, deseasonalised) as observed at KAS station against wind speed and wind direction. Data has been binned according to season and the time of the day (daytime, nighttime).

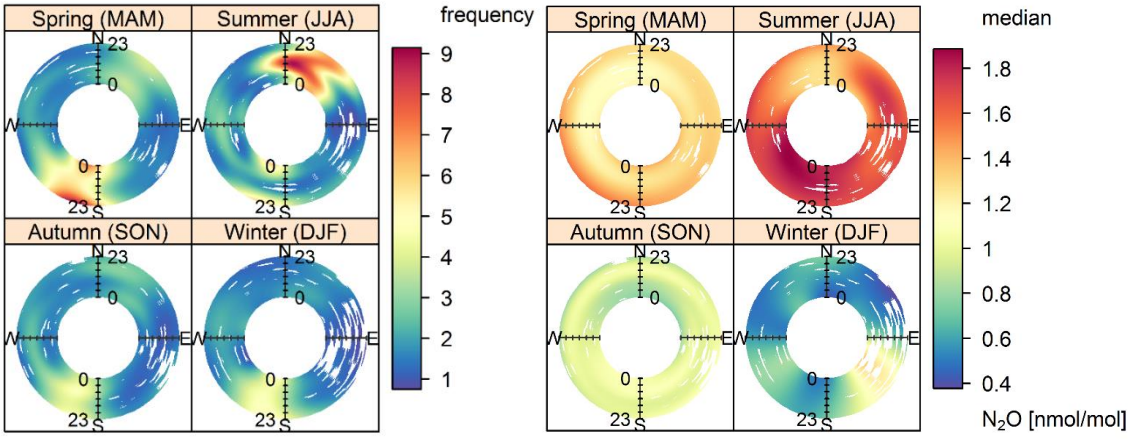

Figure 3.20. Kasprowy Wierch. Left: Diurnal patterns of wind direction - frequency of occurrence during 2013-2014, plotted by season. Right: Diurnal patterns of nitrous oxide concentration medians plotted against wind direction and by season.

The pattern visible on daytime bivariate plot closely follows topographical conditions around the station, pointing to the importance of local advection.

Seasonal variations in the emission and transport patterns were investigated by dividing the available measurements into 8 distinctive subsets, first by separating nighttime and daytime data (based on local sunrise and sundown times) and by grouping data seasonally into four subsets (Figure 3.19.). Again, it is clear that variability in transport patterns of N_2O concentrations is more pronounced during daytime. Another distinctive feature is that higher N_2O mixing ratios were observed during spring and summer months (bin average up to 4 ppb) than during winter and autumn (in the order of 1 ppb). This suggests that the main source of nitrous oxide that influences continental background conditions observed at KAS is connected to biological activity, and not with transport or combustion sources.

To gain insight into diurnal variation of these patterns, N_2O was plotted against wind direction and hour of the day, for each calendar season separately (Figure 3.20.). No diurnal cycle is observed for any season, but this might be caused by smaller sample size.

3.10. Analysis of near-field emission sources with the use of meteorological data – Kraków.

An analogous approach to that described in the preceding section was undertaken to describe N_2O ambient air transport and emissions at KRK station. For Kraków, meteorological data from a weather station located at the rooftop of the Faculty of Physics and Applied Computer Science building, several meters from to the inlet port of the GC system, were used. Meteorological data (wind speed, wind direction, air temperature and pressure) were measured and stored with frequency of 1 min and averaged to hourly values with *timeAverage* function of the *openair* package.

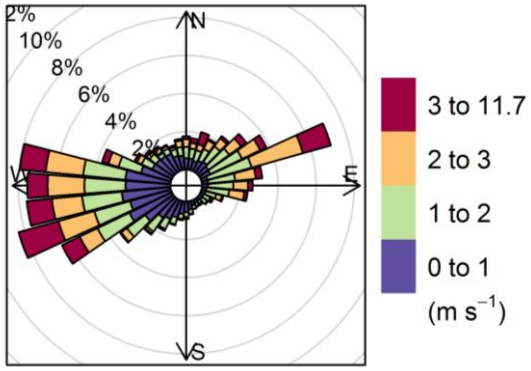

Figure 3.21. KRK - Frequency of counts by wind direction in percent of occurrence. Calm events: 3.4%.

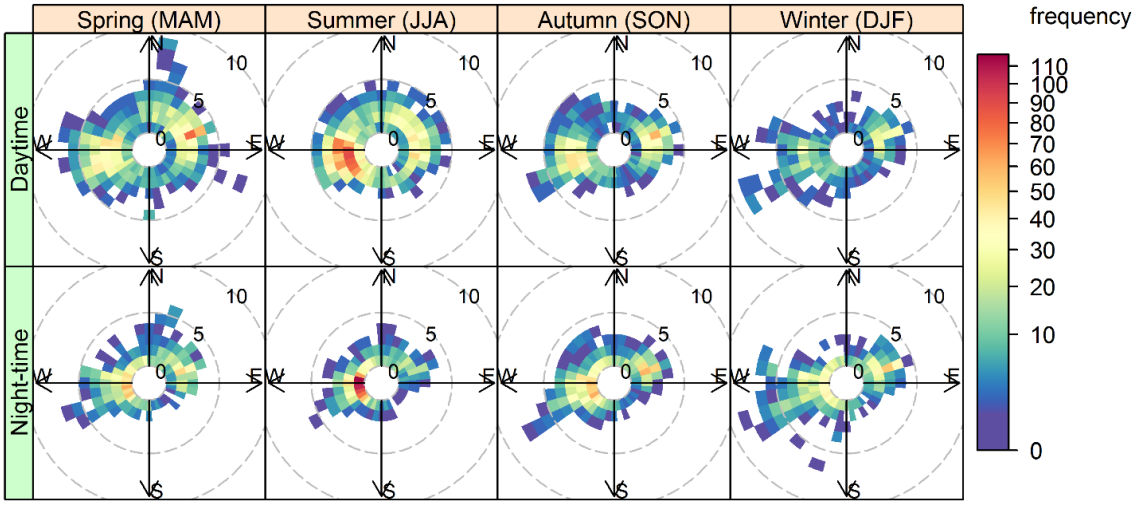

Figure 3.22. Basic statistics of wind speed and wind direction observed at KRK station in 2013-2014. Frequency of observed hourly means is conditioned for season and daytime (sunrise to sunset) and binned according to wind speed and wind direction values.

Statistics (Figure 3.21.) show that wind speeds observed in Kraków are usually much lower than at KAS, a phenomenon common for lower tropospheric stations that is linked to higher ground resistance and wind shear. Another characteristic feature is a distinct anisotropy of the wind direction, with a clear preference for westerly and, to smaller degree, easterly winds. This pattern is true for both daytime and nighttime, and holds regardless of the season (Figure 3.22.). Due to this anisotropy, only a limited amount of information can be extracted from other directions, especially S and SE, which have almost no coverage.

Highest concentrations of N_2O were observed at KRK during low wind speeds – conditions usually associated with presence of a stable inversion layer. As advective transport is mostly inhibited under

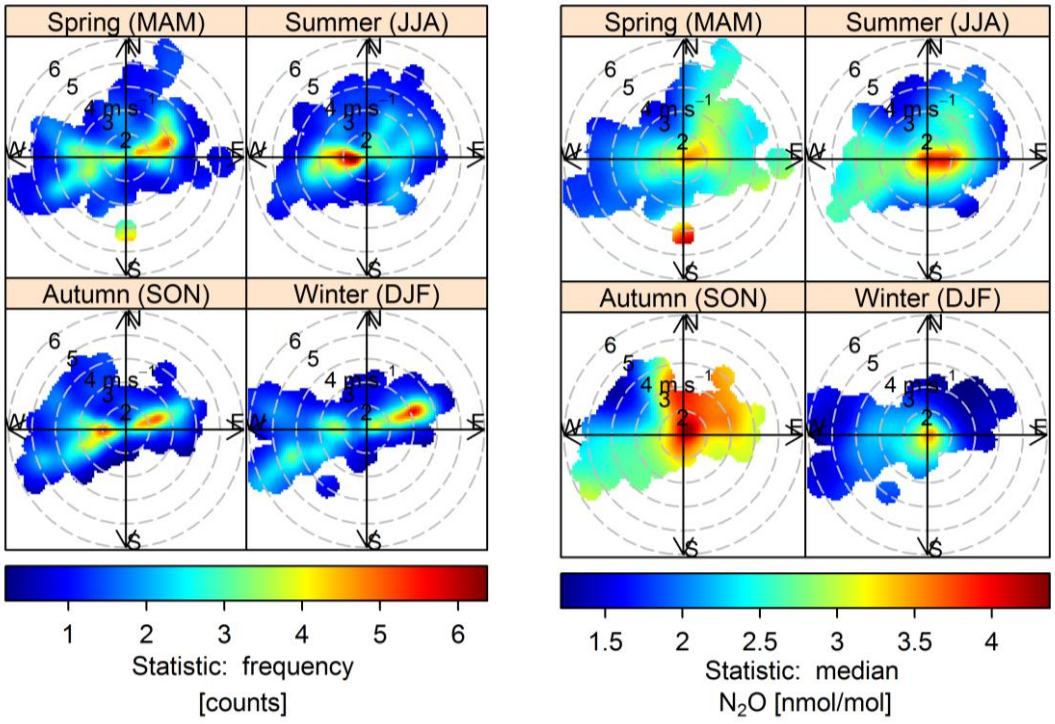

Figure 3.23.Kraków. Left: Density of observations plotted against wind direction and wind speed, separately for each season. Right: Observed nitrous oxide concentrations (hourly, detrended, deseasonalised) plotted against wind speed and wind direction. Data has been binned according to season.

such conditions, data for which the wind speed is smaller than 1 m/s has been excluded from further analysis.

Detrended and deseasonalised nitrous oxide concentrations were seasonally binned and plotted against wind direction and wind speed (Figure 3.23.) to test for the characteristics of the nearby emission sources. As can be seen, a significant variability in the observed patterns is observed, with the difference between winter and other seasons being the one most pronounced. During spring, summer and autumn months, elevated N_2O concentrations were observed under both strong and weak north-easterly, easterly, and westerly winds. During winter, only westerly winds caused a rise in the observed mixing ratios, with very low values during relatively frequent easterly-wind events. To further investigate the nature of the local sources, diurnal cycle of observed N_2O ambient concentrations was also plotted against simultaneously measured wind direction (Figure 3.24.), to further test if a characteristic morning or afternoon traffic peaks are observed. Indeed, when data measured during low wind speeds (typical during night-time inversions) are excluded, elevated values of N_2O are observed between 4 and 12 local time, with higher concentrations observed for south-easterly and north-westerly wind directions. No peak is visible in the afternoon values, which can be explained by well-mixed conditions present in the atmosphere at that time.

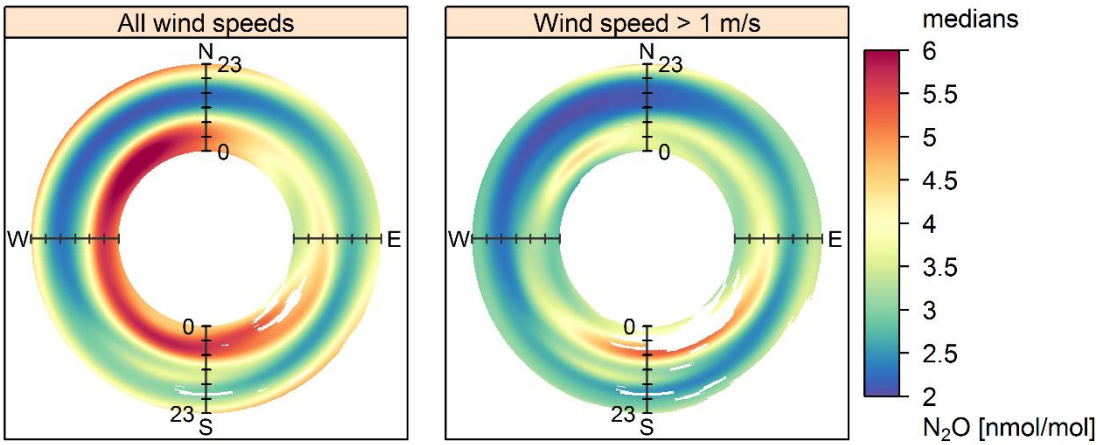

Figure 3.24.KRK: Medians of measured N_2O concentrations calculated for a given hour and wind direction. Left: Low wind speeds (smaller than 1 m/s) are removed to exclude typical inversion conditions, responsible for highest night-time concentrations. Left: Full dataset.

4. EMISSIONS OF N_2O FROM AGRICULTURAL AND URBAN SOILS

The second part of this PhD thesis focuses on the description of the spatial and temporal characteristics of the most important distributed N_2O sources in the Małopolska region, i.e. agriculture, and on the reconnaissance measurements of the urban fluxes of N_2O in the Kraków agglomeration. Temporal changes on diurnal to weekly scales caused by fertilization and/or precipitation events were of particular interest, as these were performed in this region for the first time. Direct measurements of N_2O emissions were performed with the use of static chamber method coupled with the gas chromatography analyses.

4.1. Methods of N_2O soil flux measurements.

Measurement-based studies of nitrous oxide emissions from agriculture fall into two main categories. The first are process-focused laboratory experiments, aimed at describing the behaviour of a carefully extracted subset of the soil system, e.g. specific type of microbial communities (Włodarczyk et al., 2002). The second category are *in-situ* studies that are focused on N_2O emissions from various agricultural systems, thus providing information on the current state of nitrogen budgets at local, regional and – when upscaled – even global scales.

On the local scale, emissions of nitrous oxide can be measured either with micrometeorological methods or with the use of chambers. Micrometeorological methods rely on precise measurements of nitrous oxide concentrations, coupled with observations of meteorological parameters, such as wind speed, air temperature, relative humidity etc. The most widespread of these are the flux gradient (FG) and eddy-covariance (EC) techniques.

The FG method relates the vertical gradient of atmospheric N_2O concentrations, usually measured at two vertical levels, to the surface N_2O flux. If a steady state, one-dimensional atmospheric transport is assumed, then it is possible to calculate the emission from a following relation (Denmead et al., 2000, Phillips et al., 2007):

$$\overline{\mathrm{F}}_{\mathrm{N}} = -\mathrm{K}_{\mathrm{N}} \frac{\partial \overline{\chi}_{\mathrm{N}}}{\partial \mathrm{z}}, \tag{4.1}$$

where F_{N} is the surface N_2O flux density, χ_{N} is the N_2O concentration at the height *z* and K_{N} is the eddy diffusivity. The bars over the variables represent time averages. The difficulty in calculating the eddy diffusivity can be overcome when another scalar is simultaneously measured at the same heights. It can be shown that the flux can then be calculated as:

$$\overline{\mathrm{F}}_{\mathrm{N}} = \overline{\mathrm{F}}_{\mathrm{a}} \frac{\partial \overline{\chi}_{\mathrm{N}} / \partial \mathrm{z}}{\partial \overline{\chi}_{\mathrm{a}} / \partial \mathrm{z}} \approx \overline{\mathrm{F}}_{\mathrm{a}} \frac{\Delta \overline{\chi}_{\mathrm{N}}}{\Delta \overline{\chi}_{\mathrm{a}}}, \tag{4.2}$$

where ‘a’ index denotes the quantities associated with the analogue quantity. If the analogue is a sensible heat, then its flux can either be measured by eddy-covariance or calculated using the Bowen ratio approach (Phillips et al., 2007).

The main advantage of the gradient method is its ability to reliably measure N_2O fluxes over large, homogenous areas with relatively high temporal resolution (hours). However, it has been shown that this technique has limited usability during low wind-speed and very stable conditions (Phillips et al., 2007).

Following the recent advances in the optical spectroscopy equipment, gradient method has given way to the eddy-covariance (EC) and its derived eddy accumulation (EA) and relaxed eddy accumulation (REA) methods. Originally developed in mid 1950s (Swinbank, 1951, Chojnicki et al., 2008), the EC method allows to estimate the surface fluxes through measurements of minute mixing ratio differences in the up- and downward eddies in the turbulent layer over the homogenous source, following the equation:

$$F_x = \overline{\omega' c_x'}, \tag{4.3}$$

where F_x denotes the soil flux of the measured compound, ω' is the momentary deviation of the vertical wind speed component from the mean value over the averaging period and c_x' is the momentary deviation from the mean value of the measured mixing ratio. The overbar represents the time average.

Although the theoretical basis of the EC method has been developed over 60 years ago, appropriate instrumentation, required to measure precisely very small fluctuations in wind components and concentrations of the measured compound at high temporal resolution (1 – 10 Hz) only became available in the last decade of the XX century. Over the last twenty years, EC techniques have been extensively used for measuring water, heat and CO_2 fluxes, within large international observation networks focussing on studies of the global carbon budget (e.g. FLUXNET, 2015). In Poland, the pioneer work concerning the EC measurements of carbon dioxide fluxes have been performed at the Poznań University of Life Sciences. Regular monitoring of CO_2 fluxes over selected ecosystems (wetland, forest) is conducted there since 2004 (Urbaniak, 2006, Chojnicki et al., 2007). EC technique is also used to measure heat and CO_2 fluxes in urban environment by researches from Department of Meteorology and Climatology and University of Łódź, Poland (Pawlak et al., 2011).

The feasibility of using the EC methods for measurements of non-CO_2 greenhouse gases has mainly been hampered by persisting difficulties in high-frequency, high-precision measurements of CH_4 and N_2O. Recent developments in laser spectroscopy (LGR, Picarro, Aerodyne, 2015) resulted in full implementation of EC methods to measure CH_4 fluxes over various ecosystems such as forests (Sakabe et al., 2012), wetlands (Jackowicz-Korczyński et al., 2010, Kowalska et al., 2013), croplands (Dengel et al., 2011) and landfills (Eugster and Plüss, 2010). EC N_2O flux measurements are also becoming feasible nowadays, with studies published across a variety of environments (Mammarella et al., 2010, Jones et al., 2011, Järvi et al., 2014, Merbold et al., 2014).

Although the micrometeorological methods of N_2O flux measurements are becoming increasingly popular in the scientific community, most of the field studies conducted up to now still rely on chamber techniques, either as a basis of the performed studies or as means of quality control. The main advantages of the chamber techniques is their relative simplicity, low costs of operation and usefulness in *in-situ* process-based studies of N_2O emissions (Smith, 2010).

In the most widely used, non-steady state (NSS) close-chamber technique (de Klein and Harvey, 2012), the surface flux of N_2O is determined through an enclosure of a volume of air over ground surface (usually smaller than 1 m^2), by an airtight container (chamber). The gas exchange (flux) between the soil and the ambient air causes the concentration change inside the chamber headspace. This change can either be analysed in real time (when optical instruments are used) or

later in the laboratory (when air samples are collected for GC analyses). Once the concentration function in the chamber headspace is known, the flux of the analysed compound can be calculated using one of the available flux calculation schemes (discussed in more detail in Annex B). The simplest of these schemes assume that the concentration rise in the headspace volume can be approximated by a linear function, and that the flux at the beginning of the enclosure remains unchanged throughout the deployment time and is directly proportional to the slope of the least square linear regression function:

$$F = \left.\frac{dC}{dt}\right|_{t=t_0} \times \frac{\rho V}{A}, \tag{4.4}$$

where:

F – flux, in nmol m^{-2} s^{-1},
$\left.\frac{dC}{dt}\right|_{t=t_0}$ – rate of concentration change inside the chamber headspace at the start of the enclosure period (t_0), expressed in nmol mol^{-1} s^{-1},
ρ – density of air in mol m^{-3},
V – volume of the chamber headspace in m^3, and
A – the area covered by the chamber in m^2.

However, the chamber method also has numerous drawbacks. One of its main disadvantages is the low spatial coverage. Chamber measurement guidelines (e.g. de Klein and Harvey, 2012) recommend at least 3 replicates for every site when measuring soil fluxes of N_2O, due to its high spatial variability (e.g. Velthof et al., 1996). Another issue is high temporal variability of the N_2O flux. Previous studies (Parkin, 2008) indicated that a three-day sampling regime resulted in a cumulative annual N_2O flux value inside 10% of the cumulative flux obtained with daily sampling interval. This difference increased in range of +60% and -40% when 21-day sampling interval was used. Thus, it was suggested to use 2-3 daily sampling interval during the times when elevated emissions are expected and at least 1 measurement per week when the fluxes are expected to be constant (Smith and Dobbie, 2001, Parkin, 2008).

The chamber methods may also disturb the measured environment, e.g. through modification of the pressure gradient when the chamber is deployed or by causing the horizontal diffusion in the soil then the enclosure time is too long. Rochette and Eriksen-Hamel (2008) assessed the confidence of the N_2O flux values obtained in over 350 studies, by applying 16 criteria to chamber designs and measurement techniques described in those studies. They showed that in almost 60% of the studies the confidence of the reported flux value may be described as “low” or “very low”. In order to ensure high quality of chamber N_2O flux measurements, they have provided a set of specific requirements for chamber deployments and designs. Similar recommendations can be found in several other studies (e.g. de Klein and Harvey, 2012 and references therein). These requirements were taken into consideration when planning the measurement campaigns described in Section 4.5.

4.2. Description of measurement sites.

In order to study the agricultural emissions of nitrous oxide, a cooperation was established between AGH University of Science and Technology and the Institute of Institute of Plant Acclimatization and Husbandry (ZDHAR – *Zakład Doświadczalny Hodowli i Aklimatyzacji Roślin*) in Grodkowice. The

Institute is responsible for field-testing of the crops available at the market, and for providing a recommended set of seed varieties for local farmers. Typical crop testing cycle lasts 3 years, during which their estimated crop, response to ambient conditions, possible vulnerabilities etc. are determined.

The site where N_2O flux measurements were made (49.976°N, 20.261°E, 250 m a.s.l.) is located between the Sandomierz Basin (Kotlina Sandomierska) and Carpathian Foothills (Pogórze Karpackie), some 30 km east of Kraków, Małopolska. The climate of the site is temperate, with vegetation period of approximately 220 days (Molga, 1983), usually starting between March and April and ending in October. Total crop area of ZDHAR in Grodkowice is approximately 600 ha, which allows large-scale cultivation of a multitude of crop species, including maize, rapeseed, wheat and others. For each of the crop species, several types of management techniques are tested, with varying fertilizer types, applied fertilizer amounts, tillage conditions, etc.

Two campaigns have been performed in 2014 to estimate the N_2O emissions from the crops typical for Małopolska region. During the spring campaign (March – April 2014), nine experimental field sites (Table 4.1.) were chosen to monitor N_2O emissions on 3 crop types: corn (one site), rapeseed (three sites) and wheat (four sites) with one control site located in the uncultivated and ungrazed

Table 4.1. Overview of field sites for N_2O flux measurements.

Site code	Crop [type]	Treatment code	Duration of sampling campaign [days]	Sowing	Fertilization	Fertilizer type	N added [kg N ha^{-1}]
Spring campaign							
A	Maize *Zea mays L.*	st	34	May 2, 2014*	Apr 2, 2014	Urea, 46% N, 300 kg/ha, granulate	138
E	Rapeseed *Brassica napus L.*	st	31**	Aug 26, 2013	Mar 4, 2014		78
G	Rapeseed *Brassica napus L.*	t	28**	Aug 30, 2013	Mar 3, 2014	Ammonium nitrate + ammonium sulphate, 26% N, 300 kg/ha, granulate	78
H	Rapeseed *Brassica napus L.*	st	28**	Aug 23, 2013	Mar 3, 2014		78
B	Wheat [w] *Triticum aestivum L.*	st	34	Sep 25, 2013	Mar 6, 2014	Ammonium nitrate + ammonium sulphate, 26% N, 200 kg/ha, granulate	52
C	Wheat [lw] *Triticum aestivum L.*	t	34	Nov 18, 2013	Mar 4, 2014	Ammonium nitrate, 32% N, 200 kg/ha, granulate	64
F	Wheat [s] *Triticum aestivum L.*	st	34	Mar 13, 2014	Mar 5, 2014	NPK 3.5% N, 250 kg/ha + Ammonium nitrate 27% N, 200 kg/ha, granulate	63
K	Wheat [w] *Triticum aestivum L.*	t	34	Sep 2013	(1) Mar 14, 2014 (2) Apr 03, 2014	(1) Ammonium nitrate 30% N, 200 kg / ha (2) Urea, 46% N, 150 kg/ha, granulate	129
I	Grassland *Poaceae (R. Br.)*		34	None	None	None	0
Autumn campaign							
E	Wheat [w] *Triticum aestivum L.*	st	22	Oct 8, 2014	Aug 18, 2014	Lime (no nitrogen added)	0
B	Oat *Avena sativa L.*	t	22	Sep 24, 2014	None	None	0
C	None		22	None	None	None	0
F	Rapeseed *Brassica napus L.*	st	22	Sep 7, 2014	Sep 6, 2014	Ammonium nitrate, 32% N, 100 kg/ha, granulate	32
I	Grassland *Poaceae (R. Br.)*		19	None	None	None	0

Crop types: w – winter; lw – late winter; s – spring. Treatment codes: st – shallow tillage, i.e. mixing of the top 20cm of the soil with a cultivator; no overturning; t – deep tillage, with overturning of the soil.

** - sowing occurred after the campaign has ended*

*** - measurements in the last week were impossible due to insufficient chamber height*

grassland. The measurement locations were chosen to be representative of the respective crop field and underwent the same treatments as the rest of the area, including fertilizer application, cultivation and tillage.

During the spring measurement campaign, replicates of wheat and rapeseed measurement points were selected in order to compare possible differences between N_2O emissions due to differences in the sowing times (e.g. spring, winter and late-winter wheat) or tillage techniques (shallow tillage and deep tillage). Deep tillage here means ploughing of approximately 20 cm of the top layer of the soil with harrowing (5 cm) afterwards, while shallow tillage means mixing of the top 20 cm layer without soil overturning (no ploughing).

Figure 4.1. Site B (oat) during the autumn campaign. View to N and NE directions. Photograph from personal archives of the author of this thesis.

During the autumn campaign, only 5 sites were surveyed: winter wheat, oat (Figure 4.1.), rapeseed, grassland (control) and 1 field that remained unsown after the summer harvest. This last field was not sown in preparation for catch crop sowing (broad bean, *Vicia faba L.*) in November. The autumn campaign was less intensive, as lower fluxes were expected to be low due to smaller nitrogen fertilizer amounts applied.

N_2O flux measurements from urban soils in the largest city of Małopolska (i.e. Kraków) were also performed in the framework of this PhD thesis. First, short reconnaissance campaign was performed in autumn of 2012 (Ciaciek, 2013). A large green area of Błonia Park (48 ha) was chosen as a study site (Figure 4.2), as it was already previously studied extensively for soil CO_2 emissions (Jasek et al., 2014). It is located approximately 2 km west of the city centre and is mainly used as a recreational area.

The N_2O flux measurements were also performed on the lawn in front of the Faculty of Physics and Applied Computer Science building located ca. 500 meters north of the Błonia Park site (cf. Figure 4.2). The measurements at this site were performed during late summer of 2013, between 5th and 21st of September.

Figure 4.2. Błonia Park in Kraków as viewed from Kościuszko Mound, 2008. Approximate locations of the N_2O flux measurement sites marked with arrows. Source: Wikimedia Commons, the free media repository. Author: RaNo.

4.3. Equipment set-up and measurement methodology.

All N_2O flux measurements presented in Section 4.5. were performed using a well-established closed static chamber technique (also called non-steady-state, *NSS*), coupled with gas chromatography. In the course of N_2O flux measurement, a number of samples was taken from the headspace volume of the chamber during the deployment time and then subsequently measured for N_2O mixing ratios in the Laboratory of Gas Chromatography at the AGH University of Science and Technology. The methodology of the measurements was adopted in accordance with a set of recommendations published by de Klein and Harvey (2012), which was based on the previous works by Smith and Dobbie (2001), Parkin (2008), Rochette and Eriksen-Hamel (2008) and others.

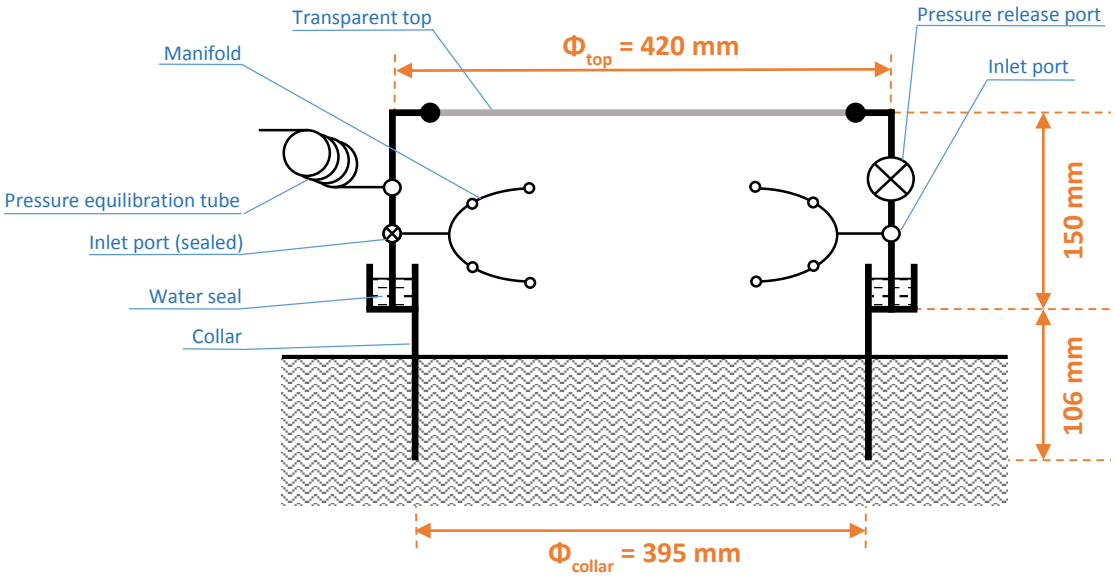

Figure 4.3. Schematic design of the chamber used for N_2O flux measurements in the presented study.

The chamber used in the presented study was constructed primarily to measure CO_2 soil fluxes (Jasek et al., 2014). Its design (Figure 4.3.) was slightly modified by adding additional pressure release port, in order to diminish the negative effect of pressure disturbance at the start of the deployment time. Three identical chambers (coded as α, β, γ) were built. One was used during urban campaigns and all three during measurements of agricultural N_2O emissions.

Both the chamber and the collar were made of stainless steel. Water seal was used to provide an air-tight connection between both parts. Before the measurements, the collar was inserted into the ground to the depth of approximately 50 mm. Once inserted, the collars usually remained in the same spot, except in case of cultivation at the agricultural fields and measurements in Błonia Park, where the collar was removed after each measurement. After insertion, water was poured into the collar as a seal and was refilled when necessary.

Prior to the deployment, the chamber was flushed with atmospheric air and carefully placed on the collar with the pressure release port open. The port was closed immediately after the chamber was placed in the collar. This moment marked the beginning of the deployment time.

Each chamber was equipped with two inlet/outlet brass manifolds, designed to provide a uniform sampling field when a closed-path instrument was connected to the chamber. As the measurements performed in the scope of this study were performed only with manual sampling, only one of the manifolds was utilized, with the second permanently sealed. Usage of the manifold system,

however, was advantageous even when one manifold was used, as it assured that the sample was simultaneously taken from several locations inside the chamber thus compensating for lack of internal fan. Pressure equilibration during the deployment time was maintained through approximately 15 cm long, 1/8" PVC tube. The same type of tube, approximately 100 cm long, was used to connect the outer inlet port with the sample container (syringe).

Enclosure times varied between the measurements according to the expected N_2O flux values. For every deployment, 5 or 6 samples were taken in regular time intervals. It was found that for sites with expected low N_2O fluxes, 40-50 min deployment time was sufficient. When the expected fluxes were higher, the deployment time was shortened to 15-20 minutes.

During urban campaigns performed in 2012-2013, the first sample was collected from the ambient air outside the chamber and its analysed N_2O concentration was assigned to 0 (zero) on the time scale of chamber deployment. During the agricultural measurements, first sample was collected from the chamber headspace approximately 30 – 60 seconds after the start of deployment.

Medical syringes (60 ml PVC) were used as sample containers to ensure sufficiently large sample volume required for high-precision GC measurements. The syringes used during N_2O flux measurement campaigns were filled with atmospheric air collected at the University campus on the day before the measurements. On site, each syringe was flushed with local atmospheric air (five times) immediately before the sample from the chamber headspace was collected. Then, after connecting to the inlet tube, 10 ml of air from the chamber was collected and released from the syringe through a 3-port valve, to prevent contamination with unmixed air remaining in the tubing. The sampling was performed at the rate of approximately 5 – 10 ml s^{-1}. After collecting 50 ml of air, the syringe was closed with a PVC seal. The inlet tube remained closed until the next sample was to be collected.

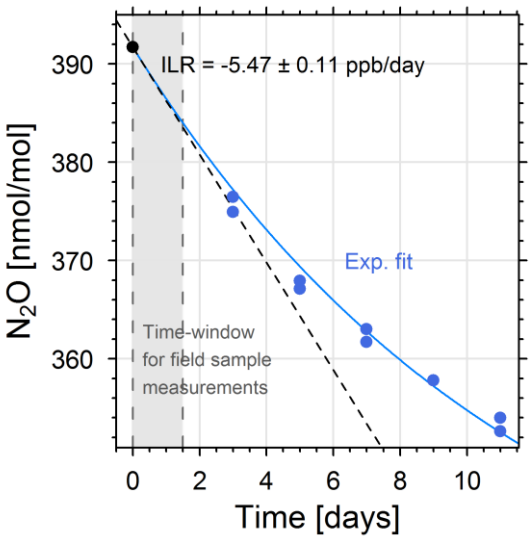

Figure 4.4. Results of leakage test. Blue dots – individual syringe measurements. Black point – the initial concentration in each syringe. ILR – initial leakage rate. Period during which all samples from field measurements were analysed is marked in grey.

All syringes and seals used for N_2O flux measurements were tested for leakage (Figure 4.4). The initial leakage rate was found to be equal to 5.47 ± 0.11 ppb/day. Based on the assumption that all the syringes displayed similar leakage behaviour, the correction factor was applied to all measured concentrations. Additionally, to minimise other effects of leakage and storage, all the collected samples were measured immediately upon arrival in the laboratory, in series, not later than 36 hours after being taken. The measurement procedure was similar to the one used for ambient air measurements, which is described in detail in Annex A. The estimated uncertainty of a single N_2O mixing ratio measurement was in the order of 0.5 ppb, allowing for high precision of analyses and short deployment times even for low (i.e. background level) N_2O flux values.

Uncertainty calculations of measured N_2O flux values were based on uncertainty propagation principle. Detailed description of the calculation scheme for N_2O flux determination can be found in Annex B.

4.4. Measurements of N_2O releases from agricultural soils.

Two intensive measurement campaigns focused on N_2O emissions from agricultural crops grown in Małopolska region were performed in 2014. A comprehensive analysis of the data collected during these campaigns will be presented in the following section.

The first, spring campaign, started on March 1st, immediately before application of fertilizer to the measured fields of rapeseed and wheat. The main goal of the campaign was to estimate springtime emission of N_2O following addition of N_r compounds to the soil. Nine sites with various configuration of crops and tillage techniques were measured. Preliminary results from the spring campaign were briefly described in the diploma thesis of K. Ciaciek (2014).

Second campaign took place between 3rd and 25th of October 2014. Due to lower autumn N fertilization, caused by economic situation of the agricultural sector in 2014 (lower revenues from crops), and manpower shortages the overall number of observations was reduced in comparison with the spring campaign, with only 5 sites monitored for approximately 3 weeks. The measurement locations were not changed since the spring campaign, however new species were introduced prior to the new crop season (cf. Table 4.1.).

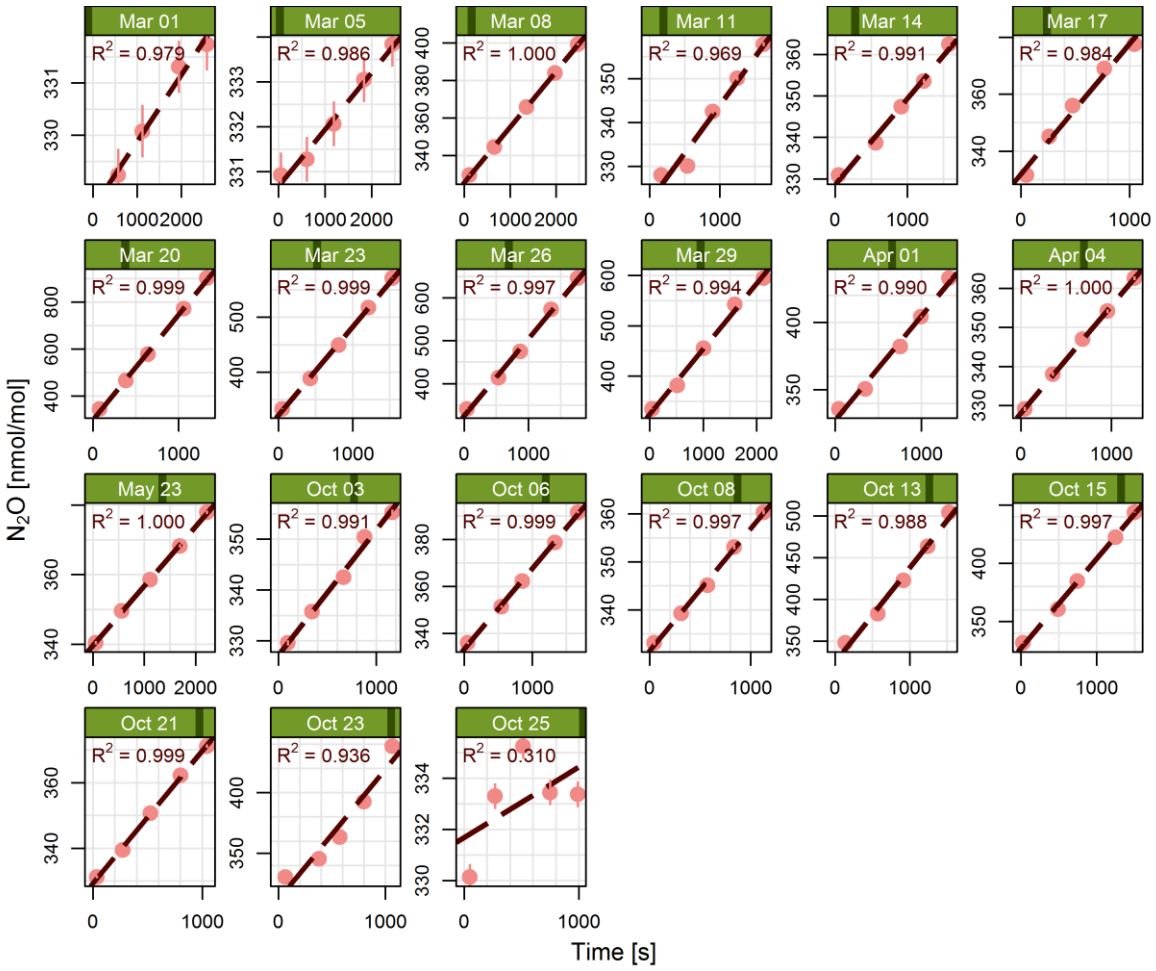

Figure 4.5. N_2O mixing ratios with their uncertainties as observed at site F site of ZDHAR, Grodkowice during spring and autumn sampling campaigns. Calculated linear regression fits and R_2 correlation coefficient are also plotted. Data points were excluded when marked as "questionable" in the laboratory log file. Measurement from October 25th was not excluded, however the reason behind the observed variability is unknown.

An example of typical measurement runs of N_2O mixing ratios is shown in Figure 4.5., presenting the results of all analyses performed at site F. The site was chosen here due to highest observed variability in the measured N_2O concentrations, with maximum values ranging from approximately 332 ppb (40 min enclosure, March 1st) to 900 ppb (20 min enclosure, March 20th).

Table 4.2. Small-scale spatial variability of N_2O fluxes at site F.

Code	N_2O flux	Uncertainty
	[ng N-N_2O m^{-2} s^{-1}]	
F	7.97	0.39
ST1	26.7	1.7
ST2	22.7	1.2
ST3	13.63	0.72
ST4	12.67	0.75
Mean	**16.7**	
St. dev.	**7.7**	

In order to estimate small-scale spatial variability of N_2O flux at a single site, a test measurement run including a total of 5 chamber deployments was performed during the spring campaign (April 4th) at one of the wheat crop fields (site F). Four additional collars were inserted next to the F site in a linear pattern, approximately 2 meters apart. Because only 3 chambers were available, deployments were performed in 2 series, separated by approximately 20 minutes. It was assumed that the N_2O flux does not change significantly during his time interval. The results of this test (Table 4.2.) confirm that even in close proximity, the N_2O emissions can differ by a factor of three.

4.4.1. Spring campaign.

The spring campaign took place between 1st of March and 4th of April 2014. A total of 98 individual flux measurements were performed, with number of analyses varying between the sites. The minimum and maximum N_2O fluxes recorded during this campaign were 0.028 ± 0.067 ng N-N_2O m^{-2} s^{-1} and 134.8 ± 6.8 ng N-N_2O m^{-2} s^{-1}, respectively.

Regardless of large variability of the observed fluxes, a common pattern can be distinguished in the temporal evolution of N_2O emissions at the investigated sites (Figure 4.6). Initially, low N_2O fluxes were observed, with a small increase following the N-fertilizer application. The largest growth of emissions was recorded after a rainfall event on March 16th and 17th (11.7 mm and 6.6 mm of precipitation in the previous 24 hours) (NCDC, 2015), after which the emissions remained high for several days (7 to 14). Afterwards, a reduction of the N_2O flux was observed. The observed temporal evolution of N_2O emissions can be explained by the activity of denitrifying bacteria stimulated by the availability of reactive nitrogen compounds and anaerobic soil conditions following the rainfall events, as indicated by the increased soil water content (not shown). The observed delay between the fertilization campaign and the increase of N_2O flux may stem from the need of the applied fertilizer pellets to dissolve, which can take several weeks under dry conditions.

Two notable exceptions from this general pattern were observed. First is the grassland control site (site I), where maximum of N_2O flux occurred before major rainfall events. However, N_2O fluxes at this site were at least several times lower than those observed at cultivated sites. Another irregularity of N_2O emission was observed at site A (maize). Here, a granulate urea (138 kg N ha^{-1}) was applied in early April, causing immediate and prominent increase of the measured N_2O flux. The kind of urea granulate that was used at ZDHAR in 2014 was not equipped in the coating that would have prevented the evaporation and dissolution of the fertilizer. Without it, the urea has infiltrated the soil and made the reactive nitrogen compounds available to the microbial community immediately after fertilizer application. Unfortunately, only one measurement was performed after

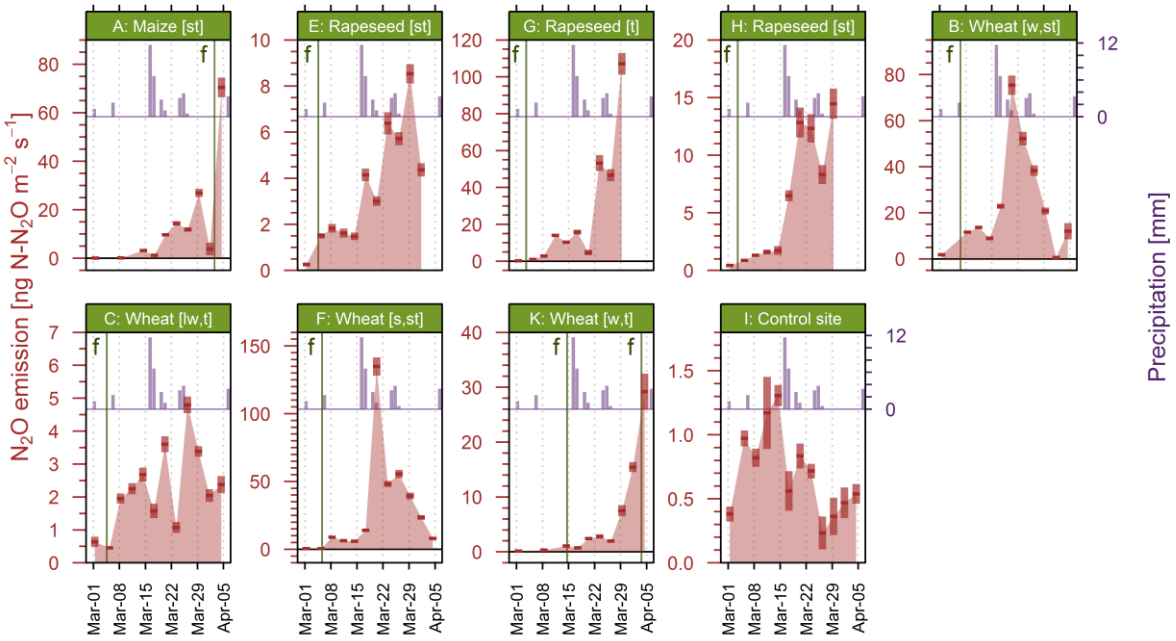

Figure 4.6. The results of spring N_2O flux measurement campaign at ZDHAR agricultural sites. Green vertical lines indicate respective fertilization dates. Red bars indicate the calculated flux values with their corresponding measurement uncertainties. Purple bars denote daily precipitation rates at Balice weather station. Balice, located approximately 30 km west of ZDHAR, was the nearest meteorological station for which relevant data were available from World Meteorological Organization Climatic Data Online database (NCDC, 2015).

the fertilizer was applied (two days after), and no information regarding further changes of N_2O emission is available. The same urea compound was also applied at site K during a second application, however the observed increase was less pronounced than in case of A site. The probable reason behind the observed difference is the fact that the last sample collection was performed only one day after the fertilizer was spread and the flux might have been in the early phase of rise

Total N_2O emissions for the spring campaign were calculated using a linear integration method of the daily fluxes. The obtained values (Table 4.3) show large variability of the N_2O fluxes between the sites, with smallest average emissions observed at the grassland control site (0.63 g N-N_2O ha^{-1} d^{-1}) and the largest occurring from non-tilled wheat sites (B and F, 19.97 g N-N_2O ha^{-1} d^{-1} and 26.03 g N-N_2O ha^{-1} d^{-1}, respectively) and tilled rapeseed (G, 20.94 g N-N_2O ha^{-1} d^{-1}).

The results of the spring campaign suggest a possible connection between tillage and cultivation techniques used at the fields and the releases of N_2O. Higher N_2O emissions for rapeseed field (G)

Table 4.3. Total emissions of N_2O during the spring campaign.

Site	Crop	Campaign duration	N added	Total emitted	Daily mean
			[kg N ha^{-1}]	[g N-N_2O ha^{-1}]	[g N-N_2O ha^{-1} d^{-1}]
					Spring campaign
A	Corn [st]	34	138	316.5	9.31
E	Rapeseed [st]	31	78	97.9	3.16
G	Rapeseed [t]	28	78	586.2	20.94
H	Rapeseed [st.2]	28	78	145.9	5.21
B	Wheat [w, st]	34	52	679.1	19.97
C	Wheat [lw, t]	34	64	67.6	1.99
F	Wheat [s, st]	34	63	885.1	26.03
K	Wheat [w, t]	34	129	140.0	4.12
I	Grassland (control)	34	0	21.4	0.63

that underwent ploughing at the beginning of the growing season (in autumn 2013) were observed than in case of non-ploughed sites (E, H). An opposite pattern is visible for wheat, where higher emissions seem to be associated with shallow tillage, with differences in both cases of approximately one order of magnitude. These differences, however, could stem from intrinsic spatial variability of soil N_2O emissions not captured when measurements are performed at a single location. Another explanation might be associated with the variability in the amount of nitrogen present in the soil, which in general is a sum of nitrogen added during fertilization campaign and that available from previous treatments. More information could be gained through (i) extension of the monitoring period, (ii) an increase in the number of chambers deployed per site and (iii) measurements of the total mass of nitrogen available in the soil.

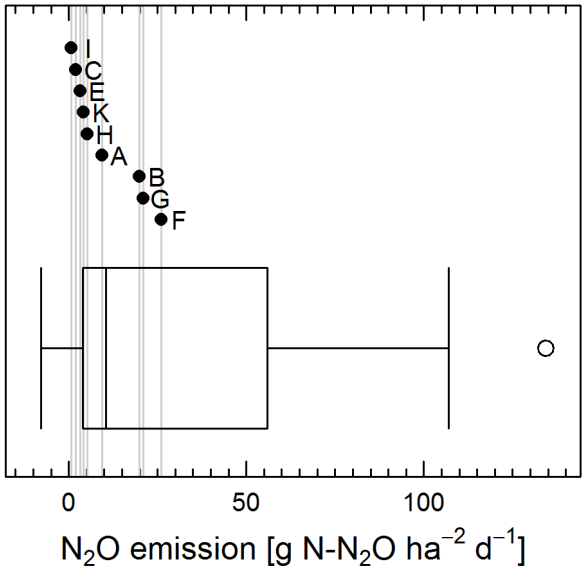

Figure 4.7. Comparison of average daily N_2O fluxes measured during the spring campaign (black points) with the boxplot representing statistical distribution of cropland N_2O fluxes from Nicolini et al. (2013). The box borders denote the 1st and 3rd quartile, with the median in between. The whiskers denote lower and upper fence, with white points for values outside the fences.

Nicolini et al. (2013) have conducted a study of N_2O flux values measured with micrometeorological methods (i.e. gradient method, eddy-covariance method) that were published in the past 10 years. Their published list of cropland sites also included cultivated grasslands, which have been excluded from this analysis, as this type of ecosystem was not surveyed in the present study. Descriptive statistics have been calculated for the remaining subset of croplands and are presented in the form of boxplot in Figure 4.7. These summary data were compared ZDHAR results. The measurements at five of the monitored sites (C, E, H, K, A) revealed average N_2O fluxes smaller than the median of previously reported cropland values (i.e. 10.40 g $N\text{-}N_2O$ ha^{-1} d^{-1}), and the remaining 3 (B, F, G) larger, albeit well below maximum reported (107 g ha^{-1} d^{-1}).

It is important to note that in their work Nicolini et al. have compared 61 campaigns of various lengths, performed at many different sites. Many of those campaigns were in fact continuous monitoring efforts, and the reported averages included periods of enhanced N_2O emissions following fertilization as well as periods with low N_2O fluxes.

A logical assumption is that the daily averages reported from this study are overestimated, as the spring N_2O emissions are higher than during the rest of the year due to N fertilization. Therefore, it is very likely that yearly totals for ZDHAR sites are in fact even smaller than those reported for croplands by Nicolini et al.. The estimation of such yearly totals for ZDHAR would require the measurements to be performed at least twice a week due to large temporal variability of the flux. Such an effort would be not feasible with the use of manual sampling. Other N_2O flux measurement methods (e.g. automatic chambers, EC) are recommended to provide an annual budget.

4.4.2. Autumn campaign.

During autumn sampling campaign (3rd to 25th October, 2014) only one of the monitored sites have received N fertilization treatment (cf. Table 4.1.). Rapeseed (site F, previously wheat) was fertilized with 32 kg N ha^{-1} in the form of ammonium nitrate, on September 5th, one month before first measurements were done on this site. The wheat field (site E, previously rapeseed), received only lime treatment, with no N added altogether. Other monitored sites (oat – B, grassland – I and unsown site C) received no additional N in autumn altogether.

The reduced N input resulted in generally smaller overall N_2O emissions. The highest N_2O flux was observed, similarly to the spring campaign, at site F: 30.6 ± 2.4 ng N-N_2O m^{-2} s^{-1}. The lowest flux was observed at the grassland control site on the last day of campaign (October 25th) and was equal to -0.03 ± 0.20 ng N-N_2O m^{-2} s^{-1}.

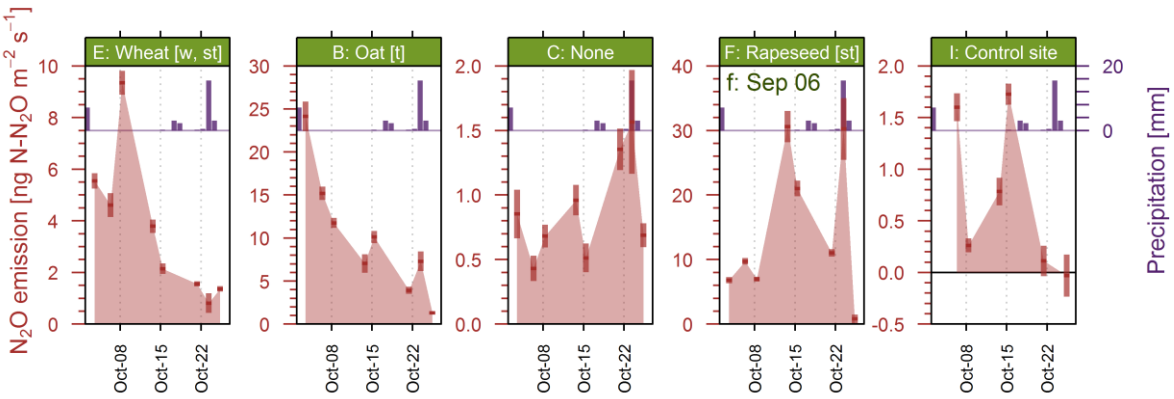

Figure 4.8. The results of autumn N_2O flux measurement campaign at ZDHAR agricultural sites.Ffertilizer application date for F site is given in green. Red bars indicate the calculated flux values with their corresponding measurement uncertainties. Purple bars denote diurnal total precipitation rates at Balice weather station. Balice, located approximately 30 km west of ZDHAR, was the nearest meteorological station for which data were available from World Meteorological Organization Climatic Data Online database (NCDC, 2015).

No clear, common temporal patterns of N_2O emissions could be discerned in the results of the autumn campaign (Figure 4.8.). Sites E and B display a declining rate of emissions, with a maximum at site E possibly caused by fertilization. The remaining three sites (C, F, I) display a large variability of the N_2O flux values that cannot be easily explained. Similar to the results of the spring campaign, the total emissions of N_2O during autumn campaign were also calculated (Table 4.4.). While average daily emissions are generally smaller (with the exception of site E, for which they were 9% larger than during the spring), comparison between the sites has uncovered that where the observed spring emissions were high, relatively higher values were also observed in autumn, even without fertilization input. Sites B and F are both displaying such behaviour, with average N_2O flux values of 44% (8.69 g N-N_2O ha^{-1} d^{-1}) and 54% (13.97 g N-N_2O ha^{-1} d^{-1}) of their respective springtime N_2O

Table 4.4. Total emissions of N_2O during the autumn campaign.

Site	Crop	Campaign duration	N added	Total emitted	Daily mean
			[kg N ha^{-1}]	[g N-N_2O ha^{-1}]	[g N-N_2O ha^{-1} d^{-1}]
					Fall campaign
E	Wheat [w, st]	22	0	75.6	3.43
B	Oat [t]	22	0	191.3	8.69
C	none	22	0	17.5	0.79
F	Rapeseed [st]	22	32	307.4	13.97
I	Grassland	19	0	11.1	0.58

releases still being emitted. Grassland site showed no change in the emissions between spring and autumn campaigns.

Daily averages of N_2O fluxes measured during autumn campaign were also compared to the reported cropland N_2O fluxes summarized by Nicolini et al. (2013). It was found out that only one site (F) was characterized by emissions larger than the median of the total distribution (Figure 4.9.). The remaining crop sites were either in the 1st (C, E) or 2nd quartile range.

The agricultural soils surveyed during both spring and autumn campaigns appear as strong sources of N_2O. Larger emissions were observed during the spring, following fertilization input and precipitation events. Importance of the form of fertilizer was also highlighted through the case of urea application at the maize field (site A). During the autumn campaign, the measured N_2O fluxes were usually smaller, in line with much lower level of fertilizer input.

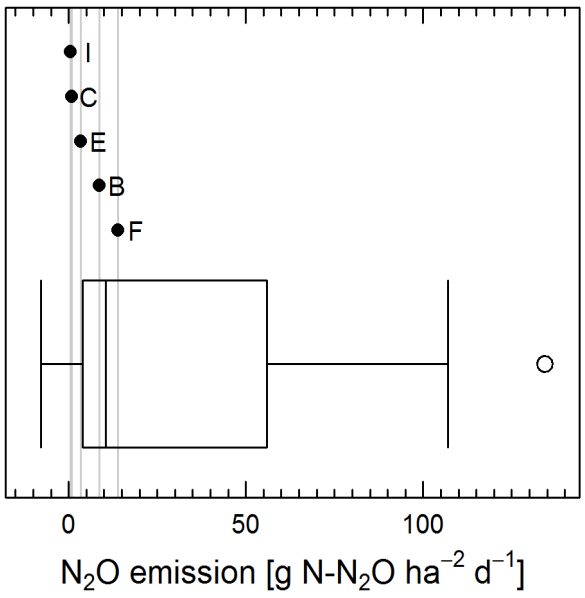

Figure 4.9. Comparison of average daily N_2O fluxes measured during autumn campaign (black points) with the statistical distribution (boxplot) of cropland N_2O fluxes from Nicolini et al. (2013). The box borders denote the 1st and 3rd quartile, with median in between. The whiskers denote lower and upper fence, with white points for values outside the fences.

4.5. Emissions of N_2O from urban soils.

The results of two reconnaissance campaigns of nitrous oxide flux measurements performed on urban soils are presented below. To the best of author's knowledge, these are the first results from this type of environment reported in Poland, and one of a few reported elsewhere (cf. Hall et al., 2008). The first campaign was performed in October 2012 and consisted of only five individual measurements. The second campaign, which took place in September 2013, lasted for 16 days and covered a total of 11 chamber enclosures, accompanying a parallel campaign of CO_2 flux measurements. Both campaigns described here were aimed mainly at quantifying the range of N_2O fluxes to be expected for the urban soils of Kraków.

During the first campaign, N_2O fluxes were measured between October 16th and 25th of 2012 at the Błonia Park in Kraków (Figure 4.2.). The results varied from 1.73 ± 0.23 ng $N\text{-}N_2O$ m^{-2} s^{-1} to 8.81 ± 0.72 ng $N\text{-}N_2O$ m^{-2} s^{-1} (Figure 4.41.). Average daily emission per hectare was estimated to be 4.65 g $N\text{-}N_2O$ ha^{-1} d^{-1}, higher than some of the fertilized sites measured at the field site of ZDHAR institute in Grodkowice.

A similar range of N_2O flux was observed during the second campaign (September 5th – 21st, 2013), with the minimum equal to 1.017 ± 0.068 ng $N\text{-}N_2O$ m^{-2} s^{-1} and maximum of 6.82 ± 0.40 ng $N\text{-}N_2O$ m^{-2} s^{-1}. A steady increase in the N_2O flux was observed since September 10th and continued until the end of the campaign on September 21th. This rise in N_2O emissions is well correlated with the outbreak of a rainy period which started on September 10th and lasted until the

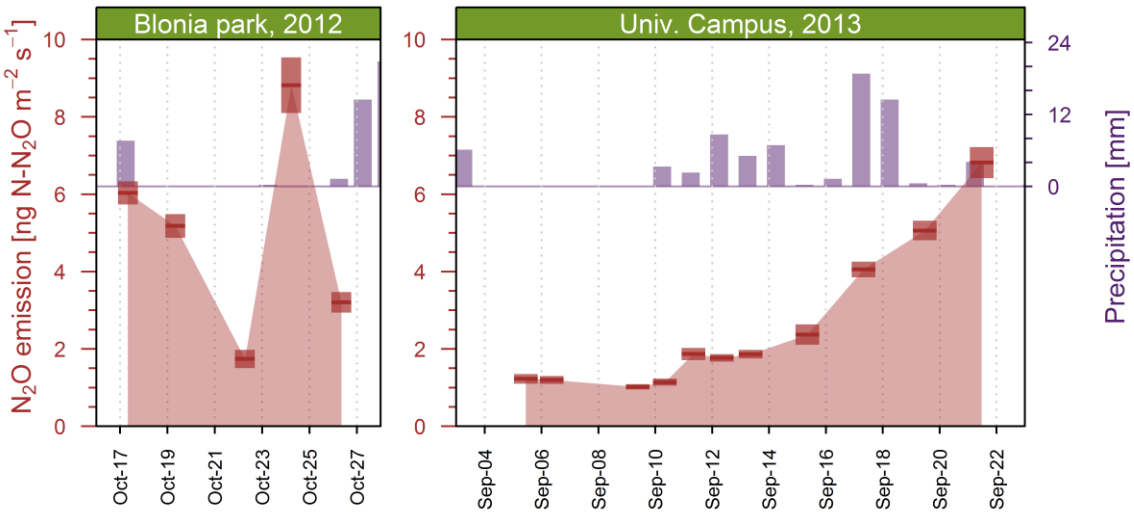

Figure 4.41. The results of two urban campaigns of N_2O flux measurements performed in Kraków. Green vertical lines indicate respective fertilization dates. Red bars indicate the calculated flux values with their corresponding measurement uncertainties. Purple bars denote diurnal total precipitation rates at Balice weather station. Balice, located approximately 30 km west of ZDHAR, was the nearest meteorological station for which data were available from World Meteorological Organization Climatic Data Online database (NCDC, 2015).

end of the campaign. Increased water content (confirmed by measurements) led to enhanced occurrence of anaerobic conditions in the soil, stimulating the activity of denitrifying bacteria and thus leading to higher N_2O emissions.

As in case of agricultural sites, the total N_2O emissions were calculated based on linear interpolation of the measured values (Table 4.5). Similar results were obtained for both campaigns: 41.8 g N-N_2O ha^{-1} for autumn 2012 and 40.6 g N-N_2O ha^{-1} for autumn 2013, albeit with two times higher daily average for the first campaign (4.65 g N-N_2O ha^{-1} d^{-1} and 2.54 g N-N_2O ha^{-1} d^{-1}, respectively). These values are higher than that reported for some of the agricultural sites described in the previous section, and in particular, 4-8 time higher than in case of the grassland control site in the Grodkowice experimental field. One possible reason behind that enhancement could be the increased availability of reactive nitrogen thanks to the presence of clover (*Trifolium L.*), which is common in urban grasslands of Kraków and able to fix atmospheric nitrogen through BNF (*Biological Nitrogen Fixation*) process. Nevertheless, the observed values are relatively low, and similar to the emissions reported from forest soils (Nicolini et al., 2013).

Overall, the urban soils were found to be sources of nitrous oxide. The level of measured N_2O emissions was higher than for some of the agricultural sites in Grodkowice, which would suggest an increased input of nitrogen, possibly through BNF of nitrogen fixing species. The measurements performed in 2013 confirm that soil water content control temporal patterns of N_2O emissions on diurnal and weekly scales.

Table 4.5. N_2O emissions from urban soils in Krakow.

Site	Campaign duration	Total emitted [g N-N_2O ha^{-1}]	Daily mean [g N-N_2O ha^{-1} d^{-1}]
October 2012 campaign			
Błonia Park	9	41.8	4.65
September 2013 campaign			
University Campus	16	40.6	2.54

5. NUMERICAL MODELLING OF REGIONAL TRANSPORT OF N_2O

In this PhD thesis, Stochastic Time Inverted Lagrangian Transport model (STILT) was chosen as a numerical tool for auxiliary analyses of the transport and emission patterns to support the observations performed at KRK and KAS stations. The use of STILT not only provided insight into the information on the range of surveyed station's footprints, i.e. the areas that have the greatest impact on the measured concentrations, but has also provided the possibility to distinguish the relative importance of the regional N_2O sources on the mixing ratios measured at KAS and KRK stations, for which external emission information was necessary. An attempt has also been made to estimate the emissions from ZAT chemical plant in Tarnów, utilizing a forward mode of calculations.

Chapter 6 is divided into six sections. First, an overview of the available numerical methods used in atmospheric transport and chemistry modelling will be provided, focusing on tools frequently used in scientific community in similar types of analyses. Second, a presentation of the chosen numerical tool (STILT) will be given, describing the main assumptions and general structure of the model. Third, the emission inventories discussed in the chapter will be overviewed. Fourth section will describe in detail the set-up of the model, including domain description, particle release locations, chosen parameterizations etc. Fifth and sixth sections will describe the obtained results, i.e. calculated footprint ranges and mixing ratios predicted by the STILT model coupled to one of the available emission databases.

5.1. Available methods of atmospheric transport modelling – an overview.

The atmospheric system, due to its inherent complexity and a multitude of driving factors, cannot be described by a set of simple mathematical formulas that could be solved analytically. Rather than that, the motions of the air masses need to be represented by a system of equations, often very complicated, each describing a subset of processes that influence the state of the atmosphere at any given moment.

These equations are rooted in thermodynamics, which laws have been described in XIX century. It took several decades, however, before it was recognized that it is possible to predict the behaviour of the atmosphere through numerical forecasting. The first trial, based on previous theoretical work by Vilhelm Bjerknes, was performed by Lewis Fry Richardson and consisted of 23 "Computer Forms", resembling modern day Excel sheets, in which Richardson has tried to forecast the weather for a single day relying on the observations of previous state of the atmosphere and a set of numerical equations, governing pressure changes, humidity, wind velocities, etc. The results were discouraging, with a predicted pressure change of 146 mbars, while virtually no change was observed. The reason behind the mistake was later shown to be caused by not applying the smoothing filter to the observational data. Once done, the Richardson prediction yielded realistic results (Lynch, 2008).

Numerical modelling of weather flourished after the revolution in electronic computing. Development of faster machines spurred rapid advancement of atmospheric sciences, particularly

in weather forecasting. Nowadays, some of the most powerful supercomputers are used by organizations responsible for weather forecasting on a global, regional and national scales (e.g. European Centre of Medium-range Weather Forecasting, ECMWF).

As processes of pollutant transfer are governed by the same atmospheric processes that are being described in numerical weather forecasting (NWS), it is not surprising that the development of atmospheric sciences was closely followed by studies focused on the transport and chemistry of the atmosphere's components. The discovery of the ozone hole and following works of Crutzen, Molina and Rowland (Nobel Prize, 1995) have shown that pollutants emitted by anthropogenic activities and transported in the atmosphere can have a direct impact on Earth System's components that are critical for climate. To understand this impact and the magnitude of human influence on the environment, it is critical to obtain a detailed knowledge on the sources and sinks of the gaseous substances present in the atmosphere, particularly greenhouse gases and ozone depleting substances (Mooney et al., 1987, Lin et al., 2003). This can be achieved from atmospheric observations, however the complex nature of the transport process needs to be taken into the account.

Constraining the emissions of N_2O with observations is possible on a set of scales through several methods. On a global scale, top-down budgets based on atmospheric observations can be utilized (Crutzen et al., 2008, Prather et al., 2012), albeit the possibility of apportioning of emission source is limited. Atmospheric observations can also be used to describe spatial variability of N_2O releases on a regional scale through inversion modelling (Corazza et al., 2011). The inverse approach is very promising for constraining the continental N_2O budgets, however it requires extensive networks of atmospheric observation sites, only possible via multinational cooperation (see section 3.1.)

Therefore, atmospheric transport modelling is crucial for obtaining quantitative information on the surface emission patterns on a regional scale. This is especially true for observations performed in the Planetary Boundary Layer (PBL), in which most of the emission sources are located. Modelling of the transport in the PBL is difficult, however, due to high variability of concentration data associated with inhomogeneous surface fluxes and due to difficulties in proper representations of PBL dynamics in the numerical models (Lin et al., 2003, Shin and Hong, 2011).

There is currently a multitude of numerical models that can simulate the transport of atmospheric pollutants, covering a wide range of components as well as temporal and spatial scales. The simplest of these are Gaussian models that take into the account only several parameters. The most complicated models are currently capable of simulating atmospheric chemistry processes of hundreds of compounds, together with their feedbacks on meteorological parameters on time scales of seconds, while covering spatial extents of whole continents (e.g. WRF-Chem, COSMO-Art).

Below, a short description of three types of transport models will be presented that are commonly used in the studies of nature similar to the presented work.

5.1.1. Gaussian plume.

Gaussian plume model is one of the simplest and most intuitive methods of describing pollutant transfer in the atmosphere (Figure 5.1). First described in 1936 (Bosanquet and Pearson), it is probably the oldest method of calculating the dispersion of pollutants. The Gaussian plume model can be derived by solving the continuity equation under several assumptions:

a) the state of the system is time-independent,
b) wind speed vector in homogeneous in space and time,
c) advection along the wind direction is much stronger than turbulent diffusion,
d) the turbulent diffusivity coefficients are homogeneous in space,
e) no chemical reactions are occurring.

Under these assumptions, the continuity equation takes the form of the Gaussian equation. If we assume that the wind is blowing along the x axis. It can be written as:

$$U\frac{\partial C}{\partial x} = D_y\frac{\partial^2 C}{\partial y^2} + D_z\frac{\partial^2 C}{\partial z^2}, \tag{5.1}$$

where C is the pollutant concentration, U is the wind speed and D_y and D_z denote the horizontal and vertical diffusion coefficients, respectively.

The solution to the eq. (5.1) can be calculated analytically and can have many variations, depending on the specific modelling needs of the end user, e.g. if maximal value over a certain period of time is required, or in case when only the concentrations on the surface are needed. In the most common version (wind-oriented Cartesian system), the equation can be written as:

$$C_{xyz} = \frac{E_g}{2\pi\bar{u}\sigma_y\sigma_z}\exp\left(-\frac{y^2}{2\sigma_y^2}\right)\left\{\exp\left[-\frac{(z-H)^2}{2\sigma_z^2}\right] + \exp\left[-\frac{(z+H)^2}{2\sigma_z^2}\right]\right\} \times 1000, \tag{5.2}$$

where:
C_{xyz} – mean hourly concentration of the compound, given in mg/s.
x, y, z – coordinates of the point, for which the concentration is calculated,
E_g – emission of the gaseous compound, given in mg/s,
$\bar{u}$ – mean horizontal wind speed, given in m/s,
σ_y, σ_z – standard deviations (horizontal and vertical) of the plume concentration spatial distribution; these are calculated from empiric formulas which depend on the atmospheric turbulence states,
H – effective emission height (i.e. height of the stack plus the plume rise).

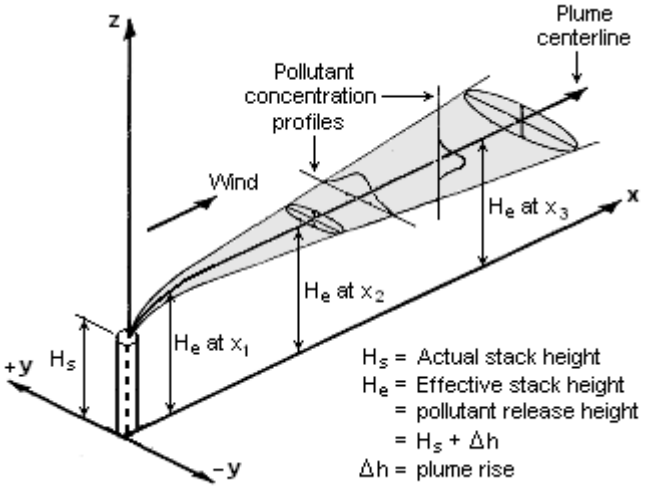

Figure 5.1. A visualization of a Gaussian air pollution plume. Author: Milton Beychok. Copied from Wikimedia Commons under GNU licence.

The formula (5.2) refers to the stationary, i.e. time-independent, state that is also homogeneous with regard to the wind

and the turbulent state of the atmosphere. The also displays a singularity when $\bar{u} \to 0$, so in most algorithms it is recommended to use a minimal wind value of 0.5 m/s. The usage of hourly averages is motivated by the fact that in real conditions neither homogeneity nor stationary assumptions are fulfilled for any given time, due to the stochastic nature of the plume transport on a small scale (formation of eddies, small wind direction changes etc.). However, when averaged, these variations are often smoothed out, and the concentration distributions can be described using the Gaussian distributions.

The results of the model rely heavily on the correct calculations of σ_y and σ_z dispersion parameters. In general, there are two main methods of obtaining these. The first is based on calculation of dimensionless functions that utilize available meteorological measurements that describe the turbulent state of the atmosphere (Pasquill, 1971, Draxler, 1976). In the second approach, computation of dispersion parameters is done with semi-empirical formulas based on categorised stability classes of the lower atmosphere (Pasquill classes) that are attributed to the studied system based on a set of meteorological parameters. This can be done using one of several possible methods, e.g. Pasquill-Gifford scheme (Gifford Jr, 1961), Brookhaven scheme (Singer and Smith, 1968) or Briggs scheme (Briggs, 1973). The choice of specific computation scheme for quantifying σ_y and σ_z depends on the context of the numerical experiment.

Nowadays, the Gaussian model is frequently used by governmental agencies responsible for air quality assessments to predict the influence of existing (or proposed) industrial facilities on the concentrations of the gaseous compounds in the surrounding environment. Another possible application is related to emergency scenarios developed in case of critical malfunctions of certain installations (chemical or nuclear). Gaussian model is also often used to predict possible areas of contamination and can be used by respective agencies to develop evacuation scenarios.

5.1.2. Eulerian models.

Eulerian approach to numerical weather predictions and pollutant transfer relies on the simulations of the modelled processes in a spatially fixed grid. The simulated quantities follow continuity equations that are based on mass-balance and thermodynamics principles. When considering atmospheric pollutants, these equations take into the account four most important processes: emission, transport, chemical changes and deposition. The Eulerian form of the continuity equation can be written as:

$$\frac{\partial \mathrm{n}}{\partial \mathrm{t}} = -\nabla \cdot \mathrm{F} + \mathrm{P} - \mathrm{L}, \tag{5.3}$$

where n is the molar concentration (i.e. in units of particles per unit volume) of the compound, $\nabla \cdot \mathrm{F}$ is the flux divergence, P is the production process inside the grid cell and L is the local sink.

The three-dimensional Eulerian models discretize the modelled area into grids and solve the above partial differential equation in each grid point (or grid cell). Together with initial and boundary conditions (usually in the form of fluxes, which can also be the results of process-based modelling), this allows for predictions of the system's evolution, and in particular, the chosen compound concentration changes.

The scales of Eulerian model computations vary depending on the application, and can range from global to local. It is important to note that the spatial and temporal scales are connected through Courant-Fredrichs-Lewy criterion (CFL), which states that the for a given grid set, propagation of information (wave) inside this grid can only be properly described if the size of the grid is bigger than the distance travelled by that signal during a single time step. In other words, the time step of calculations must be sufficiently small to allow the fastest signals (waves) to propagate at most to the neighbouring cell. Failure to comply with CFL criterion may result in numerical instabilities which can make the results of the model unreliable or unstable. A balance must ever be achieved between the desired spatial resolution and available resources when using the Eulerian models, as calculating fine grids with large number of grid cells becomes costly with increasing resolution.

Many of the processes that need to be included in the numerical models are occurring in scales smaller than the one set up for the modelled system. In that case, it is impossible to write and solve mathematical equations pertaining to those processes, and the model must rely on empirical or semi-empirical descriptions. A classic example is the process of convection, which is a critical one in terms of heat, water and also pollutant transport, and which usually takes place on a spatial scale of one to several kilometres and time scales of several hours. In case of global models, even with relatively high resolutions of 1°x1° (approximately 100 km x 100 km in mid latitudes) the convection cannot be directly described.

Modern numerical weather prediction (NWP) models are almost exclusively Eulerian models, forecasting meteorological parameters on global and regional scales. The state of the art models now have the ability to simultaneously predict weather and chemistry of many gaseous compounds (e.g. ECMWF IFS, IFS-C, WRF, WRF-Chem) on global to regional scales. However, increasing complication of the process description is directly connected with the increased resource usage, and simulating pollutant transport with an Eulerian model on a high spatial and temporal resolution can become costly (i.e. requiring the usage of powerful computing clusters or even supercomputers). For example, in order to predict concentrations of a given compound at a chosen site, the Eulerian model would need to perform simulation on the whole modelled domain. In a typical case of regional emissions, with 10 km x 10 km domain over Europe, and with 30 vertical levels, this would mean solving transport equations for 1 875 000 grid cells at every time step (which can be on the order of seconds).

A way out from this dilemma has been developed in the transport modelling that allows to take advantage of high resolution of Eulerian models while reducing the cost of simulations. The idea of nesting assumes that the most accurate information (i.e. highest resolutions of simulations) is usually only necessary in the small region of interest, and the rest of the domain can be solved with lower resolutions. This idea reflects the physical phenomenon where the small-scale variations in the concentrations are driven mostly by local effects (both in case of emissions and meteorology). When more distant sources are considered, the signal is smoothed out by diffusion, therefore high-resolution predictions are not needed in the whole simulated domain.

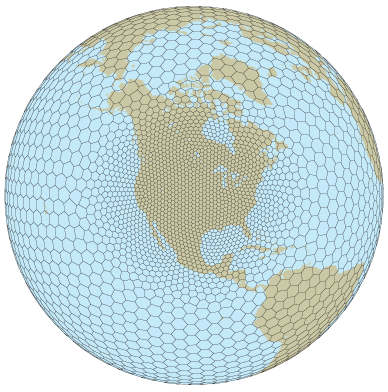

Figure 5.2. MPAS Voronoi mesh. Source: MPAS website (MPAS, 2015).

The nesting procedure has several issues, with the most notable one being related to the boundary effects that occur on the interface between parent (i.e. coarser) and nested domains. These boundary effects often cause unphysical numerical noise which can reduce gains from using high-resolution altogether. A possible solution to that problem might be through the usage of

variable resolution grids. For example, U.S. National Centre of Atmospheric Research (NCAR) and Los Alamos National Laboratory (COSIM) are currently developing the MPAS (Model for Prediction Across Scales), which utilizes the Voronoi mesh (Figure 5.2) and modified ARW (Advanced Research WRF) code to simulate weather on meso-scales.

Nevertheless, Eulerian models are rarely directly used in the simulations of pollutant transport due to high costs of computations, as Lagrangian models allow for accurate results without the need to solve the continuity equation in each grid cell. In most cases however, the Lagrangian models are in fact relying on pre-calculated weather parameters (e.g. horizontal and vertical winds) that were simulated and stored on a 3D Eulerian grid. This is also the case for STILT.

5.1.3. Lagrangian models.

This section is largely based on the description of Lagrangian models provided in (Lin et al., 2003).

The continuity equation can also be transformed to describe the change of mixing ratio inside the volume element moving along the wind field. In contrary to the Eulerian form, no fixed frame of reference is considered, and the general formula of the continuity equation can be written as:

$$\frac{\mathrm{dC}}{\mathrm{dt}} = \mathrm{P}' - \mathrm{L}', \tag{5.4}$$

where C is the mixing ratio of pollutant in the considered volume, P' and L' are the local production and loss terms, respectively, and $\frac{\mathrm{d}}{\mathrm{dt}}$ denotes the Lagrangian operator, which can be expanded to:

$$\frac{\mathrm{d}}{\mathrm{dt}} = \frac{\partial}{\partial \mathrm{t}} + \vec{\mathrm{u}} \cdot \nabla,$$

where $\vec{\mathrm{u}}$ is the local wind velocity.

In order to consider the tropospheric transport in a realistic manner, the turbulent motions of the lagrangian air parcels cannot be neglected, however. In the works published by Obukhov (1959), Smith (1968) and Hanna (1979), it has been shown that turbulent diffusion can be described through a Markov chain. This assumption serves as a foundation of all modern Lagrangian transport models. Particle's velocity vector $\vec{\mathrm{u}}$ can be expressed as a sum of a mean component $\langle\vec{\mathrm{u}}\rangle$ and a turbulent component $\vec{\mathrm{u}}'$, which in turn can be written as (Lin et al., 2003):

$$\vec{\mathrm{u}}'(\mathrm{t} + \Delta\mathrm{t}) = \mathrm{R}(\Delta\mathrm{t})\vec{\mathrm{u}}'(\mathrm{t}) + \vec{\mathrm{u}}''(\Delta\mathrm{t}), \tag{5.5}$$

where R is the autocorrelation coefficient, $\vec{\mathrm{u}}''$ is a random vector and $\Delta\mathrm{t}$ is the time step.

R can be expressed as an exponential function: $\mathrm{R}(\Delta\mathrm{t}) = \exp(-\Delta\mathrm{t}/\mathrm{T_{Li}})$, where $\mathrm{T_{Li}}$ denotes the Lagrangian time-scale in the horizontal $(\mathrm{i} = \mathrm{u})$ or vertical $(\mathrm{i} = \mathrm{w})$ direction. The value of $\mathrm{T_{Li}}$ determines the behaviour of the particle motion, with random walk occurring for $\mathrm{T_{Li}} = 0$ and movement along mean wind for $\mathrm{T_{Li}} \gg 0$.

Random velocity $\vec{\mathrm{u}}''$ is defined as:

$$\vec{\mathrm{u}}''(\Delta\mathrm{t}) = \lambda\sqrt{1 - \mathrm{R}^2(\Delta\mathrm{t})}, \tag{5.6}$$

with λ usually calculated using a Gaussian distribution centred at zero with a standard deviation characterizing the spread of random velocity. Using these formulas and calculating an ensemble of particles allows the Lagrangian models to describe the turbulent flows.

Forward mode of Lagrangian model simulation predicts the motion of particles for the values of *t* greater than zero, i.e. forward in time. This mode is used when the *a-posteriori* distribution of the released mass is the desired outcome of the simulation (Lamb et al., 1979, Ryall et al., 2001). For example, Lagrangian models have successfully been used in a forward mode to explain the transport patterns of ash after the Eyjafjallajökull volcano (Iceland) eruption in 2010 (Stohl et al., 2011) or of radionuclides after the Fukushima Dai-Ichi nuclear power plant event (Park et al., 2013).

Lagrangian models can also be used in the backward mode, under the assumption that the particle transport is a time reversible process. In the backward mode, the simulations are performed following the same equations, with *t* values decreasing below zero. The increased number of particles in the upstream regions can be interpreted as reflecting the higher impact of the emissions in these areas on the concentrations observed at the receptor point, thus providing a "receptor-oriented framework" (Uliasz and Pielke, 1990, Lin et al., 2003).

Mathematically, the backward-in-time particle distribution is an estimation of the influence function $I(\overrightarrow{x_r}, t_r|\vec{x}, t)$ that describes the relation between the sources (or sinks), $S(\vec{x}, t)$, and the concentrations of a conservative tracer $C(\overrightarrow{x_r}, t_r)$, as observed at time t_r in the receptor point located at $\overrightarrow{x_r}$. The I function is interpreted as "the fraction of a fluid element found at $\overrightarrow{x_r}$ at time t_r given that the fluid element was at $\vec{x}$ at time t" (Lin et al., 2003, and references therein):

$$C(\overrightarrow{x_r}, t_r) = \int_{t_0}^{t_r} \int_V I(\overrightarrow{x_r}, t_r|\vec{x}, t) \times S(\vec{x}, t)\ d^3x\, dt + \int_V I(\overrightarrow{x_r}, t_r|\vec{x}, t_0) \times C(\vec{x}, t_0)\ d^3x. \qquad (5.7)$$

In the equation (5.7), the I function has the unit of m^{-3}, concentrations (C) – mmol mol^{-1} (denoted as ppm), and source function S – mmol mol^{-1} h^{-1} (mixing ratio per unit time). The first integral term can be interpreted as the concentration change due to sources and sinks activities during the simulation time (from t_0 to t), and the second integral describes the contribution from the initial conditions. In particular, if no initial concentrations are provided, the second term is effectively equal to zero and the simulated concentrations will only reflect the additional signal coming from the upstream emission fields.

It can be shown that for discretized values of the functions described in equation (5.7), the source/sink term in that equation can be rewritten as a relatively simple formula (Lin et al., 2003):

$$\Delta C(\overrightarrow{x_r}, t_r) = \sum_{i,j,m} f\left(\overrightarrow{x_r}, t_r \mid x_i, y_j, t_m\right) \times F\left(x_i, y_j, t_m\right), \qquad (5.8)$$

where $\Delta C(\overrightarrow{x_r}, t_r)$ denotes the predicted increase in pollutant concentration over the initial concentration coming from the boundary conditions, with value in mmol/mol, $F\left(x_i, y_j, t_m\right)$ is the spatial and temporal distribution of net surface sources/sinks provided in units of μmol m^{-2} s^{-1} and fdenotes the footprint function which directly links fluxes occurring at x_i, y_j, t_m over a single time step to the concentration change ΔC at the receptor. The f footprint function can be calculated directly from the simulated particle locations using the formula:

$$f\left(\overrightarrow{x_r}, t_r \mid x_i, y_j, t_m\right) = \frac{m_{air}}{h\bar{\rho}\left(x_i, y_j, t_m\right)} \frac{1}{N_{tot}} \sum_{p=1}^{N_{tot}} \Delta t_{p,i,j,m}, \tag{5.9}$$

where: $\overrightarrow{x_r}, t_r$ – space and time coordinates of the receptor point, x_i, y_j, t_m – space and time coordinates of the emission point, $\Delta t_{p,i,j,m}$ – total amount of time that the particle p spends in the cell at x_i, y_j coordinates during the respective time step, $\bar{\rho}$ – average air density below h, N_{tot} – number of particles released from the receptor, m_{air} – molar mass of air, h – turbulent mixing height (below which we assume that air is perfectly mixed) and p, i, j, m – indexes of particles (p), space coordinates (i, j) and time step (m), respectively.

It has been shown that in order to provide realistic source-receptor relationship, the Lagrangian particle model must fulfil a number of physical requirements (Lin et al., 2003): (i) well mixedness, (ii) simulation of interaction between wind shear and vertical turbulence, (iii) high temporal resolution (to resolve the decay of the autocorrelation in $\vec{u}'$), and (iv) consistent representation of particles as air parcels of equal mass.

The well-mixed criterion is directly related to the Second Law of Thermodynamics, and states that "models of turbulent dispersion must retain an initially well-mixed particle distribution and not spuriously unmix particles" (Lin et al., 2003, following Thomson, 1987). The violation of the well-mixed criterion can stem, for example, from violations of mass conservation in the mean wind fields, where the amount of air mass that enters a given grid box is not equal to the amount of mass that exits that grid box, which leads to the artificial dilution of simulated particles. It has been shown by Thomson (1987) that the well-mixed criterion is a theoretical equivalent of time-reversibility.

The wind-shear and vertical turbulence interaction criterion reflects the complexity and inherent coupling between the horizontal and vertical components of a particle motion during wind shear. Without the proper implementation of this relation in the model code, the particles can be transported vertically without simultaneous horizontal advection by the mean wind, or *vice-versa*, transported horizontally without being redistributed vertically at the same time, which could yield unrealistic simulation results.

The third criterion requires high temporal resolution of the simulation, so that the decay in the autocorrelation term in equation (5.5) can properly be represented. Failure to provide small enough time step will mean that the particle velocity is not affected by the random components and the $\vec{u}'$ does not change over the time step. A critical parameter that needs to be considered here is the Lagrangian timescale (T_L). Time step used in the simulations should be smaller than 10% of the local T_L value (Lin et al., 2003).

The last criterion, regarding the consistent representation of particles as parcels of equal mass, states that the model parameterisations of turbulence needs to use the gradient of atmosphere's density. Neglecting that criterion will lead to systematic underestimation of tracer concentrations near the surface and overestimations at the higher levels of the model (Lin et al., 2003).

A number of Lagrangian particle dispersion models is currently available to the scientific community, with many studies published in the previous 20 years utilizing tools like LPDM (Uliasz, 1993), FLEXPART (Stohl et al., 2005), NAME (Jones et al., 2007), HYSPLIT (Draxler and Hess, 1998) and STILT (Lin et al., 2003).

5.2. Stochastic Time-Inverted Lagrangian Transport model STILT – an overview.

The core of the STILT model is based on the code of the Hybrid Single-Particle Lagrangian Integrated Trajectory (HYSPLIT) model, described by Draxler and Hess (1998), and is developed by a group of researchers from Harvard University (USA), Max Planck Institute for Biogeochemistry in Jena (Germany), University of Waterloo (Canada) and Atmospheric & Environmental Research (AER, Boston, USA). STILT can be used for analyses of past concentration changes or for campaign planning purposes (with the forecasted meteorological fields.

The main difference between HYSPLIT and STILT is that the latter utilizes an improved turbulent motion module, described in detail in works by Lin et al. (2003) and Gerbig et al. (2003). The most important improvements are related to (i) the Planetary Boundary Layer parameterization, where a modified Richardson number has been applied, and (ii) vertical transport of the released particles themselves, where a reflection/transmission scheme first described by (Thomson et al., 1997) has been applied to ensure that the well-mixed criterion is satisfied.

STILT utilizes the pre-prepared meteorological fields to drive the transport of the released particles. Different sources of meteorological data are currently supported, including output files from EDAS archive (*Eta Data Assimilation System*), GDAS (*Global Data Assimilation System*, both developed by National Centers for Environmental Protection, NOAA), BRAMS (Brazilian implementation of Regional Atmospheric Modeling System, BRAMS, 2015), Aladin (MeteoFrance), WRF (Weather Research and Forecasting, Nehrkorn et al., 2010) and IFS models (ECMWF).

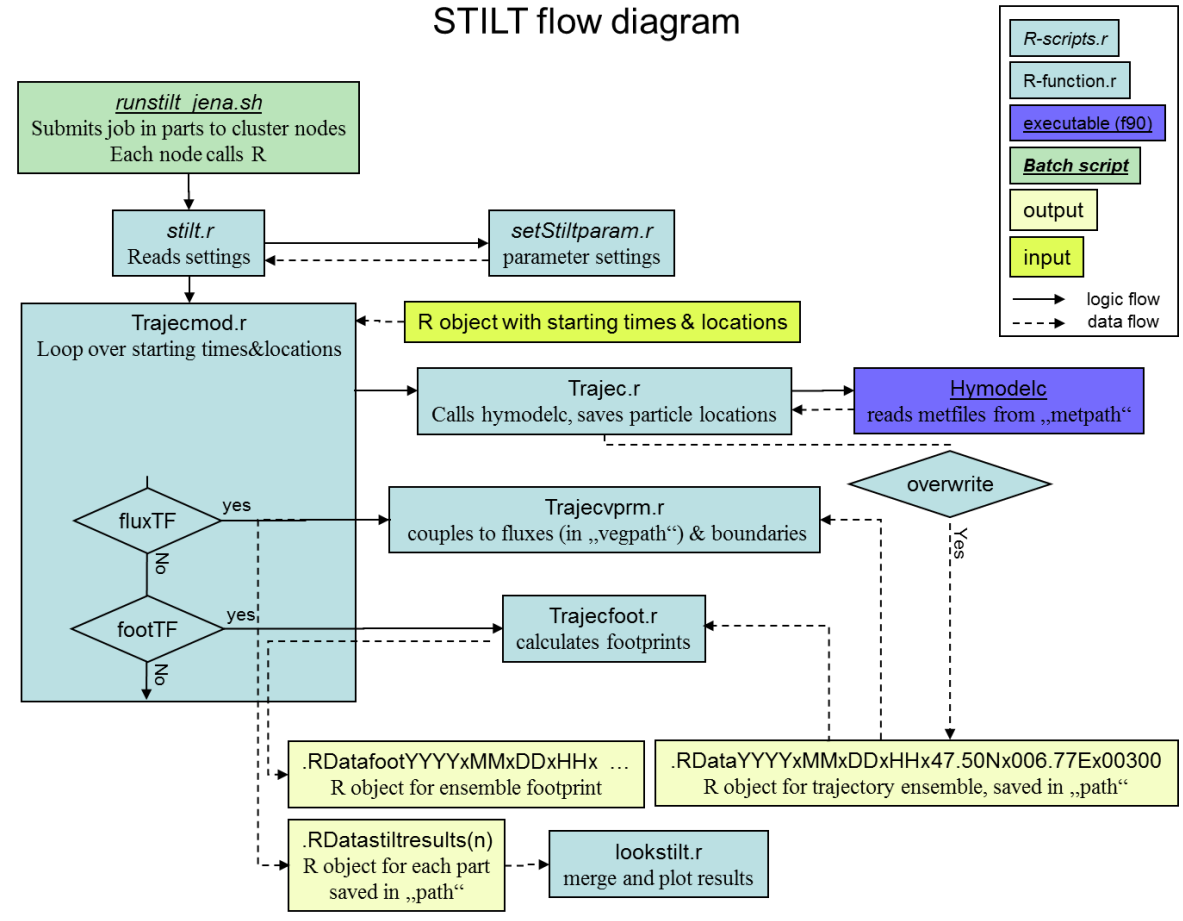

Figure 5.3. STILT model flow chart. Source: STILT (2015).

The user interface of the STILT model is mainly based on a series of scripts and functions written in R software (RCT, 2014), with the conceptual flow chart of the data and the parameters presented in Figure 5.3. In the most basic version, the model allows for the calculation of an ensemble of particles for a single release, based only on the meteorological data files provided. When requested (*footTF* set to *true*), the model also allows for the calculation and output of the footprint objects (*.RDatafootYYYYxMM…*), which stores information on the footprint fractions pertaining to the modelled domain for all of simulated time steps. When the information on the fluxes values are provided, the calculated footprints can be multiplied by the respective emission fields to simulate the concentrations predicted at the receptor point (*.RDatastiltresult*). In order to reduce computational costs of model operation, this calculation is in fact performed without explicitly using the *.RDatafoot* objects.

A limited parallelization of the model code has been implemented. The model run can be submitted to a queue system (e.g. *bsub*) on a multi-node server by a set of scripts available with the distribution, allowing to increase the calculation speed and reduce the computation time.

Apart from the predicted concentration and footprint, a set of auxiliary model output variables is also available. These can be used for detailed analysis of gaseous compound transport between the respective emission sources and the receptor point during the surveyed events. Some of the most important of these are associated with the vertical transport, e.g. time-distributions of: (i) particle locations, (ii) particle heights (*agl*), (iii) mixing height in the grid cell (*zi*) in which the particles resided in, and (iv) vertical path of particles through convection (*zconv*).

5.3. Model set-up.

In the presented study, STILT has been used as the supporting tool to interpret the N_2O concentration records measured at two surface sites located in South Poland, namely Kraków (KRK) urban station and Kasprowy Wierch (KAS) high mountain station. Detailed description of these sites can be found in Chapter 3, in sections 3.3.1 and 3.3.2.

In order to perform this task, a modelling framework has been set up, in cooperation with the Department of Biogeochemical Systems, Max Planck Institute for Biogeochemistry (MPI BGC) in Jena, during a 5 week scientific visit of the author of this thesis. The software was installed on the MPI's *panorama* server, in accordance to the instructions available on the STILT website (STILT, 2015).

The model domain (Figure 5.4) covered the area of continental Europe, between 12°W and 35°E longitude and between 35°N and 62°N latitude, with resolutions

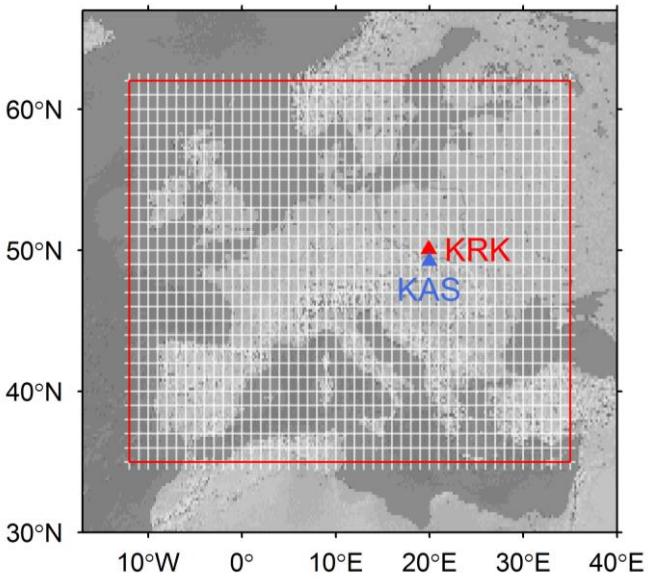

Figure 5.4. STILT model domain used in the presented study. Gridlines plotted every 1°.

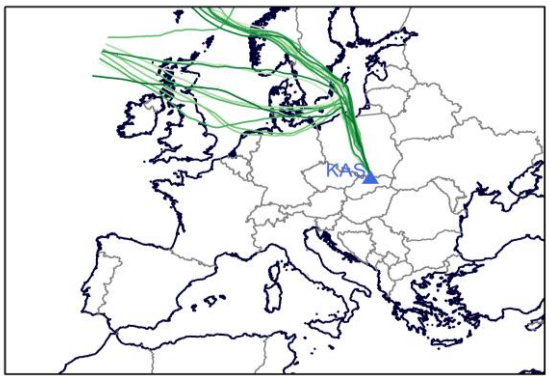

Figure 5.5. Example of particle trajectories calculated by STILT.

Table 5.1. Receptor locations.

Site	AGL [m]	Longitude	Latitude
KRK	17	19.913° E	50.067° N
KAS	700	19.981° E	49.232° N

of $1/8$ and $1/12$ degrees, respectively, which is roughly equal to 10 km x 10 km square grid and exactly the same as in case of the flux emission fields from IER database available at the *Panorama* server.

Integrated Forecasting System (IFS) high resolution (HRES, 0.125° x 0.125°, 137 vertical levels) data have been used to drive the simulations performed in the presented study. The data has been downloaded to the MPI server and pre-processed to be readable by STILT prior to the simulations.

Unless otherwise stated, every simulation consisted of a release of 100 particles in the backward mode, with the simulation period of 10 days and hourly outputs of the particle positions and footprint elements. Figure 5.5. presents an example of calculated particle trajectories, released from KAS station on 16.04.2014 at 00:00 GMT. Convection parameterization was always turned on, as well as dynamic resolution of the time step (to ensure that Courant criterion is satisfied). Other parameters were set to their default values.

For footprint calculations, an optimal surface layer height h was defined as half (0.5) of the respective mixing height in the equation (5.9), in accordance with findings published in Gerbig et al. (2003). Horizontal size of the footprint elements was dynamically changed to prevent the effect of underrepresentation of flux that occurs when the particles are distributed during the latter part of the simulation. As the gaps between the emitted particles grow, the grid cells resolution is degraded and the respective footprint is distributed over the larger area. An example of the sum of footprint elements calculated for a single release (also started at 16.04.2014 at 00:00 GMT) is shown in Figure 5.6.

The receptor points (Table 5.1.) were chosen to best represent their location in the modelled domain. In case of KAS, it has been decided that the release point should be located 700 m above model ground level due to misrepresentation of the local topography in the coarse driving meteorological fields. In the used datasets, the ground elevation in the grid cell pertaining to the station's location was around 1300 m AMSL.

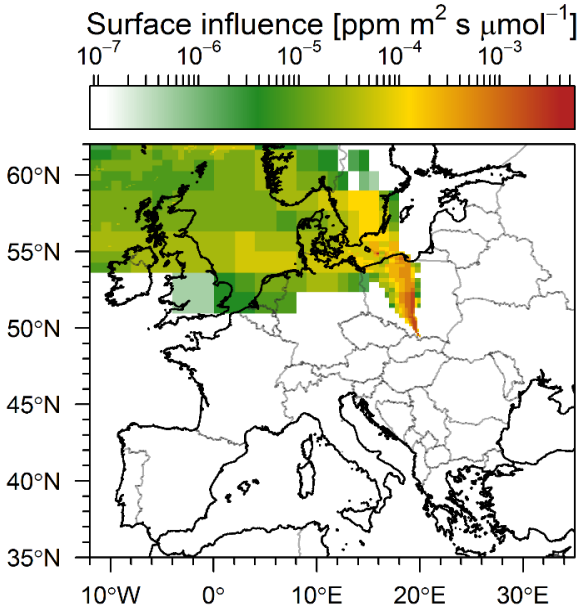

Figure 5.6. Example of a total footprint (surface influence) calculated for a single release of one thousand particles, described as pollutant concentration enhancement (in ppm) at the receptor point per flux unit (in μmol m^{-2} s^{-1}).

5.4. N_2O emission inventories.

In order to predict concentrations at the receptor point, STILT needs to be provided with the external flux emission maps of a given compound defined for the respective simulation domain. It is important to note, however, that in order to be used, it is necessary for the emission inventory to be provided on the timescale of 1 hour. There are currently several databases of gridded anthropogenic N_2O emissions available to the scientific community, covering either global (Emission Database for Global Scientific Research – EDGAR) or regional (IER_hourly, E-PRTR and GESAPU with N_2O emissions from Europe) spatial extents. Short description of these databases will be given below.

EDGAR v4.2. (EDGAR, 2011) is a global database managed by Joint Research Centre (JRC) of the European Commission and Netherlands Environmental Assessment Agency (PBL). It is commonly used as a reference-database thanks to the commonly accepted bottom-up methodology based on the Intergovernmental Panel on Climate Change guidelines for reporting of greenhouse gas emissions (IPCC, 2006). EDGAR v4.2 provides annual datasets of a multitude of anthropogenic gaseous components, including N_2O, on a high spatial resolution of 0.1° x 0.1° (Figure 5.7., left).

Two database updates have been issued since the original publication, including the releases of v4.2 FT2010 (where FT stands for *Fast Track*, i.e. without strict quality control procedures) and v4.2. FT2012 datasets that extended the annual emission maps, until 2010 and 2012, respectively. These releases, however, include some erroneous allocation of the N_2O sources in southern Poland (not shown). Therefore in this study, only the emissions for 2008 from the original dataset have been used for reference purposes, which will hereafter be referred to as "EDGAR emissions".

The main disadvantage of the EDGAR database is lack of time-dependence of the emitted components. While it is possible to include time-dependence through the usage of per-sector time-variation factors provided by EMEP (European Monitoring and Evaluation Programme, see Vestreng,

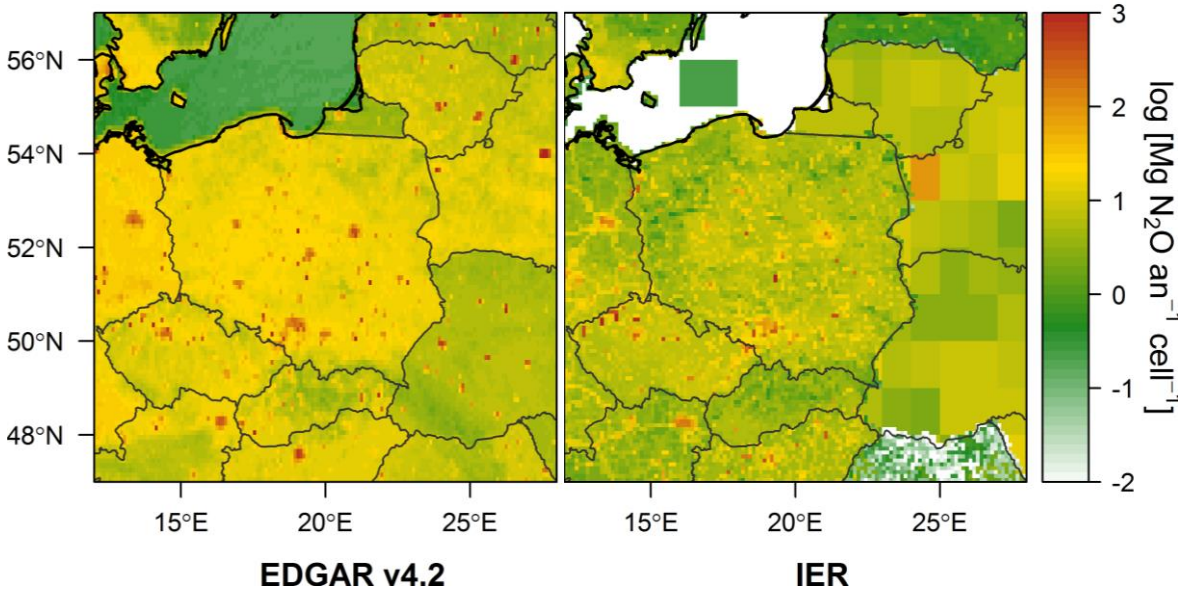

Figure 5.7. Comparison between total anthropogenic emissions of N_2O for central Europe quantified by EDGAR v4.2 and IER databases. Logarithm of emission given in tonnes per year per cell is displayed. See text for description.

2005), its application would require additional efforts. Therefore another, already available N_2O emission database was used in STILT experiments in the framework of this PhD thesis.

IER_hourly dataset (hereafter referred to as simply IER) is a time-dependent anthropogenic greenhouse gas emission inventory for the year 2000, prepared by the IER (*Institute for Energy Economics and the Rational Use of Energy*) of the University in Stuttgart in the framework of the CarboEurope project (CarboEurope-IP, 2000). The spatial extent of the database is limited to Europe, and its resolution is 10 km x 10 km for most of the EU countries and coarser, 1° x 1° resolution for other countries (Figure 5.7., right). Temporal resolution of 1 hour is available. The bottom-up methodology used during the creation of the IER database was similar to the one adopted by EDGAR, and is described in detail in Pregger et al. (2007).

The IER database has been pre-processed and made available for STILT simulations at the *panorama* server of the MPI BGC in Jena. Only total emissions were included. Both databases differ in the total emission values attributed to the respective cells and country totals, and only a small part of these differences can be explained due to changes in emissions that occurred between 2000 and 2008 (IER and EDGAR, respectively; comparison not shown). However the spatial distribution of the emission sources is similar in both datasets.

GESAPU (*Geoinformation technologies, spatio-temporal approaches, and full carbon account for improving accuracy of GHG inventories*) database is the result of a EU 7th Framework Programme Marie Curie Actions project, which main aim was to develop a spatial inventory of GHG for Poland. The methodology of this bottom-up inventory closely followed IPCC guidelines, with high resolution of the dataset obtained thanks to the application of a nouveau spatial data disaggregation described in Horabik and Nahorski (2015), allowing to obtain very high spatial resolution of the dataset, i.e. 2 km x 2 km.

European Pollutant Release and Transfer Register (E-PRTR, cf. section 2.3.2.) is the database where the releases of the most important environmental pollutants need to be reported under the EU Regulation (EC) No 166/2006, which is the European implementation of the UNECE (United Nations Economic Commission for Europe) PRTR protocol, signed by the European Community and 23 Member States in May 2003 in Kiev. The PRTR is a protocol to the Aarhus Convention, which grants the citizens of the signatory countries the rights to receive information on environmental pollution and to participate in environmental decision-making. The E-PRTR database was established in 2006, and since 2007 industrial facilities that emit pollutants above their respective annual threshold values, are required to report these releases to the database.

5.5. Regional footprint estimation for KRK and KAS stations.

One of the main aims of this chapter was to quantify the influence of local and regional sources of nitrous oxide on the atmospheric concentrations of this gas observed at KAS and KRK stations. Assessment of the station footprint and estimation of the impact of individual sources on the measured mixing ratios of N_2O are necessary steps in characterizing the regional representativeness of the results obtained at these stations.

In each case, total station footprint was calculated as a sum of single-release footprint elements, each derived from 10-day long backward simulations with 100 particles released. The releases were

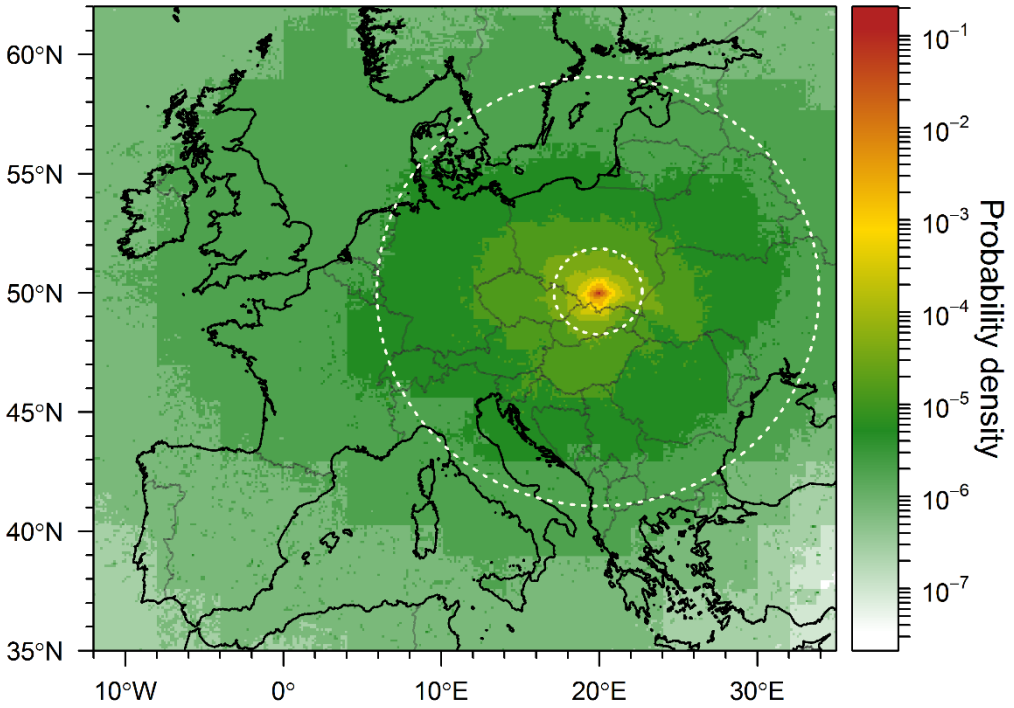

Figure 5.8. Footprint of the KRK station integrated for period 2012-2014. Shown is the probability density function defined as the ratio of total footprint element from a single grid cell divided by sum of footprint elements over the whole domain. White circles denote 200 km and 1000 km distance from the station.

simulated every 3 hours, since 01.01.2012 until 01.10.2014 (excluding the data from 11th to 26th of June 2013, for which the meteorological driving fields were not available).

Figure 5.8. shows the long-term footprint of KRK station as calculated by STILT. Main sources of influence are located in the close vicinity (< 200 km) of the station, with the relative influence of the emission sources located further at least two orders of magnitude lower. When footprint distribution is analysed on the local scale (Figure 5.9.), it is apparent that KRK station is best suited for analyses of the emission sources that are located inside of Kraków agglomeration, or in its close vicinity.

Footprint for KAS station (Figure 5.10) shows much smaller variability, with the maximum values of the total footprint function two orders of magnitude smaller than for KRK site. This stems from the fact that KAS station is located 700 m AGL, with PBL height often much lower than that value. Therefore many of the particles that arrive at the station were uplifted further away (via turbulence or convection) and didn't pass through the PBL close to the measurement site. KAS is not, however, completely free of local influences, as can be seen in Figure 5.11. Sensitivity to the sources located within approximately 50 km radius are c.a. an order of magnitude higher than from

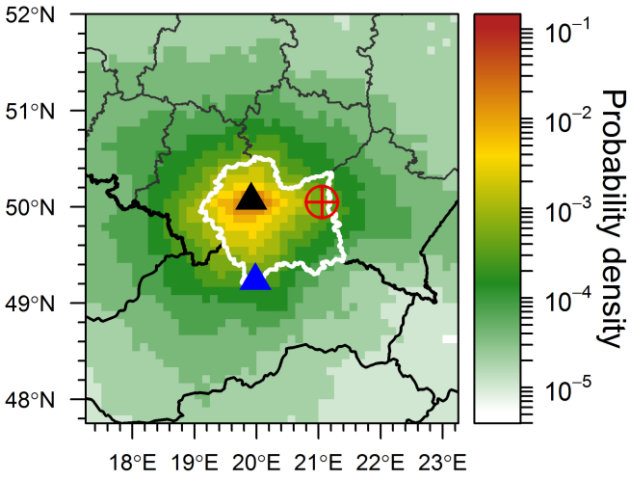

Figure 5.9. Regional footprint of KRK station integrated for period 2012-2014. Shown is the probability density function defined as the ratio of total footprint element from a single grid cell divided by sum of footprint elements over the whole domain. Triangles denote KRK (black) and KAS measurement sites. Red circle with cross marks the location of Z.A.T. in Tarnów. Małopolskie voivodoship marked with white borders.

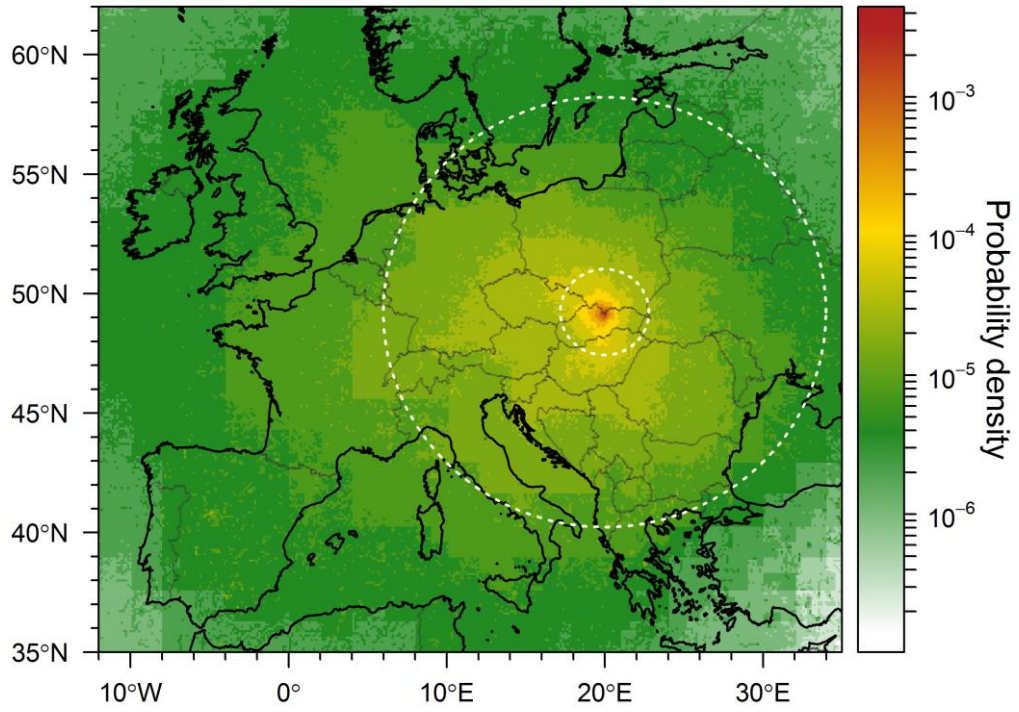

Figure 5.10. Footprint of the KAS station integrated for period 2012-2014. Shown is the probability density function defined as the ratio of total footprint element from a single grid cell divided by sum of footprint elements over the whole domain. Dashed circles denote 200 km and 1000 km distance from the station.

more distant ones. The relative importance of this area is low, however, as there are no significant emissions of N_2O in that area (see section 5.4). The influence of local sources on the results can be reduced if daytime data are excluded from the concentration record, as convective transport is the most probable cause of the footprint function increase in this case. Footprint of KAS station shows that the site can be used for the estimation of the strength of sources distributed over the region of central Europe, covering Poland, Slovakia, large part of Czech Republic, Hungary, and, to a lesser degree – Austria, eastern part of Germany, Romania, Balkan countries and Ukraine.

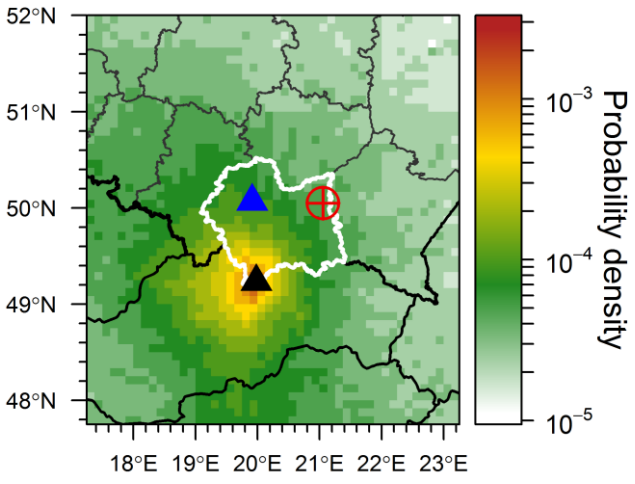

Figure 5.11. Regional footprint of KAS station integrated for period 2012-2014. Shown is the probability density function defined as the ratio of total footprint element from a single grid cell divided by sum of footprint elements over the whole domain. Triangles denote KRK (black) and KAS measurement sites. Red circle with cross marks the location of Z.A.T. in Tarnów. Małopolskie voivodoship borders are outlined in white.

Summarizing, the footprints calculated with STILT confirm the assumptions about the station's areas of influence presented in Chapter 3. For KRK site this means that the station's N_2O representativeness is heavily biased to the local area (i.e. Kraków agglomeration), and it will be difficult to draw information on the emission sources located beyond it. For KAS, smaller variability and a lack of significant sources of N_2O supports the choice of the station as a regional background monitoring site for N_2O (and other greenhouse gases as well).

5.6. Comparison of measured and modelled atmospheric N_2O mixing ratios.

A comparison between the mixing ratios predicted by STILT coupled to the IER N_2O emission database forms a basis for the following section. Through careful analysis of the differences between the modelled values and in-situ observations, additional insight into the transport patterns and the sources of influence responsible for elevated N_2O concentrations can be gained.

As the initial N_2O fields (term $C(\vec{x}, t_0)$ in equation (5.7)) were not available for STILT simulations, it was not possible to directly compare atmospheric observations performed at KRK and KAS stations with the predictions from the model. The latter procured only information on anthropogenic addition, coming from the inside of the model domain, to the continental background values. It was necessary to exclude this N_2O background from the observation records, and a procedure proposed to perform this task is described in section 5.6.1.

In order to establish the relative influence of the near-field N_2O sources located in Małopolska, 3 scenarios of emissions were compared for each of the stations for the years 2012-2014. In the first scenario (BASE), STILT footprints functions were coupled to the original IER N_2O emission database. In the second scenario (MP), the emission database was limited to the grid cells pertaining to the Małopolska voivodoship in order to estimate relative influence of the emissions from this area on the predicted concentrations. Similar approach was taken in case of third scenario (ZAT), where only the emissions from ZAT chemical plant in Tarnów (20.9°E, 50.0°N, Figure 5.9.) were considered. The plant, part of Grupa Azoty S.A., is one of the largest regional sources of N_2O, mainly producing nitrogen-based fertilizers and polymers, with nitric acid as well caprolactam facilities operating inside the plant. These known to be responsible for large amounts fugitive N_2O releases during the oxidation of ammonia, a necessary stage in both production chains (IPCC, 2006). Annual N_2O releases by ZAT reported in various bottom-up inventories for the past 15 years differ significantly: 187 Mg N_2O for 2000 (IER), 2010 Mg N_2O (EDGAR v 4.2) and 936 Mg N_2O (GESAPU) for 2010. This variation is also reflected in the emission values reported officially to the E-PRTR. Information contained in that database show that between 2007 and 2013, the total emission of N_2O varied between 3750 Mg (2007) and 1350 Mg (2013), with a generally declining tendency. It is unclear at this point if this variability comes from physical changes in the emission rates or differences in methodologies of bottom-up estimations used in these databases.

5.6.1. Decoupling of the regional background from N_2O measurement records.

Initial fields of N_2O concentrations for the STILT model (see eq. (5.7) in section 5.1.2) are usually obtained from a chemistry/transport model (e.g. TM5) which yields the respective concentrations on a coarse grid typical for a global model. These are necessary to predict total N_2O concentrations at the receptor points, and without them, only the additions coming from the modelled domain can be calculated. No global field of N_2O was readily available at the time of writing this thesis, therefore an additional procedure to subtract the regional background from detrended and deaseasonalised data from the measurement station is necessary in order to validate the STILT-IER results against *in-situ* observations.

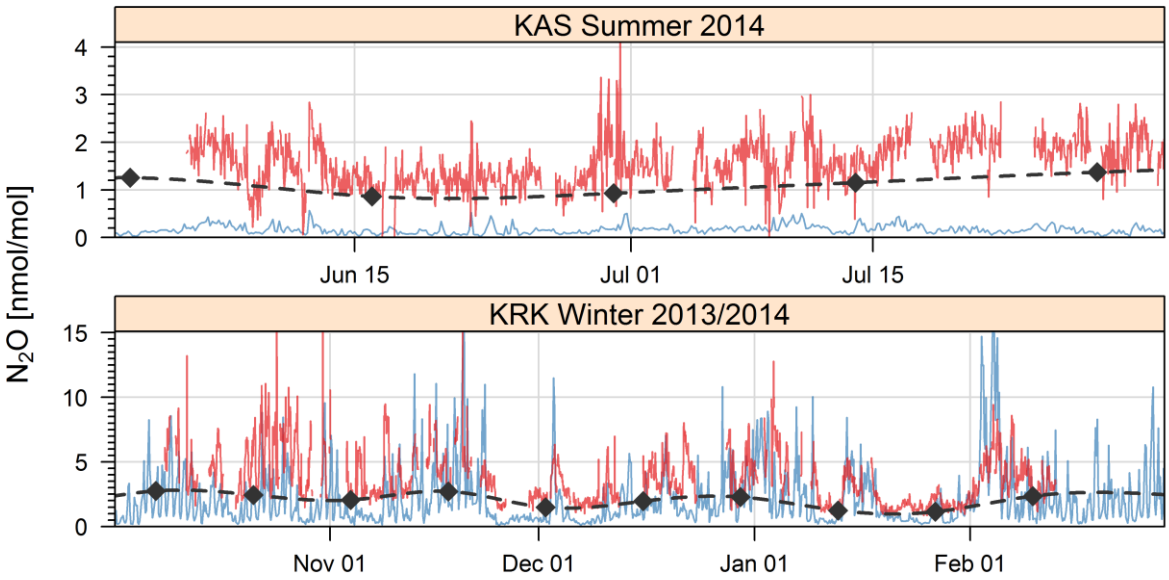

Figure 5.12. Decoupling of regional background. Detrended and deaseasonalised KRK N_2O concentrations – red; STILT-IER model results – blue; 10th percentile of bi-weekly statistics – black points. Smooth fit of the background – black dashed line.

The issue is clearly visible in Figure 5.12., on which selected fragments of previously calculated detrended and deaseasonalised (D&D, cf. section 3.5.2.) data from KRK and KAS stations is superimposed on the predictions of STILT-IER. The D&D data baseline values are elevated, most probably due to a large-scale synoptic variability that cannot be reproduced by the model due to a lack of initial N_2O fields.

In order to extract the regional part of the signal, a background-subtraction approach has been adopted. First, bi-weekly statistics were calculated for both D&D records. Second, 10th percentile values were selected as baseline values (to exclude possible negative outliers occurring due to measurement uncertainty). Third, a smooth curve was calculated from these baseline values, using a cubic interpolation (Forsythe et al., 1977) available in the R software (see *spline* function). The last step was the subtraction of this smooth curve from D&D data. The result of the decoupling can be seen in Figure 5.13. The procedure was applied to all available N_2O observations from KRK and KAS stations.

5.6.2. KRK urban station.

The results obtained from STILT-IER for KRK station span the period between 01.01.2012 and 30.09.2014. The first part of this section will discuss the validation of the obtained model results by comparison of the STILT results (BASE scenario) to the measurements performed at KRK during three periods:

- “winter”, spanning 01.10.2013-01.03.2014,
- “spring”, from 01.04.2014 to 01.06.2014, and
- “summer”, from 01.06.2014 to 01.08.2014.

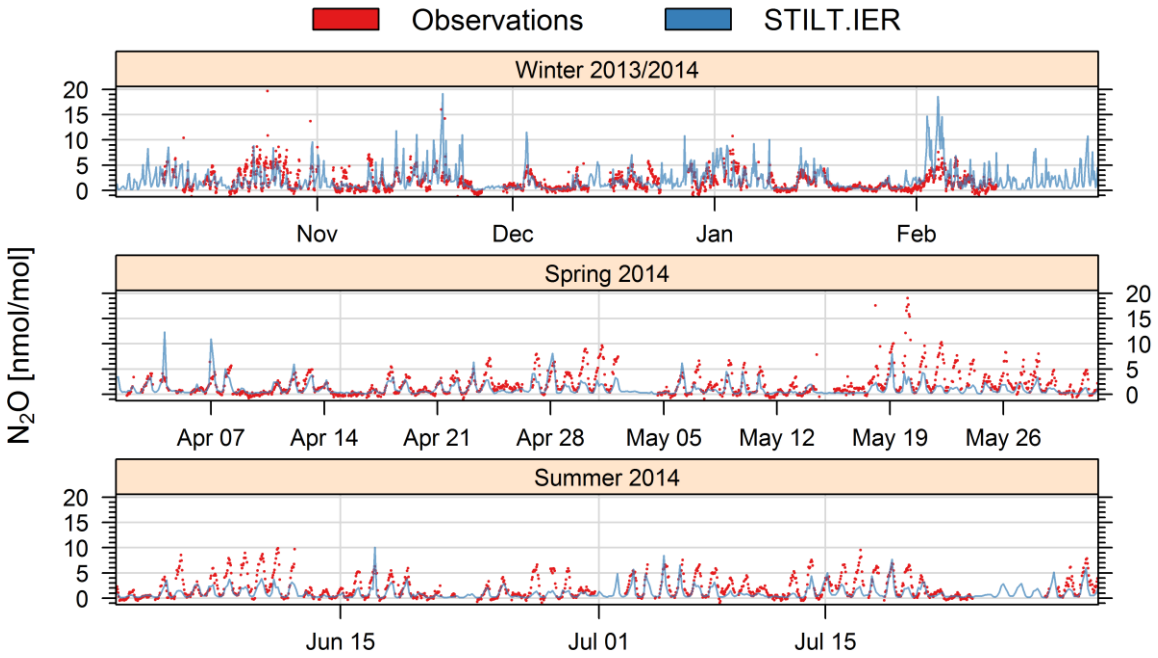

Figure 5.13. KRK STILT-IER model predictions (blue) against N_2O ambient concentrations measured by gas chromatography (red) for wintertime (top), spring (middle) and summer (bottom) period.

These three distinct periods were selected due to (i) the availability of long-term continuous measurement records of N_2O from KRK station, i.e. with no significant maintenance periods and (ii) different characteristics of the model response in comparison with the observations.

Results of the STILT N_2O validation for KRK station can be seen in Figure 5.13. The model performs best in wintertime, with most of the patterns occurring on a time-scale of days and weeks reproduced by the model framework, without the need to apply any scaling factors. The similarity of diurnal patterns is smaller, with some of the short-term peaks of N_2O simulated for KRK being higher than in-situ observations by a factor of three. For spring and summer, the overall tendency is opposite, with modelled results underestimating the values of N_2O in comparison with in-situ observations. The transition between these two distinct modes (underestimation and overestimation of mixing ratios) occurs in the spring, as can be seen in Figure 5.13. (middle).

The largest differences between the modelled results and the observations occur in the late spring and summer during night-times (Figure 5.14.), which points to two possible causes. The first is inappropriate attribution of sources strength in the IER database, and the

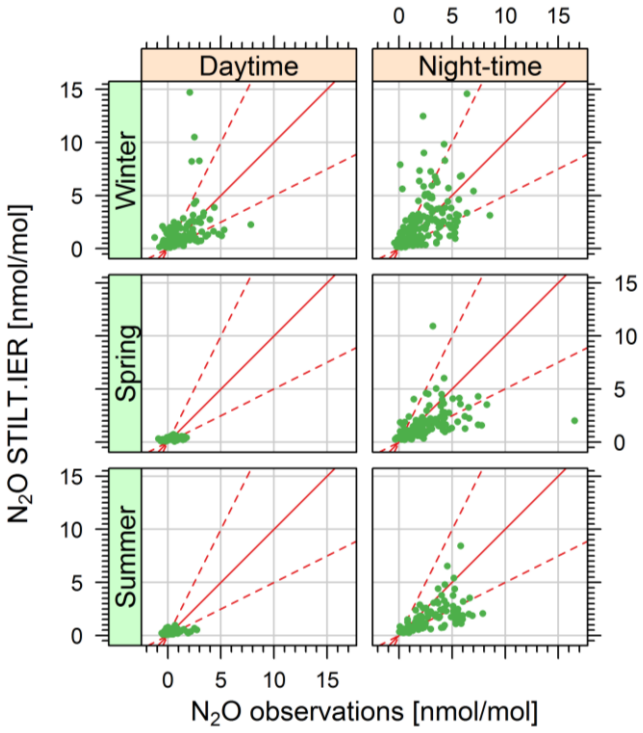

Figure 5.14. Scatterplot of modelled vs. observed N_2O values for springtime. Data from 00:00 and 03:00 were selected for night-time plot. For daytime plot, only values from 12:00 and 15:00 were selected Solid line marks 1:1 ratio. Dashed lines mark 0.5:1 and 2:1 ratios.

second is possible errors in the results of PBL parameterisations during strong and quickly-developing night-time inversions, typical for summer nights.

If the main source of the model-observation misalignment is the wrong attribution of sources strength in the emission database, then the time when over-/underestimation mode change occurs would suggests correlation with the vegetation period, and thus with the biogenic activity inside the station's footprint. The hypothesis of stronger than expected biogenic emissions is supported by the findings from chapter 3 (sections 3.8-3.10), where simultaneous observations of N_2O concentrations and meteorological parameters also suggested the importance of biological sources for the N_2O observed in Kraków.

Erroneous calculation of transport, and in particular, of the values of night-time PBL height, could be another source of observation-model misalignment. It has been demonstrated in the past that the PBL height is difficult to simulate, especially in the stable conditions (Lin et al., 2003, Shin and Hong, 2011). The most reliable way of estimating the role of the PBL parameterisation in the errors of modelled concentrations is to use *in-situ* observations, e.g. with LIDAR or SODAR (cf. Zimnoch et al., 2010, 2014).

Estimating the influence of misalignment of database sources (i.e. their strengths, locations and temporal patterns) on the observed model – observation differences is much more difficult, due to multitude of configurations which need to be tested. A most desirable course of action would be to establish an inversion framework, which would allow to solve the issue numerically, albeit this was outside of scope of this PhD. A simpler way might be to compare the results obtained with other available emission databases (e.g. EDGAR, GESAPU). Such a study is planned in the near future.

Source apportionment has been performed for KRK station using the results from three scenarios: BASE, MP and ZAT, as described in section 5.6. The results (Figure 5.15.) indicate that during night-time, the concentrations at KRK station are influenced mostly by the near-field sources (located in Małopolska voivodoship), due to frequent development of the stable inversion layer. The relative

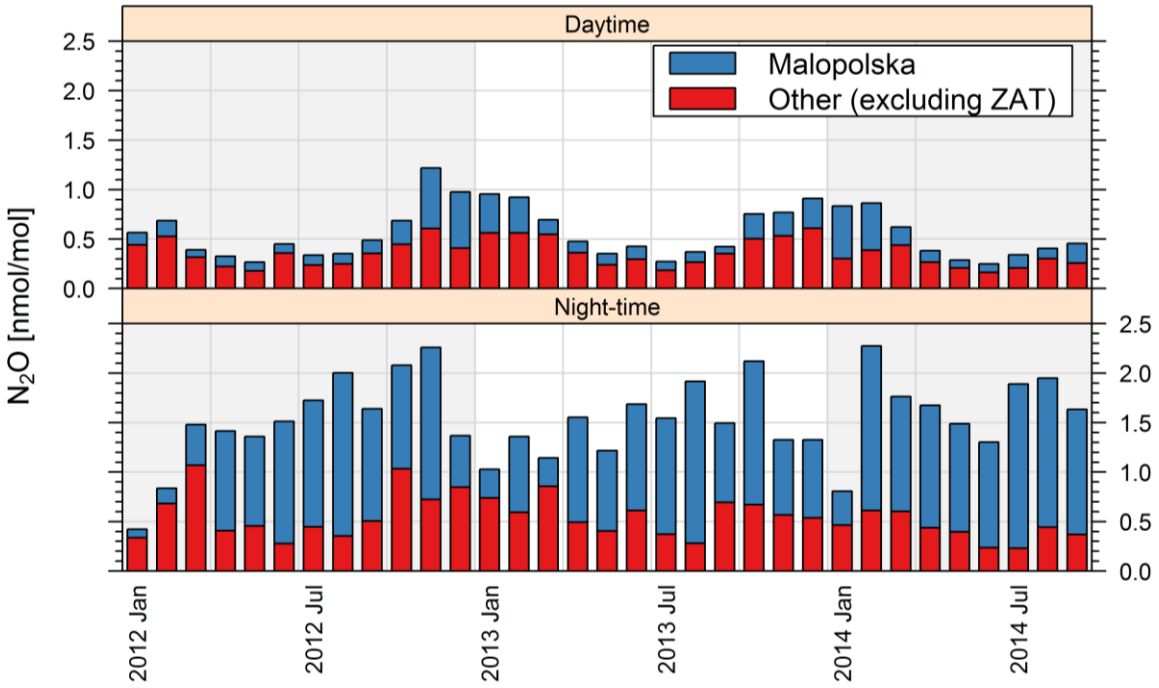

Figure 5.15. STILT-IER N_2O source partitioning for KRK station. Shown are monthly medians of the respective influence enhancements. 3 scenarios described in the text were analysed. ZAT scenario not displayed due to negligible values. Daytime values were selected between 10:00 and 15:00 local time, night-time values: between 23:00 and 04:00 local time.

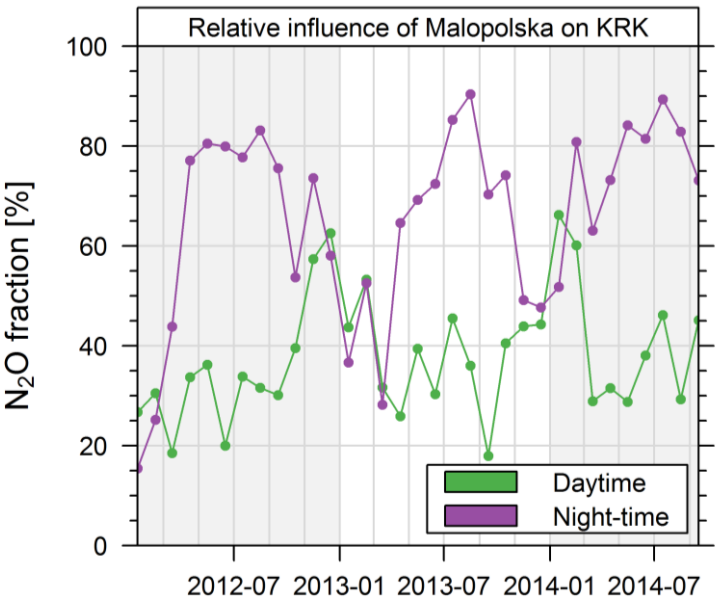

Figure 5.16. Median of monthly statistics of N_2O fractions related to emissions from anthropogenic sources in Małopolska voivodoship. Daytime values were selected between 10:00 and 15:00 local time, night-time values: between 23:00 and 04:00 local time.

influence of these local sources (Figure 5.16) varied throughout the year, reaching the lowest values in winter (20-50%), and highest in the summer (more than 80%). During daytime, the relative importance of long range transport increased, and STILT predicted that during summertime up to 80% of N_2O addition to the background had sources located outside of voivodoship. In winter, the atmospheric dynamics was reduced, and N_2O emitted from near-field was not transported vertically to the same degree, resulting in high relative importance (50-70%) of local sources in the N_2O measured at the station.

The results of ZAT scenario show low overall influence of nitrous oxide emissions from that facility on the N_2O concentrations measured at KRK, never exceeding values of 2.5 nmol/mol (Figure 5.17.). While this value is close to the lower limit of measurement precision characterizing in-situ measurements at KRK station, it might be possible to use STILT framework to select a range of events during which the signal from ZAT might be significant. These have proven to be difficult to capture, however, as the diurnal amplitude of N_2O measured at KRK was too high to easily discern the local background to which the N_2O from ZAT is being added. A similar experiment has been performed for KAS record, where stable N_2O baseline should allow to discern the peaks caused by ZAT emissions more easily

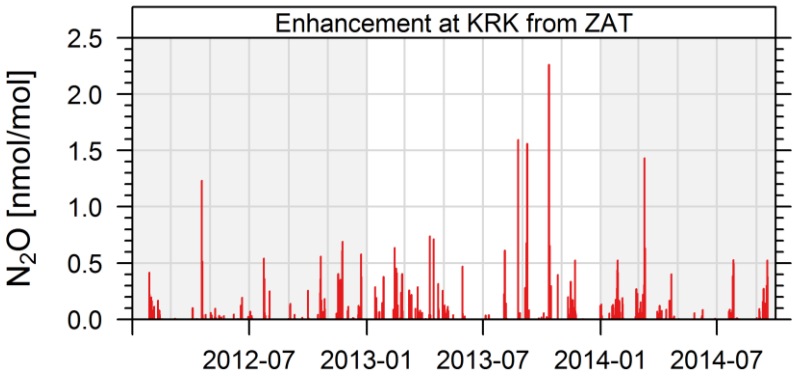

Figure 5.17. Predicted N_2O additions at KRK from ZAT facility.

.

5.6.3. KAS mountain station.

The main difficulty in analysing atmospheric composition at high-mountain stations arises from the complexity of local orography, which is very challenging for numerical modelling of transport processes. High-altitude sites can be affected by valley winds blowing along the terrain slope and

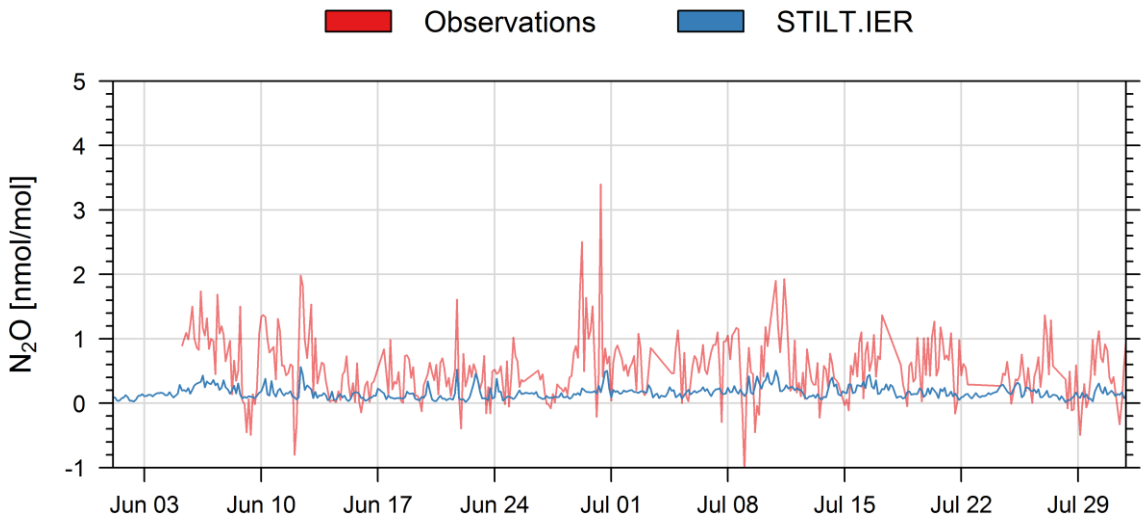

Figure 5.18. KAS STILT-IER model predictions (BASE scenario, blue) against N_2O ambient concentrations measured by gas chromatography (red) for summertime period.

advecting the air masses enriched in pollutants emitted at lower altitudes. This effect was shown to be very important for diurnal variation of greenhouse gases concentrations measured at KAS (2003, Necki et al., 2013), and is not fully reproduced in transport models even if high spatial resolution (2 km x 2 km) is used in the simulations (Pillai et al., 2011, Sheridan and Vosper, 2012).

Validation of the STILT-IER modelling framework (Figure 5.18.) reveals the difficulties associated with such analyses in the high-mountain environment. The overall level of the ambient N_2O signal measured at the station is low, with the observations variability higher than the predicted additional N_2O emitted by the European sources (BASE scenario). From the modelling perspective, low predicted values are accompanied by large relative uncertainties that stem from possible transport errors, misrepresentation of the receptor point's location in the model domain and from lack of

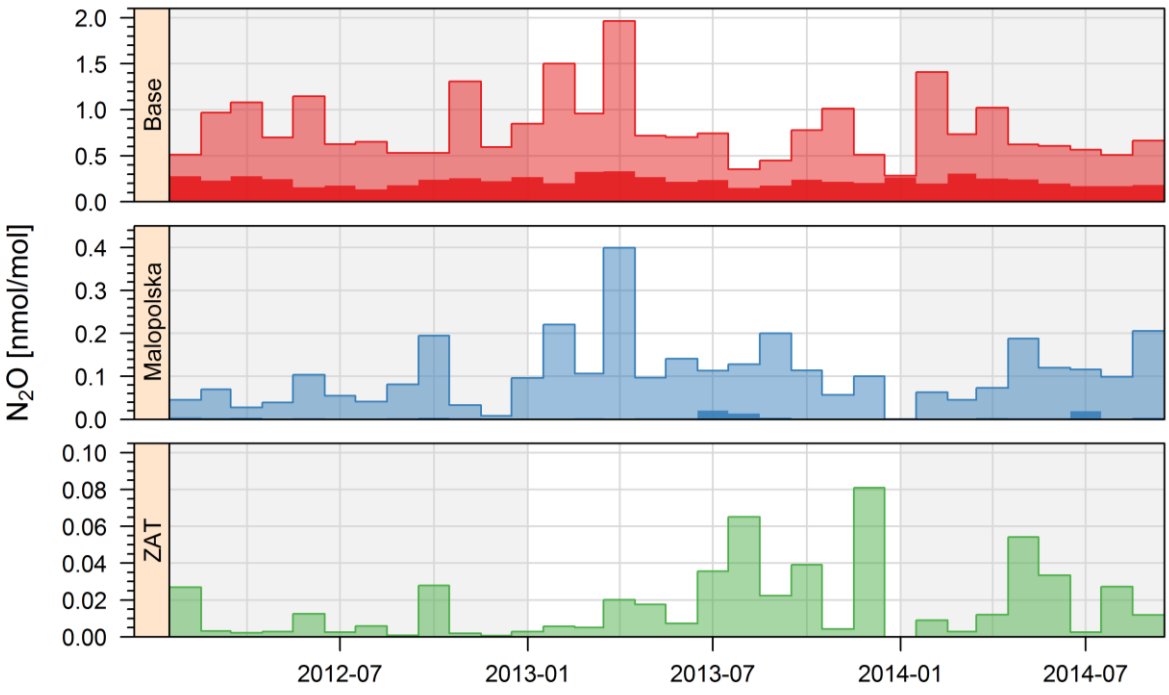

Figure 5.19. Statistics of predicted enhancements of N_2O at KAS station as calculated by STILT-IER. Light shaded areas denote monthly maxima. Dark shaded areas denote monthly medians (not distinguishable for ZAT scenario due to low value).

representation of very local effects (e.g. foehn and katabatic winds) that could significantly influence the initial particle dispersion, and thus change the overall footprint fields dramatically.

Predicted values of N_2O mixing ratios usually remain below 1 ppb, even for base simulation scenarios, where all available European sources were included, with maximum recorded enhancements close to 2 ppb (Figure 5.19., top). The relative influence calculated from Małopolska voivodoship (MP scenario) is much lower, with monthly medians of N_2O concentrations never reaching above 0.05 ppb, and maximum recorded enhancement close to 0.4 ppb (Figure 5.19., middle). This is in line with identified difficulties in application of gas chromatography to analyse the European N_2O balance (Corazza et al., 2011), and underlines the need for analysers with enhanced performance, characterised by reproducibility level an order of magnitude lower than that offered by present GC methodology.

Despite of this situation, simulations by STILT-IER model can be used to help interpret some features of N_2O records available for KAS station. In the scope of this work, an attempt was made to estimate the influence of emissions from a strong, single point-source (ZAT industrial facility) on the N_2O concentrations measured at KAS. Although nitrous oxide emitted by this large chemical plant, located approximately 150 km north-east of Kasprowy Wierch is generally not traceable with the analytical technique in use at this station (gas chromatography), the model simulations suggest that single, short-term episodes of elevated N_2O can still be detected under favourable meteorological conditions.

Before simulations with STILT-IER were performed, however, a feasibility study was performed with the use of a classical Gaussian plume model (equation (5.2), see section 0.), in order to estimate possible range of N_2O concentration changes due to emissions from ZAT facility. The parameters used in the calculation procedure are given in Table 5.2. The results (Table 5.3) depend linearly on the emission strength of the ZAT facility that is assumed. Several estimations were considered, with ranges of resulting concentrations from approximately 0.010 ppb (IER), to 0.107 ppb (EDGAR v4.2). These values are low, but indicate that in the favourable conditions, the emission plume from ZAT facility might be measurable by the equipment available there.

Table 5.2. Parameters used for Gaussian plume model.

Parameter	Value	Unit
Distance to KAS	110	km
Stack height	30	m
Plume rise	10	m
Mean wind speed	4	m/s
Terrain roughness	0.3	
Stability index	4	
Receptor height (KAS)	1793	m AGL

Table 5.3. N_2O addition at KAS as predicted by the Gaussian plume model for different emission databases.

	N_2O Emission [ton/year]	KAS concentration [nmol/mol]
E-PRTR (2013)	1350	0.072
E-PRTR (2007)	3750	0.200
EDGAR v4.2	2010	0.107
IER	**187**	**0.010**
GESAPU	936	0.050

In the second step, STILT-IER framework was used to simulate the ZAT additions to the N_2O measured at KAS site (Figure 5.19., bottom). The STILT simulations indicate that the events when the air masses arriving at KAS have been influenced by ZAT emissions are not frequent (33.5%). This is not surprising, as (i) the spatial extent of this particular source is comprised of a single grid cell and (ii) ZAT is located NE of KAS site, not on a preferential, westerly direction. Only several cases when the fraction of ZAT-emitted N_2O comprised more than 5% to the total enhancement predicted

by STILT were recorded during the 2013-2014 period. Median value of that fraction for the presented period was very low – only 0.04%.

It is important to note that the predicted N_2O ZAT fraction may be underestimated due to the low values of N_2O releases values attributed to this source by the applied emission database (IER). If the emissions from EDGAR v. 4.2 were used, then the median fraction of ZAT N_2O would be 0.44%, with the highest recorded value of almost 88% of the enhancement coming from that facility. Regardless of that, predicted N_2O enhancements attributed to ZAT would still remain low. ZAT emissions would need to be at least an order of magnitude larger to be detectable at Kasprowy Wierch.

The relation between the STILT-IER and in-situ observations shown in Figure 5.18 cannot simply be attributed to misrepresentation of the fluxes in the emission databases, but can also stem from errors in the modelled transport. These in turn can be caused either by the model parameterisations or might be associated directly with the chosen release location, which was arbitrary assigned so that the height of the station in the model domain, relative to the mean sea level, was the same as in reality. Due to the coarseness of the horizontal resolution of the underlying meteorological field, however, the predicted wind fields at the chosen height might not have represented the wind fields around the station well. This is especially important for mountain sites like KAS station, for two distinct reasons. First, the vertical profiles of the wind are crucial in the first hours of simulation. If the station release point was misrepresented, then the initial wind direction at the model release point height might have been slightly different, resulting in errors in the assigned footprint. Second, the station height is crucial from the PBL scheme point of view. The higher the station location in the model is chosen, the longer the simulated air parcels will spend above the PBL, where the concentrations are lowered due to mixing with air masses without N_2O enhancements from the surface. The long-term effect of that phenomenon in the simulation would be overall lower values of predicted concentrations.

It was initially planned that the independent estimations of the ZAT source strength will be produced by applying a simple scaling-factor approach to the predicted STILT-IER N_2O enhancements, which is possible thanks to the linearity between fluxes and receptor concentrations in the model. The envisioned procedures included a several-step algorithm. First, the events where influence from ZAT was predicted to be high were needed to be found and correlated with the observable increase in the N_2O mixing ratios in the in-situ data. Once such an event was found, the second step was to perform a least-squares fit regression in order to find an optimal correction factor, by which the ZAT emission values were to be multiplied to assure the best fit, thus procuring the estimated emissions without formally performing the inverse procedure.

However, due to overall low signal to noise ratios obtained from the in-situ N_2O record and the inability to estimate the location representativeness error, such estimation was not performed at this point, as – in the opinion of the author of this thesis – it would not yield sufficiently precise results. It might be possible to improve the proposed method, however, by obtaining the high-resolution meteorological data (100 m x 100 m or better), thus reducing the influence of misrepresentation of the station model height. This was outside the scope of this work, but is considered as a topic of a future study.

Nevertheless, STILT in combination with IER can still be used as a qualitative indicator that can identify synoptic conditions which potentially may allow for the occurrence of ZAT-caused events at KAS site. In case of very high enhancements, it might be possible to plan a sampling-collection campaign for subsequent analysis of the isotopic composition, which could also provide information on the source strength. However, such a campaign would first require to obtain information on the isotopic composition of the ZAT facility sources. Another difficulty is that such high-pollution events

are very rarely recorded at KAS station. A more feasible approach might be to use a collection point closer to the ZAT facility itself. Providing that a well-planned sampling campaign is performed, the proposed methodology can be applied to independently verify the emissions from a strong point-emission source such as ZAT.

6. CONCLUSIONS AND OUTLOOK

Growing impact of anthropogenic activities on the Earth's system functioning, realized on a wide array of spatial and temporal scales, has become a part of our everyday life. There are two most serious environmental threats the human civilization is currently facing: (i) progressing climate change, induced by ever-growing emissions of greenhouse gases into the atmosphere, and (ii) growing ecosystem strain that can be attributed to large inputs of reactive nitrogen compounds in the form of fertilizer and manure.

Nitrous oxide lies at the intersection of these two central environmental problems. It is both a nitrogen compound, released mainly through microbial processes that occur in a multitude of terrestrial, aquatic and marine ecosystems, and a potent greenhouse gas and ozone depleting substance, also emitted due to industry and fossil-fuel burning activities.

Despite of its importance, the global budget of N_2O and the factors that drive its emissions are highly uncertain. These uncertainties need to be reduced if the mitigation measures aimed at diminishing the negative effects of the nitrogen excess and greenhouse gas releases, are to be effective. In order to achieve this goal, better knowledge of emission and transport patterns of N_2O needs to be obtained on a wide range of spatial and temporal scales.

6.1. Conclusions.

The presented regional study of nitrous oxide circulation in the region of Małopolska was aimed at providing a detailed description on the transport and emission patterns of this gas on a scale usually not considered in the available bottom-up or top-down assessments. The limited study area should have, in theory, allowed for more accurate source attribution, thus enhancing the precision of available emission estimates and their driving factors. At the same time, characteristics of the chosen study area required that most types of known sources of N_2O needed to be taken into the account.

The presented thesis encompassed three distinct parts, each focused on fulfilling a set of specific goals.

The first part of the work (Chapter 3) was focused on obtaining high-quality records of atmospheric N_2O concentrations at two stations of distinct characteristics (Kraków urban station – KRK, and Kasprowy Wierch mountain station – KAS). The obtained dataset is now available to the scientific community upon request. The results from KRK and KAS stations were robustly analysed in order to characterise the transport and emission of N_2O in the southern Poland. The comparison between the KAS mountain station and other continental background sites (Section 3.6) revealed elevated background values, most probably caused by the continental emissions of N_2O. It also hinted at possible stratospheric influences in the station's record, although this could not be fully confirmed at the moment. Temporal characteristics of the KRK and KAS stations were then compared (Section 3.7), revealing significant local influences at the urban site. Unexpectedly, the local sources were more pronounced in the spring and summer times, suggesting that predominant source of N_2O at KRK site is of biogenic rather than anthropogenic origin. This conclusion was supported through

comparison between records from KRK and from a tall tower of Białystok (BIK; Section 3.8), as well as through coupled concentration and meteorology analyses (Sections 3.9 and 3.10).

The second part of this work (Chapter 4) was aimed at quantifying the N_2O emissions from soils in Małopolska region. Field work comprised four intense *in-situ* measurement campaigns that utilized well-established non-steady state chamber methodology coupled with gas chromatography analyses of the collected samples. Two campaigns were performed at selected agricultural sites, on which species of crops typical for the region were planted. All the sites were located in the ZDHAR institute, responsible for testing crop species available on the markets under varying treatment methods. This has provided a unique opportunity to test the influence of treatment methods (e.g. tillage versus shallow-tillage) on N_2O emissions. Another two campaigns were performed on the urban soils which, to the best of author's knowledge, have not been previously studied in the Central and Eastern Europe with respect to N_2O emissions.

The goals set in this part of the presented work were not achieved completely. While the measurements were performed in intense campaigns spanning two to four weeks, with analyses every three to four days, the obtained information turned out to be insufficient to provide a realistic annual budget of N_2O emissions. The main cause was too high spatial and temporal variability of the N_2O flux measured at the sites. Thus, it was not possible to scale-up the obtained emissions and to provide realistic, independent verification of N_2O emissions from agriculture for the Małopolska region.

Nevertheless, valuable knowledge and experience have been gathered. The results show that agriculture in Małopolska is a significant source of N_2O, and that the temporal variability of that source is high (Section 4.4.). Rapid changes in emission values were observed following the fertilizer application and subsequent rainfall, in line with previous scientific findings. The emission values obtained through *in-situ* measurements suggest that the total annual releases from agriculture in Małopolska are probably smaller than those previously reported in scientific literature for similar conditions. Even with N_2O production strengthened by addition of fertilizer, the observed average N_2O emission values are mostly in the lower part of distribution of similar emissions reported previously from long-term measurement campaigns. This finding is consistent with lower overall annual N addition (per hectare) in Małopolska, when compared to Western Europe. The comparison between various crop management techniques showed significant differences in N_2O releases from the fields under different tillage techniques, with higher N_2O emissions for rapeseed on the tilled crop fields, and the opposite for wheat. The cause behind the observed differences is unclear at the moment and require further studies.

Similar to the agricultural sites, the urban lawns and meadows of Kraków have also shown consistent positive emissions, correlated with precipitation events (Section 4.5.). These emissions were not negligible in comparison to the agricultural fields, and in some cases exceeded them. The reason behind these elevated N_2O releases is unknown, as no fertilizer was applied at the surveyed sites. It is possible that nitrogen inputs from such a large human settlement are sufficient to generate increased N_2O emissions, either through nitrogen deposition or other processes. Research including measurements of other forms of reactive nitrogen would be required in order to address that question.

It is important to note that the obtained N_2O flux data must be interpreted with care in view of high spatial variability of N_2O emissions from agricultural fields. The uncertainty stemming from this phenomenon was estimated to be high.

The third part of the presented work (Chapter 5) was focused on coupling the information obtained in the first and second part of the study within a Lagrangian numerical modelling framework. At the planning stage, it was assumed that the use of Stochastic Time-Inverted Lagrangian Transport model (STILT), connected with one of the available emission databases (IER database) and external meteorological data, will make it possible to: (i) estimate the ranges of influence pertaining to each of the chosen ambient N_2O measurement sites (KRK and KAS stations), (ii) predict N_2O mixing ratios at these locations, (iii) compare these predictions with observations, (iv) modify the chosen sources strength so that the predicted results best fit the observations, thus providing the updated values of the emissions.

Most of the tasks set in Chapter 5 were successfully completed. Long-term station footprints (i.e. areas of influence) were calculated for both KAS and KRK stations (Section 5.5.), revealing distinct differences stemming from the atmospheric transport patterns. Higher sensitivity to local influences in case of KRK was confirmed, with probability of source detection in the close vicinity (c.a. 50 km) being at least two orders of magnitude higher than in case of KAS station. At the same time, the sensitivity of KAS station to more distant sources was shown to be higher than for KRK, supporting the choice of KAS as a regional background monitoring station.

Comparison of the STILT-IER results with N_2O observations performed for KRK station (Section 5.6.2.) displayed some interesting aspects. The model predictions were able to capture the main features of the baseline changes associated with synoptic scale phenomena. During wintertime period (October 2013 – February 2014), night-time N_2O mixing ratios simulated by STILT-IER were usually overestimated, while during spring and summer these were underestimated. The source of this discrepancy is unclear. One of the possible explanations might be the underestimation of the biogenic sources in the selected emission database, which would support the conclusions of the analyses described in Chapter 3. Further investigations are needed, though, as the role of the misalignment of the night-time planetary boundary layer height remains unclear.

The source partitioning performed with help of STILT-IER revealed that the relative importance of N_2O sources located in Małopolska on the concentrations observed at KRK station was high, albeit variable in time. The medians of day-time fractions of N_2O enhancements ranged from 20% to 60%, with maxima in the wintertime most probably associated with decreased atmospheric dynamics. These enhancements were usually low, however, with monthly median values never exceeding 3 ppb, pointing to the necessity of high-quality observations for verification of the modelled data.

A series of events were identified, where observations could potentially help to estimate the emissions from Zakłady Azotowe in Tarnów industrial plant (ZAT). However, the enhancements predicted by the model (2.5 ppb or lower) were low when compared to the diurnal amplitude usually observed at KRK station. Consequently, an attempt to independently verify ZAT emissions was not made. The reason was that the probability of the signals from ZAT to be successfully distinguishable from the diurnal N_2O variations (caused by sources located in close proximity) was estimated to be low.

Similar approach was chosen when analysing the predictions of STILT model for KAS station (Section 5.6.3.). In this case, however, the level of enhancements predicted by STILT-IER was at least an order of magnitude lower than in case of KRK, close to the detection limits of the utilised equipment. In order to compare these predictions with the N_2O record at KAS station, much higher precision of ambient measurements would be required. Such a level could not be achieved even with significant modifications of the GC-methodology utilized at KAS station and usage of the modern optical instrumentation is recommended in the future.

Several important issues have emerged that will help in future numerical experiments at KAS station. The first is the inherent difficulty in representing the high-altitude station in the modelled domain, which is critical in case of modelling the transport patterns of measured tracers. The misalignment of the receptor point (i.e. station) in the vertical direction could lead to large errors in the transport patterns of the modelled particles, and in consequence – to large errors in predicted concentrations. The recommended solution is an increase in the spatial resolution of the modelled domain which would diminish the negative effects of station representation, and at the same time have the added values of including the typically mountainous advection effects, e.g. valley winds, which can have large impact on the initial wind fields.

Due to the described difficulties, the verification of the emissions by ZAT through comparison of the modelled results with KAS observations was not attempted. The probability of obtaining statistically significant results was estimated to be low. A limited survey was performed in order to estimate the level of possible N_2O enhancements occurring at KAS station due to ZAT emissions using Gaussian plume and STILT-IER frameworks. Gaussian model was run for several ZAT emission values, reported in various publicly available databases. Predicted N_2O enhancement have not exceeded 0.2 ppb under most favourable conditions. STILT-IER framework predicted a similar maximum level of possible N_2O concentration increase. However, as IER database has low emissions attributed to the ZAT facility, these maximum values might be underestimated, thus suggesting that rare events of detectable N_2O enhancement of ZAT origin might occur at KAS station, and that STILT-IER might be used to identify, or even predict, such events.

6.2. Outlook.

The presented PhD thesis summarizes the large amount of data and new knowledge obtained in studying various aspects of nitrous oxide circulation on a regional scale. Despite of significant efforts put into measurements and analyses, the overarching goal of detailed description of N_2O budget of Małopolska region was only partly achieved, due to the inherent complexity of the tackled scientific issue. Several pathways of research have emerged that still need to be pursued to reach this goal and which can built upon the presented work.

Measurements of N_2O ambient concentrations at KAS and KRK stations will be continued, providing more data needed for verification of the models and statistical analysis. These could be significantly improved if both of the stations were to be equipped with state-of-the-art optical spectroscopic instruments, capable of high-precision and high-frequency analyses of the ambient air. Another interesting aspect would be associated with isotopic analyses of ambient N_2O, which could allow for independent, near-real-time source apportionment. There is an ongoing effort to obtain such instrumentation in the near future. The same optical instrumentation would be also valuable in N_2O soil flux measurements, providing new opportunities for research, including: (i) continuous measurements at a fixed location with the eddy-covariance technique that would allow to build N_2O annual budgets, (ii) multi-site chamber measurements, (iii) process analyses, using isotope labelling and possibly isotopomer analyses.

With respect to numerical modelling of atmospheric N_2O transport, several research pathways can be explored as a follow-up of this work. These include coupling of the STILT model to other available emission databases that provide information on emissions from various IPCC sectors. The results of such simulations will allow for high-frequency source apportionment not only by geographical

location (like those described in Chapter 5 of the presented work), but also by sector, further enhancing the information on regional N_2O emissions and transport patterns.

Another scientific issue opened up by the presented work is the implementation of high-resolution numerical modelling in the analyses of KAS station data. This would require independent calculations of meteorological field with one of the available models, e.g. Weather Research and Forecasting model (WRF). Some initial steps in this direction have already been taken.

ANNEX A. CALIBRATION PROCEDURES AND UNCERTAINTY ESTIMATES FOR ATMOSPHERIC MEASUREMENTS.

Measurements of atmospheric nitrous oxide described in this study have been performed in 2013 and 2014 at Kraków (KRK) and Kasprowy Wierch (KAS) monitoring stations using a well-established GC-ECD techniques. In the framework of this PhD, significant modifications have been made to the existing infrastructure and measurement methodology in order to assure high quality (accuracy and precision) of N_2O measurements performed at both sites, necessary to quantify low variability of N_2O concentrations in the atmosphere.

Changes to the equipment set-up, appropriate calibration methodology and implementation of analytical uncertainty estimates recommended by the InGOS project made possible appropriate interpretation of the measurement results presented in chapters 3, 4 and 5. A detailed description of the analytical system that was established and used in the framework of this work is presented below.

A.1. Equipment set-up.

Both monitoring stations described in this thesis had already functioning infrastructure for measurements of greenhouse gases. However, no long-term, consistent records of nitrous oxide mixing ratios have ever been made available to the scientific community. At KAS and KRK stations, gas chromatography methods were employed for atmospheric greenhouse gases measurements, using GC units equipped with FID (*flame ionization detector*) and ECD (*electron capture detector*) for simultaneous measurements of CH_4, CO_2 (FID), N_2O and SF_6 (ECD).

A detailed description of KAS station GC-FID system set-up has been published elsewhere (Nęcki et al., 2003) The description given here will be limited to the details that are important in the context of N_2O measurements. Configuration of the GC system installed at KRK station is analogous to that operated at KAS site, with only minor differences which shall be highlighted in the description, where necessary. Figure A.1. presents layout of the inlet system currently in use at KAS and KRK station.

Ambient air is sampled on the roof of the building, at approximately 2 meters above the local ground in case of Kasprowy Wierch and 19 meters in case of Kraków. At KAS station the inlet is heated to avoid ice clogging during winter. The air is sampled by a diaphragm pump (KNF N86 KN.18) with the flow rate of approx. 150 ml/min, regulated by a needle valve. Slight over-pressure maintained in the inlet system limits the possibility of sample contamination by indoor atmosphere of the building. The sampled air passes through a cryogenic dryer operating at approx. -60°C, to ensure that H_2O mixing ratio in the injected sample is sufficiently low. To ensure constant air flow in the inlet line, a release valve has been installed prior to the drying module.

After drying, the sampled air passes through the multiport inlet system (Gas selector), containing a multiposition valve (Vici Valco, 16 port, SD) with a microelectric actuator. The inlet system operating at KRK is described in detail by Nasulewicz (2009). At KAS, a modernized version of the inlet system

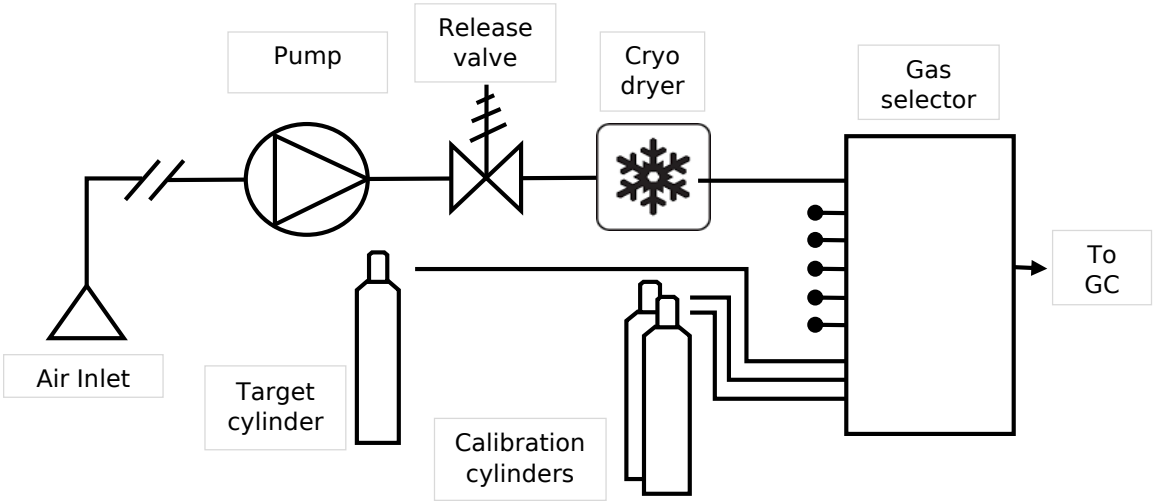

Figure A.1. Simplified layout of the inlet system used at KAS and KRK stations.

was installed, with a mass flow meter (Aaalborg, GFM Mass Flow Meter) and a cut-off valve to ensure that at least 150 ml of air sample has been flushed through sample loops in the GC unit. The communication between GC software (Agilent Chemstation) and the inlet system is achieved by "VaBo" software, written by J. Bartyzel (LabView code). Output from the selector valve is connected to the GC unit. Special care has been taken at both stations to ensure that every sample type (ambient air, secondary laboratory standard, target gas) has a similar flow rate (±10% of the adopted flow rate) to minimise possible differences in the pressure of the sample at the moment of injection.

The measurements have been performed with the use of automatic gas chromatographs: HP5890 (KAS) and HP6890 Plus (KRK). Both are equipped with a flame ionization detector (FID) and an electron capture detector (ECD). The sample loops of both detector lines are connected in series, which allows for simultaneous analyses of the mixing ratios of CO_2 and CH_4 on the FID line, and N_2O and SF_6 on the ECD line. Full analysis takes between 9-11 minutes (station-dependent, also modified throughout the described period). While ECD analysis could be successfully performed in approximately 5 minutes, longer time is needed due to long retention time of CO_2 chromatographic peak on the FID line.

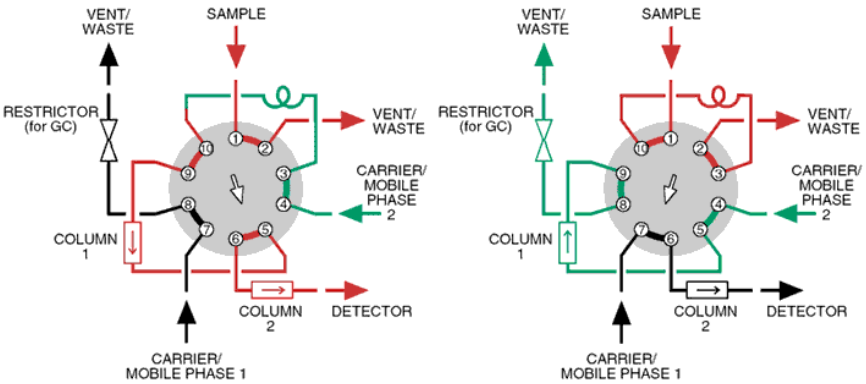

Figure A.2. A back-flush configuration of an µ-ECD GC-system used at KRK and KAS stations. Detailed description in text. Image from of www.vici.com.

For N_2O and SF_6 measurements, a double-column system (Figure A.2.) was used in the back-flush mode, with N_2 as a carrier gas. At the start of the analysis, the air from the sample loop is compressed by high pressure of the carrier gas. Then, the sample is eluted into the pre-column (2m Haysep Q 80/100), where gaseous compounds from the sample are initially separated. First stage lasts for 3 min, which allows only O_2, NF_3, N_2O and SF_6 to enter the analytical column (4m Haysep Q 80/100), after which the valve is switched again to initial position. The gases with higher retention times that are still present in pre-column are then flushed in the opposite direction and

vented outside the system. Compounds in the analytical column are eluted to the ECD detector for analysis and vented afterwards.

A.2. Measurement and calibration methodology.

The immediate result of a gas chromatographic analysis is a time series of the detector signal (*chromatogram*), which is a complicated function of mass and composition of the gas mixture that is flowing through that detector at any given time. The change in the signal occurring when eluted component emerges from the column and enters the detector volume produces a peak in a chromatogram, which cannot be related to the mixing ratio of a measured compound in a direct manner. A calibration procedure is required, which translates the peak parameters (peak height or peak area) to the mixing ratio of the measured compound. This is achieved through usage of one or more reference air mixtures, often described as *calibration standards*.

Reference air mixtures for greenhouse gas measurements are prepared by scientific centres (*Central Calibration Laboratories*, CCL) recommended by World Meteorological Organization (WMO). In case of nitrous oxide, Earth System Research Laboratory (ESRL) of National Oceanic and Atmospheric Administration (NOAA) serves as a CCL, providing sets of gravimetrically-prepared reference gas mixtures of certified composition. This set of reference gas standards defines a *primary scale* (for nitrous oxide – currently WMO N_2O X2006A). According to WMO recommendations (WMO, 2013), any measurement of greenhouse gases must be directly traceable back to the primary scale. In most cases, this is achieved through distribution of secondary and tertiary standards by the calibration facilities, which can be obtained by any interested scientific institution, where they usually become *primary laboratory standards* (PLS) – a direct link to the original scale of measurements.

From a scientific point of view, a most desirable method of scale transfer between *in-situ* measurements and the primary scale is to measure all samples directly against PLS. In most cases however, this approach is inefficient (e.g. high cost of calibrated mixtures, logistical issues when using more than two PLS cylinders). Instead, an intermediate set of reference mixtures (*secondary laboratory standards*, SLS) is used to link measured concentrations with the PLS. Using SLS is advantageous, as it reduces operating costs, limits the possibility of accidental reference mixture contamination, prolongs the usage time of PLS (decades instead of several years) and, in some cases, allows to take advantage of multi-point calibration without the need to reduce in-situ sample measurement frequency (e.g. CHIOTTO methodology – see CHIOTTO (2015) and Popa et al. (2010))

The main disadvantage of using SLS is a possibility of systematic error that may arise during calibrations, which is hard to quantify. It also increases the necessary manpower, as preparation of secondary laboratory standards (SLS) is a difficult and time-consuming procedure, often requiring corrections of the obtained mixing ratios by injecting additional quantities of the desired compound (*spiking*).

At both KAS and KRK stations, scale transfer is currently performed through two SLSs, each calibrated against two primary laboratory standards (NOAA CMDL, cylinders no. CA07494, CA07462, WMO N_2O X2006A scale) available at the Gas Chromatography Laboratory of AGH University, similar to the system described by Schmidt et al. (2014). The main purpose behind using two SLSs is to account for ECD non-linearity, further discussed below. A graphical illustration of a two-point calibration procedure is shown in Figure A.3. Two SLS cylinders with known mixing ratios *c.1* and *c.2*

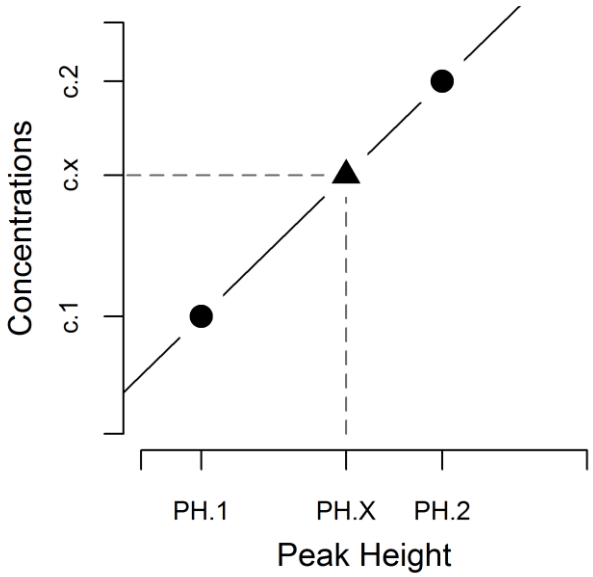

Figure A.3. Calibration scheme using two secondary lab standards (suffixes .1 and .2) against a measured sample (suffix .X).

are analysed by the GC system, providing the concentration-dependent parameter information – peak heights in case of N_2O analyses (*PH.1* and *PH.2*, respectively). Application of a linear fit allows to calculate the compound concentrations in the sample based on the measured peak height (*PH.X*).

The SLSs that have been used for GC measurements in the framework of this work had N_2O concentrations spanning the atmospheric concentrations usually observed at each station (325 – 340 ppb). Additional consideration has been given to soil N_2O flux measurements, where the samples often contained much higher amounts of nitrous oxide (usually 325-400 ppb, with several cases of mixing ratios being as high as 900 ppb; see chapter 4, section 4.4.). A similar approach was adopted for calculations of other measured trace gases (CH_4, CO_2, SF_6). A detailed information on PLSs, SLSs and target tanks used for measurements presented in this thesis is given in Table A.1.

All measurements of ambient air samples were performed in automated sequences, where a single analysis takes 9-11 minutes. To minimise measurement sensitivity to changes of laboratory atmosphere (pressure, temperature), one of the SLS mixtures was injected after every analysis, following the sequence: sample – SLS1 – sample – SLS2. This cycle was repeated indefinitely, allowing the samples to be collected and analysed every 20 min and reference cylinders every 40 minutes, approximately.

To further limit the influence of instrument noise and sensitivity to pressure and temperature changes, calibration curve was constructed using smoothed curves fitted to the measured peak

Table A.1. Detailed information on composition of reference gas mixtures used at KAS and KRK gas monitoring stations. Precisions for PLS provided by the supplier (NOAA ERSL). Uncertainties of SLS and Target mixtures calculated from calibrations performed at AGH University in Kraków.

		Mixture ID	N_2O [ppb]	CH_4 [ppb]	CO_2 [ppm]	SF_6 [ppt]
	Primary Lab Standards	CA07462	323.03 ± 0.03	1808.91 ± 0.11	369.55 ± 0.01	6.13 ± 0.00*
		CA07494	335.13 ± 0.06	1986.49 ± 0.05	401.16 ± 0.01	8.28 ± 0.01
KRK	Secondary Lab Standards	Gapcio	351.53 ± 0.24	2189.18 ± 0.48	404.488 ± 0.060	9.750 ± 0.073
KRK		Hipcio	328.43 ± 0.43	1802.74 ± 0.36	482.39 ± 0.18	7.256 ± 0.078
KRK	Target Mixtures	Krewki**	391.70	1545.01	474.77	9.138
KRK		Yak	338.798 ± 0.053	2159.78 ± 0.88	407.177 ± 0.021	8.607 ± 0.055
KAS	Secondary Lab Standards	Bang	339.44 ± 0.04	1820.32 ± 0.17	379.75 ± 0.01	9.71 ± 0.01
KAS		Helmut***	332.83 ± 0.02	1833.71 ± 0.12	400.77 ± 0.01	7.86 ± 0.01
KAS		Jasna	316.38 ± 0.06	1936.38 ± 0.14	357.97 ± 0.03	9.74 ± 0.02
KAS		Najeli	321.38 ± 0.04	2061.29 ± 0.37	422.67 ± 0.10	7.88 ± 0.02
KAS		PNS2	267.72 ± 0.16	1882.46 ± 0.12	390.14 ± 0.02	6.39 ± 0.01
KAS	Target Mixtures	Hokus	356.57 ± 0.06	2016.62 ± 0.22	417.10 ± 0.22	7.42 ± 0.01

* - Uncertainty of SF_6 calibration was lower than 0.005 ppt.

** - Cylinder was not calibrated against SLS, as it was not required at the time of usage. Values provided here were obtained indirectly, from long-term in-situ measurements.

*** - "Helmut" mixture was also used as a target tank in 2014.

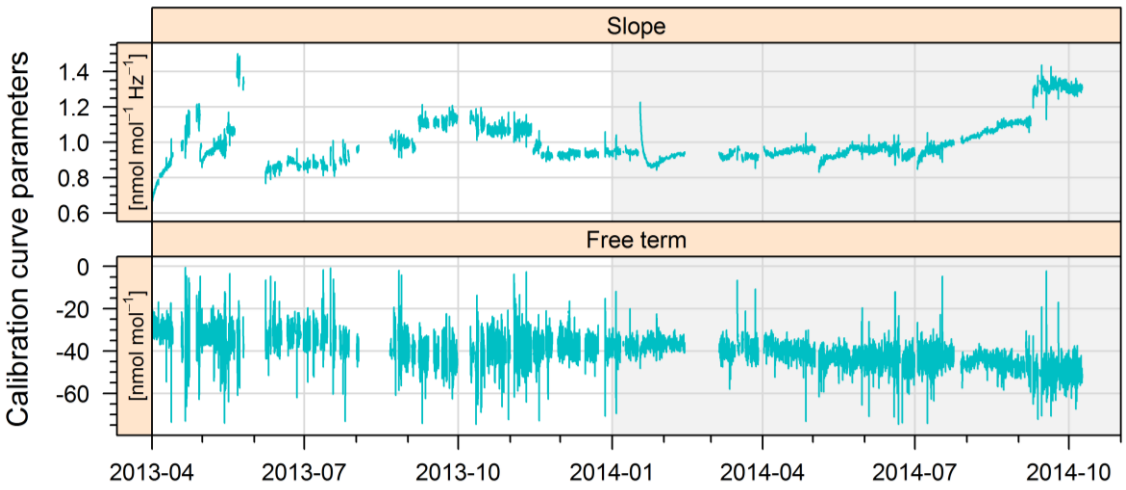

Figure A.4. Fluctuations of the slope and free-term coefficients of the linear two-point calibrations throughout the analysed period (2013-2014). Changes in the parameter values reflect long-term variability of the system performance and modifications of the equipment set-up.

parameters (height for N_2O, CH_4 and SF_6 or area for CO_2). These curves were calculated using the smooth spline by Panda software (data analysis software written by the author in cooperation with J. Bartyzel), which allows to interpolate peak parameter values at every sample injection moment, thus providing an individual, drift-corrected calibration curve for every sample.

Multi-point calibration procedure is critical in case of non-linear measurement devices, such as ECD detector. As can be seen in Figure A.4, the calibration parameters vary not only with the instrumental noise, but also show a consistent bias of the free-term that points to a significant offset in the measurements performed with one-point calibration methodology.

To illustrate the effect of non-linearity and estimate its possible magnitude, an example is presented in Figure A.5, where the concentrations of the ambient air were calculated using two-point (REF) and one-point calibration methodologies (SC1 and SC2). SC1 shows values calculated using one SLS with high N_2O concentrations (351.2 ppb), while SC2 values were obtained when using SLS with low N_2O (328.5 ppb). The analyses were done for KRK measurements performed during summer 2014 (June), when high diurnal variability of nitrous oxide was observed. The results show that using only one SLS as reference always leads to over- or under-estimation of the measured mixing ratio, with mixing ratio of nitrous oxide in the SLS being of critical importance. If SLS with N_2O concentrations close to ambient concentrations (SC2) is used, the effect of non-linearity is negligible most of the time, with

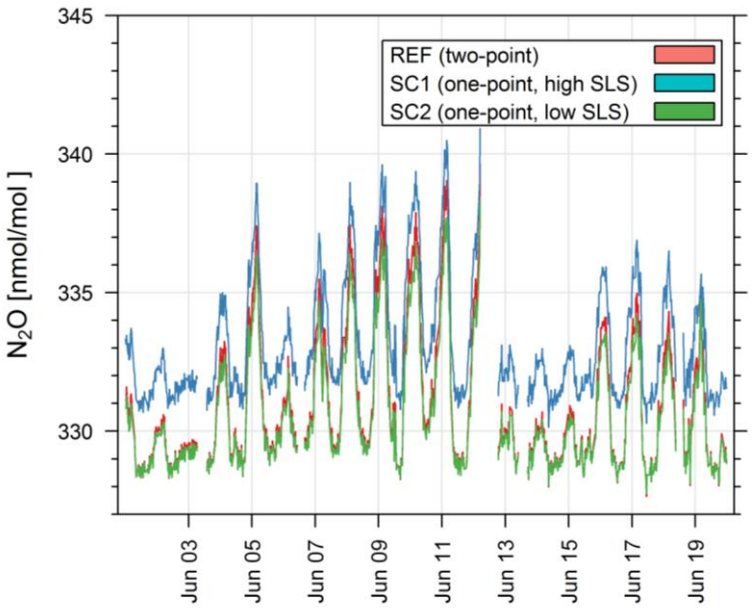

Figure A.5. Differences between ambient-air N_2O concentrations calculated using 2-point (using 2 SLS mixtures for calibration) and 1-point calibration methodologies (using SLS mixture with either low or high concentrations of N_2O as fixed reference).

significant differences occurring only during night-time build-up of this gas in the atmospheric inversion layer. However, when SLS with high concentration is used as a reference, a significant bias occurs for all analyses. This bias in the described case is linearly dependent on the concentration difference between the SLS mixture and the measured concentration.

This dependence is illustrated in Figure A.6. The reference (REF) values measured at the site during the presented period were divided into four concentration-dependent subsets. Box-and-whisker diagrams were then plotted for each of the described calibration scenarios (RER, SC1 and SC2). The results show that for the lowest measured N_2O mixing ratios (325-329 ppb), the difference of medians between REF and SC2 scenario (low concentration SLS) is equal to 0.02 nmol/mol, but rises to 1.06 µmol/mol when only the highest values (337-341 ppb) are observed. Opposite dependency occurs when using a high-concentration SLS for reference (SC1). In this case, the highest difference occurs with low measured values.

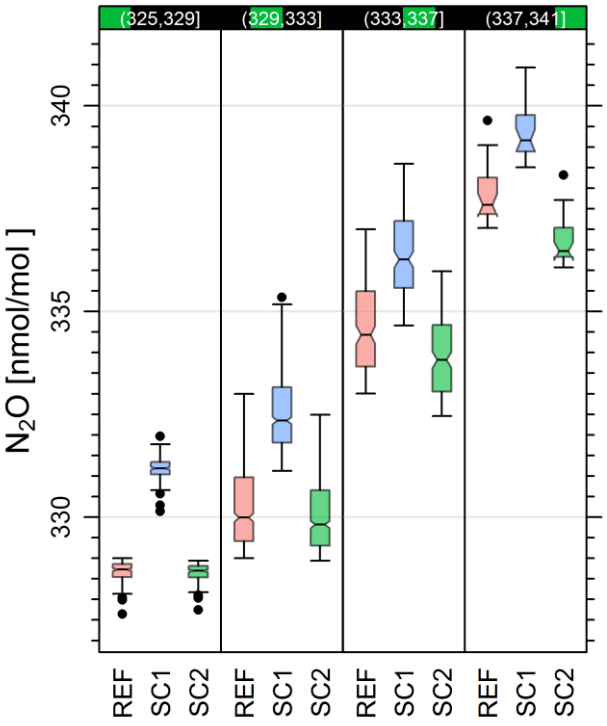

Figure A.6. Statistics of the differences between ambient-air N_2O concentrations measured at KRK in June 2014, calculated using 3 different calibration methods (bottom) applied to four distinct ranges of the measured N_2O mixing ratios (top). See text for details.

Both scenarios predict that the difference in N_2O concentration between the measured sample and the used SLS mixture in the order of 10 ppb leads to 1 ppb bias in the measured concentrations for the analysed period. This value is much larger than the random uncertainty of a single measurement and point to the fact that using one-point calibration will lead to the bias of the magnitude which is significant in regional Bayesian inversion experiments that might be dependent on such data. It is important to note that this bias depends on the slope of the calibration curve, which can vary significantly with time. Therefore, it is not possible to accurately correct the historical N_2O records obtained using one-point calibration methodology without some *a-priori* knowledge (or assumptions) concerning the linearity of the ECD detector.

A.3. Quality control / quality assurance procedures.

In long-term monitoring of atmospheric trace gas composition, special attention must be given to quality control and quality assurance (QC/QA) procedures. In case of gas chromatography this is of particular importance, as the ability to re-examine any station record becomes increasingly difficult with time, owing to consumption of reference mixtures, equipment deterioration by usage, sudden malfunctions etc.

An effort to establish scientifically-based QA/QC procedures for *in-situ* atmospheric composition measurements has been on-going in the scientific community since the first networks have been established. Its scope is not only to maintain overall high-quality of observations at any given site, but also to minimize the possibility of inter-network biases which could lead to false interpretations of the data (Corazza et al., 2011; see also section 3.1. in main text).

Two of the workpackages of the ongoing 7th EU Framework Project InGOS (*Integrated non-CO_2 Greenhouse gases Observing System*) have a goal of establishing a network of stations for measuring non-CO_2 greenhouse gases with a QA/QC procedure common to all parties in the project. The author of this thesis was active in the efforts of developing and testing these procedures in the framework of the project. In the scope of this PhD work, these recommended, state-of-the-art procedures for QC/QA were adopted at KAS and KRK stations.

The publication of InGOS QA/QC recommendations in a peer-reviewed journal is still pending at the moment of writing this thesis. It has been presented at several international conferences (e.g. NCGG7, 2014, Amsterdam, Netherlands). A short description of these recommendations will be provided here, with KAS and KRK procedures as examples. Implementation of these recommendations at KRK and KAS stations was in hands of the author of this thesis .

The InGOS QA/QC assume that there are several characteristic time-scales, over which uncertainties can be estimated and quality control procedures can be independently applied. These procedures tackle the issues of short-term variability of the measurement equipment, long-term drifts and instabilities of the measurement system (including those caused by both the equipment and calibration methodology), inter-network bias quantification and monitoring, quality control of scale transfer and detector non-linearity.

The central component of all of these QC procedures is constant (on at least daily basis) monitoring of the measurement equipment parameters by station operators. In order to achieve that, remote access to both KAS and KRK stations has been set-up via VNC protocol, which allows to monitor the system performance from any place in the world, providing that internet access is available. By using the control software (Panda), it was possible to monitor the system performance on a daily basis, which further allowed to react to the equipment malfunction as soon as it was possible.

In the framework of InGOS project, a diagnostic quantity called “repeatability” has been developed that allows to quantitatively describe the GC system performance in a short-term and that can be interpreted as an estimate of a standard deviation of a single ambient air measurement. Such quantitative assessment of a single measurement uncertainty has never been consistently adopted before, and is gaining in significance as new state-of-the-art inverse models begun to use the repeatability as a first estimate of measurement uncertainty. This new development will allow for independent assessment of the atmospheric inverse model results uncertainty, which, due to high complexity of the calculations, was up to now estimated through the analyses of model ensembles. The models with independent uncertainty calculations included have been tested in the Framework of the InGOS project. KAS data developed in the scope of this thesis was actively used in these experiments.

In an internal InGOS document, repeatability is described as “*24h centered moving 1σ standard deviation of bracketing working standards*[6]” where “*The 24h period has to be centered at the measurement interval for which the repeatability is calculated (12h prior and 12h after)*”. This means that to calculate repeatability at any given time, from all the available analyses a subset of those of

[6]*In the methodology used in the presented thesis, working standard is equivalent to secondary lab standard (SLS).*

the SLS is first needed. Then, for each of the subset points, one needs to calculate the mixing ratio of this SLS, while treating it as an unknown sample (only "bracketing" SLS analyses are used). From the calculated SLS mixing ratios, only those that correspond to the analyses performed in a 24-hour window around the chosen time needs to be chosen. In case of the system with only one SLS in use, this would mean that the repeatability can be calculated with the formula:

$$\mathrm{R(t)} = \sqrt{\frac{\sum_{\mathrm{i=1}}^{\mathrm{N}}\left[\mathrm{r_i(t)} - \overline{\mathrm{r(t)}}\right]^2}{\mathrm{N}-1}}, \tag{A.1}$$

where:

$$\mathrm{r(t_i)} = \mathrm{WS_{mixR}} \times \frac{2 \times \mathrm{PP(t_i)}}{\mathrm{PP(t_{i-1})} + \mathrm{PP(t_{i+1})}}. \tag{A.2}$$

In the equations above, $\mathrm{R(t)}$ denotes repeatability, $\mathrm{r(t_i)}$ is the intermediate quantity ("measured value of the working standard") calculated for all SLS analyses, $\overline{\mathrm{r(t)}}$ is the mean value of $\mathrm{r(t_i)}$ inside the 24-hour window, $\mathrm{WS_{mixR}}$ is the assigned value of the SLS (a known quantity, given in e.g. ppb), $\mathrm{PP(t_i)}$ – peak parameter (area / height) of a chosen compound measured in SLS at the time $\mathrm{t_i}$ and i index corresponds to the time index of the analyses that fall into the 24-hour time window centred around time $\mathrm{t_i}$.

It is worth noting that, by definition, repeatability can be calculated as soon as 12 hours after the ambient air analysis has been performed. With a small modification (e.g. by using only measurements performed in the last 12 hours) it can also be used as a near-real time diagnostic tool to monitor the measurement system performance for small changes that are otherwise impossible to detect. In KRK, for example, a diurnal cycle with elevated N_2O repeatability values were observed during summer, possibly connected with higher variability of laboratory temperature and/or improper detector insolation (Gałkowski, 2013). The repeatability is not yet used on a daily basis in the described manner in neither KAS or KRK, however future developments of control software may allow it.

Because the repeatability formula has been developed for sites that utilize one SLS, some modifications were necessary for the procedure to be applicable at KAS and KRK sites. These were devised by the author of this thesis and have been presented to the scientific community at the NCGG7 conference (NCGG7, 2014). The procedure follows the recommended protocol as closely as possible: first, the analyses of both SLSs are selected from the complete record of analyses. Then, for each of the SLS, its concentration is calculated by the calibration procedure (see above), treating the "current" SLS as an unknown sample. Thus, as there are two SLSs, two separate data sets become available. From these, and for each SLS separately, a subset of values with timestamps 12 hours prior and 12 hours posterior to the chosen time must be selected for the standard deviation to be calculated according to formula (A.1). In the last step, repeatability is calculated as a mean square root of each of two SLS repeatabilities. This procedure was used to calculate repeatabilities of KRK and KAS stations records, shown in Figure 3.9. (see main text, chapter 3, section 3.5.1.).

Another set of procedures is responsible for maintaining long-term stability of the measurements. In order to do that, a concept of a target mixture has been introduced. A target is an air mixture of composition as close to the ambient air as possible, that is meant to be measured over a long period of time – significantly larger than a typical lifetime of SLSs in use at the given site. While target mixture is usually prepared in exactly the same manner as SLSs and stored in the same type of cylinders, there are significant differences as to the philosophy of the measurements.

The main role of target mixture is to monitor long-term stability of the measurements on monthly to decadal timescales. This is achieved by measuring the target gas in the same manner as an ambient air sample, at regular intervals that are not smaller than 8 hours, allowing it to be preserved over a long time, depending on the amount originally available and the rate of usage. It is important that although the mixing ratios of the analysed gases are known, the target mixture is never used for calibration procedure in the normal operation mode, therefore it can be interpreted as a semi-independent quality assurance asset.

The main disadvantage of using the target mixture for quality control is the difficulty in the interpretation of the results. For example, in case that drift occurs, it cannot be easily distinguished if the problem originated from the malfunction of the measurement system, leakage, drift of the SLSs concentrations or the problems with the target tank itself.

Despite these issues, target tank has been included in InGOS QA/QC procedures as an obligatory asset and therefore it has been in use at both KRK and KAS stations (since 2013 and 2009, respectively). At both sites, the target mixture is stored in 50 dm^3 stainless steel cylinder and measured 3 times in series (to diminish the possibility of an outlier occurrence) at the interval of approximately 9 hours. Nitrous oxide concentrations measured in the target tank are presented in Figure. 3.9. (see main text, chapter 3, section 3.5.1.).

InGOS procedures currently require that concentrations of the analysed trace compounds of the target mixture should be known. Such knowledge can be provided either by the manufacturer or through calibration against primary laboratory standards. In case of KAS and KRK, these were established through the same calibration procedure as all SLSs used at both stations. Using that information, two additional diagnostic quantities can be calculated: (i) *Lab Internal Scale Consistency* (LISC), and (ii) *Monthly Reproducibility*.

LISC is defined as "*Difference of measured and assigned target value*", and represents the magnitude of possible errors due to scale inconsistencies between the primary and secondary scales. LISC is calculated via the following procedure: (i) Externally assigned target value is subtracted from the *in-situ* target analyses results, (ii) The dataset is divided into time-periods, by using target change dates as the base of division. Additional divisions are recommended in case when rapid system parameter change occurs, so that the possible bias is represented and quantified. This is based on the expert judgment done by the station manager, (iii) if no visible drift pattern is present, then LISC is equal to the median for each of the subsets. If there is a drift in the subset (no clear definition of the drift was provided at the moment of writing this thesis), then a linear fit should be applied to the dataset and the parameters of this fit are then reported as LISC.

Monthly Reproducibility is defined as the dataset of "*Absolute values of the (30-day) smoothed target residuals*". The recommended procedure in this case is as follows: (i) *Calculate "adjusted target differences" by subtracting the lab internal scale consistency (…) from the individual target differences (…) from their* [respective] *assigned values,* (ii) *Smooth these adjusted target differences with a centred running median with a window length of 30 days (…). In case of gaps (and the beginning or the end of the data set) mirror the existing target measurement in order to calculate a centred running median. Other gap filling strategies (e.g. constant values) are accepted as well. (…),* (iii) *Report the values of this smoothed target differences as positive or negative values of the Monthly Reproducibility*. Reproducibility values calculated for KRK and KAS records are also presented in Figure 3.9. (main text, section 3.5.1.)

It is important to note that while both LISC and reproducibility have a clearly defined numerical values, it has been agreed that they should not be used in any kind of corrections of the analysed

datasets, as the reason behind the elevated values of either could have a multitude of causes, some of which might not in fact occur in the ambient air records of the station. Currently, the main purpose of both LISC and reproducibility is to provide guidance in choosing the best filtration procedures at the measurement stations.

ANNEX B. Methods of calculating soil N_2O flux using NSS-chamber method including uncertainty estimate.

Annex B is dedicated to description of the methodology of calculating soil N_2O fluxes and their uncertainties on the basis of a set of samples collected from the chamber headspace. Section B.1 provides an overview of the available flux calculation schemes and their characteristics. Section B.2 contains a discussion of the uncertainty estimation method that was applied to all N_2O flux measurements described in Chapter 4 of this thesis.

B.1. N_2O flux calculation schemes.

Because the soil flux of N_2O is assumed to be controlled predominantly by diffusion, increase of N_2O concentration inside the chamber depends on N_2O concentration gradient between the soil and the chamber headspace, and therefore is inherently non-linear. Given enough time, the mixing ratio of the measured compound (N_2O) will reach saturation level, provided that production and destruction processes occurring in the soil are not time-dependent.

The best method of obtaining the flux (F) value at the time of the enclosure is still under debate in the scientific community. There are at least six commonly used methods of calculating F (de Klein and Harvey, 2012):

a) Linear regression (LR),
b) Hutchinson and Mosier (HM) scheme,
c) Quadratic Regression (QR) scheme,
d) Non-steady state diffusive flux estimator (NDFE),
e) HMR (based on extended HM model),
f) Chamber bias correction method (CBC).

The first three, historically most popular, "conventional" methods (de Klein and Harvey, 2012) allow the calculation of the flux (F) of the given compound through determination of time-derivative of the concentration function inside the chamber headspace (Levy et al., 2011):

$$F = \left.\frac{dC}{dt}\right|_{t=t_0} \times \frac{\rho V}{A}, \qquad \text{(B.1)}$$

where:

F – flux, in nmol m^{-2} s^{-1},
$\left.\frac{dC}{dt}\right|_{t=t_0}$ – rate of concentration change inside the chamber headspace at the start of the enclosure period (t_0), expressed in nmol mol^{-1} s^{-1},
ρ – density of air in mol m^{-3},
V – volume of the chamber headspace in m^3, and
A – the area covered by the chamber in m^2.

LR is the simplest and most popular choice for non-steady state (NSS) chamber-based soil N_2O flux studies, as it only uses the slope obtained from a linear, least-squares regression of the N_2O concentrations measured inside the chamber throughout the enclosure period. The slope serves as a proxy for dC/dt at $t=t_0$. The main disadvantage of using LR is a tendency for underestimating the flux (e.g. Matthias et al., 1978). This underestimation can exceed 25% even in situations where linear regressions show R^2 values greater than 0.997 (Conen and Smith, 2000). Furthermore, this effect is dependent on the specific soil conditions during the experiment, which could significantly hamper the results of budgeting based on LR calculations (Venterea and Baker, 2008, Venterea and Parkin, 2012). On the other hand, it has been shown that LR is less sensitive to random uncertainties (associated with sampling and measurement of the headspace air) than more complicated methods (Venterea et al., 2009). LS yields generally lower overall detection limit (Parkin et al., 2012). LR is also the only available option in cases where concentrations observed in the chamber do not saturate with time, as all other schemes assume *a priori* that the derivative of the concentration function will have a decreasing slope over time (de Klein and Harvey, 2012).

The HM method is a non-linear flux calculation scheme, first developed by Hutchinson and Mosier (1981). Its main advantage over the LR method was its underlying theoretical basis (derived from one-dimensional diffusion model with several general assumptions) and relative computational simplicity. The disadvantages of this method are: (i) sensitivity to measurement uncertainties, (ii) restriction of using only three concentration measurements, equally spaced in time, and (iii) inability to generate statistical parameters for uncertainty estimations (de Klein and Harvey, 2012). As these drawbacks were removed in the HMR model, the HM scheme is no longer recommended and should be considered as obsolete.

The QR method, described by (Wagner et al., 1997), tackles the non-linearity issue by assuming that the observed changes in the concentration can be approximated by a quadratic function. The QR scheme requires more computational effort in day-to-day use, but it has been shown that it produces the results that are less sensitive to measurement uncertainties than HM scheme and less biased than LR method. However, the bias is not eliminated entirely (Livingston et al., 2006, Venterea et al., 2009, Venterea, 2013).

The other three, more advanced schemes (NDFE, HMR, CBC) are based on a stronger and more subtle scientific models, taking into account many processes occurring in the soil beneath the chamber enclosure. These include for instance production, diffusion and accumulation of the measured compound in the pore spaces in the soil layers. For detailed description of these methods, see de Klein and Harvey (2012) and references therein. In general, these advanced schemes should be able to provide N_2O flux values more accurate than the "classical" methods. Still, all of them have their advantages and disadvantages. Moreover, it is recommended (or even necessary in case of CDC scheme) to test the obtained results against the classical methods, as there are specific cases where using either NDFE, CDC or HMR can lead to misinterpretations (Kutzbach et al., 2007, Venterea, 2010, de Klein and Harvey, 2012).

In the presented work, the linear regression (LR) method has been chosen to calculate the N_2O fluxes measured at the field sites. There are three main reasons behind this choice.

First, at one of the experimental sites (F, 20 deployments), a numerical experiment was performed, in which N_2O fluxes were calculated by both LR and HMR schemes. The HMR algorithm has recommended the calculations with the LR method in all but 2 cases (90%, results not shown). At the same time, the results obtained with the LR method have shown high degree of linearity (R^2 higher than 0.97 in all but one case). The reason behind failure of the HMR scheme might be connected to short deployment times (between 20-30 minutes), associated with high precision of

the GC analyses. It should be noted that other phenomena, not tackled in the above-mentioned schemes (such as disturbance of the soil during chamber placement), might have more impact on possible N_2O flux uncertainties, diminishing the gains from using advanced flux calculation schemes.

Second, the main focus of the measurements carried out in the framework of the presented study was to provide a general overview of the N_2O fluxes typical for Małopolska region. The adopted research plan utilizing short, intensive campaigns, made it impossible to use the obtained results in building a detailed budget of N_2O emissions in the surveyed environments. Therefore the presence of small biases was not critical at this point.

Finally, it should be noted that the author of this study took part in the N_2O static chamber intercomparison campaign that was held in Hyytiälä, Finland, in summer of 2014. The main goal of that campaign, which included over 20 teams from Europe and North America, was to compare and analyse the processes of N_2O flux measurements in controlled conditions. The design of the campaign followed previous, similar studies focused on CO_2 (Pumpanen et al., 2004) and CH_4 (Pihlatie et al., 2013) chamber measurements, and was focused on the effects of chamber placement, the initial soil disturbance, pressure effects from wind, etc. Although the results of this campaign are not yet available, it is hoped that a simple correction factor will become available as an immediate result of this intercomparison, which can be further used for correction of possible biases occurring when LR method is used for the specific chamber design employed in this study.

B.2. Uncertainty estimates for N_2O soil flux measurements using a linear regression scheme.

The uncertainties of the N_2O flux measurements presented in Chapter 4 was calculated using the uncertainty propagation principle. When applied to equation (B.1), the resulting relative uncertainty estimate can be described by following the formula:

$$\frac{\mathrm{u(F)}}{\mathrm{F}} = \sqrt{\left[\frac{\mathrm{u}(\alpha)}{\alpha}\right]^2 + \left[\frac{\mathrm{u}(\rho)}{\rho}\right]^2 + \left[\frac{\mathrm{u(V)}}{\mathrm{V}}\right]^2 + \left[\frac{\mathrm{u(A)}}{\mathrm{A}}\right]^2}, \qquad \text{(B.2)}$$

where F denotes the calculated flux, α is the linear slope calculated from the least-squares regression method, ρ is the molar density of air, V is the total chamber volume, A is the area that the chamber covers when deployed, and $\mathrm{u}(\alpha)$, $\mathrm{u}(\mathrm{F})$, etc. denote the respective absolute uncertainties.

Relative uncertainty of the chamber surface area was estimated through direct measurements as 2.5%. Least-square linear regression fitting function from the R statistical software (*lm* function from [*stats*] package) was used to obtain the $u(\alpha)/\alpha$ value (RCT, 2014). The uncertainty of the chamber volume was calculated using the uncertainty propagation:

$$\mathrm{u(V)} = \sqrt{\mathrm{u}^2(\mathrm{V_{lid}}) + \mathrm{u}^2(\mathrm{V_{collar}})},$$

where $\mathrm{V_{lid}}$ uncertainty was estimated through direct measurement and $\mathrm{u}(\mathrm{V_{collar}})$ was determined from the formula:

$$\frac{u(V_{collar})}{V_{collar}} = \sqrt{\left[\frac{u(A)}{A}\right]^2 + \left[\frac{u(H)}{H}\right]^2},$$

where $u(A)$ is the chamber area uncertainty and $u(H)$ was estimated as a standard deviation of collar insertion depths measured *in-situ*. This uncertainty included also the component coming from the unevenness of the terrain inside the collar, which is not taken into account in most studies.

$u(\rho)$ was estimated from:

$$\frac{u(\rho)}{\rho} = \sqrt{\left[\frac{u(p)}{p}\right]^2 + \left[\frac{u(T)}{T}\right]^2},$$

where p and T stand for pressure and temperature (in K) of air in the chamber headspace, respectively. It was assumed that the uncertainty of R (gas constant) can be neglected. Pressure uncertainty was assumed as approx. 1% (approximately 10 hPa). This relatively high value was adopted due to relatively large distance between meteorological station and flux measurement.

Uncertainty of air temperature was assumed as equal to 1 K in cases when no measurements inside the chamber headspace after the deployment were done. If the temperature inside the chamber was measured[7], then the $u(T)$ was assumed to be either equal to 1 K, or one standard deviation of the ambient temperature and the chamber temperature, depending on which of these quantities was larger:

$$u(T) = \min\left\{1\ \text{K},\ \sqrt{\sum[(T_{air} - \overline{T})^2 + (T_{chamber} - \overline{T})^2]}\right\},$$

where T_{air} is the temperature of air measured outside of the chamber, $T_{chamber}$ denotes the temperature of the air enclosed under the chamber at the end of the enclosure, and $\overline{T}$ is the average of T_{air} and $T_{chamber}$.

This part of uncertainty was meant to represent the effects of temperature change inside the chamber headspace, which were not taken into the account during the flux calculation. In case of chamber designs without pressure equilibration tube, a significant temperature increase could lead to expansion of the air enclosed under the chamber and advection, decreasing the rate of diffusion responsible for concentration rise.

As the chamber used in this work was equipped with a pressure equilibration tube, the advection through the soil was highly unlikely and could be neglected. Nevertheless, the best way to approach this issue would be to include temperature effect in the flux calculation (FC) model. The author is unaware of any available FC scheme that uses the temperature change information to correct the flux values.

Selected examples of uncertainty assessment using the above-outlined methodology are presented in Table B.1. It is apparent that the factor contributing most to the uncertainty of the calculated N_2O flux is the slope of the concentration curve. Other contributing factors, ordered by importance, are: volume uncertainty (with ground height variability included), chamber area and molar density of air. It is important to note that this uncertainty analysis concerns only a single flux measurement, and is not able to address spatial variability of the N_2O flux stemming from heterogeneity of the N_2O sources in the soil.

[7] Measurements of temperature inside the chamber headspace were only possible at the end of deployment time, after all the samples were taken.

Table B.1. Example of uncertainty components calculated for ZDHAR F site flux measurements and medians of all measurements performed in the scope of this PhD work.

Measurement date	$\frac{u(F)}{F}$	$\frac{u(\alpha)}{\alpha}$	$\frac{u(V)}{V}$	$\frac{u(A)}{A}$	$\frac{u(\rho)}{\rho}$
01/03/2014	11.3%	10.3%	3.7%	2.5%	1.1%
05/03/2014	8.3%	6.9%	3.7%	2.5%	1.1%
08/03/2014	4.7%	0.9%	3.7%	2.5%	1.1%
11/03/2014	11.5%	10.4%	3.7%	2.5%	1.6%
14/03/2014	7.4%	5.6%	3.7%	2.5%	1.8%
17/03/2014	8.7%	7.5%	3.6%	2.5%	1.0%
20/03/2014	5.0%	2.1%	3.6%	2.5%	1.2%
23/03/2014	4.8%	1.6%	3.6%	2.5%	1.2%
26/03/2014	5.5%	3.2%	3.6%	2.5%	1.2%
29/03/2014	6.4%	4.5%	3.6%	2.5%	1.2%
01/04/2014	7.4%	5.8%	3.6%	2.5%	1.4%
04/04/2014	4.9%	0.8%	3.6%	2.5%	2.1%
Global medians (i.e. from all the measurements performed in the scope of this study):					
	8.4%	**6.9%**	**3.8%**	**2.5%**	**1.4%**

REFERENCES

AERODYNE. 2015. *Aerodyne Research website* [Online]. Available: http://www.aerodyne.com/ [Accessed August 2015].

AGAGE. 2015. *The Advanced Global Atmospheric Gases Experiment website* [Online]. Available: https://agage.mit.edu/ [Accessed July 2015].

ANDERSON, B., BARTLETT, K., FROLKING, S., HAYHOE, K., JENKINS, J. & SALAS, W. 2010. Methane and nitrous oxide emissions from natural sources. *United States Environmental Protection Agency, Office of Atmospheric Programs, Washington*.

AREVALO-MARTÍNEZ, D. L., KOCK, A., LÖSCHER, C., SCHMITZ, R. & BANGE, H. W. 2015. Massive nitrous oxide emissions from the tropical South Pacific Ocean. *Nature Geoscience*.

BAGGS, E. 2008. A review of stable isotope techniques for N2O source partitioning in soils: recent progress, remaining challenges and future considerations. *Rapid Communications in Mass Spectrometry,* 22**,** 1664-1672.

BATJES, N. H. 1996. Total carbon and nitrogen in the soils of the world. *European journal of soil science,* 47**,** 151-163.

BERGAMASCHI, P., FRANKENBERG, C., MEIRINK, J. F., KROL, M., VILLANI, M. G., HOUWELING, S., DENTENER, F., DLUGOKENCKY, E. J., MILLER, J. B. & GATTI, L. V. 2009. Inverse modeling of global and regional CH4 emissions using SCIAMACHY satellite retrievals. *Journal of Geophysical Research: Atmospheres (1984–2012),* 114.

BERGAMASCHI, P., KROL, M., DENTENER, F., VERMEULEN, A., MEINHARDT, F., GRAUL, R., RAMONET, M., PETERS, W. & DLUGOKENCKY, E. 2005. Inverse modelling of national and European CH4 emissions using the atmospheric zoom model TM5. *Atmospheric Chemistry and Physics Discussions,* 5**,** 1007-1066.

BERGSTERMANN, A., CÁRDENAS, L., BOL, R., GILLIAM, L., GOULDING, K., MEIJIDE, A., SCHOLEFIELD, D., VALLEJO, A. & WELL, R. 2011. Effect of antecedent soil moisture conditions on emissions and isotopologue distribution of N2O during denitrification. *Soil Biology and Biochemistry,* 43**,** 240-250.

BOSANQUET, C. & PEARSON, J. 1936. The spread of smoke and gases from chimneys. *Transactions of the Faraday Society,* 32**,** 1249-1263.

BOUWMAN, A. 1998. Environmental science: Nitrogen oxides and tropical agriculture. *Nature,* 392**,** 866-867.

BRIGGS, G. A. 1973. Diffusion estimation for small emissions. *Atmospheric Turbulence and Diffusion Laboratory, NOAA, ATDL Contribution File***,** 83.

CARBOEUROPE-IP. 2000. *CarboEurope-IP website* [Online]. Available: http://www.carboeurope.org/ (currently not available).

CARSLAW, D. 2012. The openair manual–open-source tools for analysing air pollution data. *Manual for version 0.7-0, King's College London*.

CARSLAW, D. C. & ROPKINS, K. 2012. Openair—an R package for air quality data analysis. *Environmental Modelling & Software,* 27**,** 52-61.

CHIOTTO. 2015. *Continuous HIgh-precisiOn Tall Tower Observations of greenhouse gases (CHIOTTO), website* [Online]. Available: http://www.chiotto.org/ [Accessed August 2015].

CHMURA, L., ROZANSKI, K., NECKI, J., ZIMNOCH, M., KORUS, A. & PYCIA, M. 2008. Atmospheric concentrations of carbon dioxide in Southern Poland: Comparison of mountain and urban environments. *Polish Journal of Environmental Studies,* 17**,** 859.

CHOJNICKI, B. H., URBANIAK, M., JÓZEFCZYK, D., AUGUSTIN, J. & OLEJNIK, J. 2007. Measurements of gas and heat fluxes at Rzecin wetland. *Wetlands: monitoring, modeling and management (Okruszko, ed). Taylor & Francis Group, London: pp***,** 125-131.

CHOJNICKI, B. H., URBANIAK, M., LESNY, J., JUSZCZAK, R. & OLEJNIK, J. 2008. Nowoczesne metody pomiaru wymiany masy i energii pomiędzy podłożem a atmosferą. *Przegląd Naukowy. Inżynieria i Kształtowanie Środowiska,* 17.

CIACIEK, K. 2013. *Pomiary glebowej produkcji podtlenku azotu na terenie Krakowa, praca inżynierska.* Eng., AGH University of Science and Technology.

CIACIEK, K. 2014. *Pomiary zmienności zawartości N2O w próbkach pochodzenia naturalnego i przemysłowego, Praca Magisterska.* MSc, AGH University of Science and Technology.

CLEVELAND, R. B., CLEVELAND, W. S., MCRAE, J. E. & TERPENNING, I. 1990. STL: A seasonal-trend decomposition procedure based on loess. *Journal of Official Statistics,* 6**,** 3-73.

CONEN, F. & SMITH, K. 2000. An explanation of linear increases in gas concentration under closed chambers used to measure gas exchange between soil and the atmosphere. *European Journal of Soil Science,* 51**,** 111-117.

CORAZZA, M., BERGAMASCHI, P., VERMEULEN, A., AALTO, T., HASZPRA, L., MEINHARDT, F., O'DOHERTY, S., THOMPSON, R., MONCRIEFF, J. & POPA, E. 2011. Inverse modelling of European N2O emissions: assimilating observations from different networks. *Atmospheric chemistry and physics,* 11**,** 2381-2398.

CRUTZEN, P. J., MOSIER, A. R., SMITH, K. A. & WINIWARTER, W. 2008. N2O release from agro-biofuel production negates global warming reduction by replacing fossil fuels. *Atmospheric chemistry and physics,* 8**,** 389-395.

DAVIDSON, E. A. 2009. The contribution of manure and fertilizer nitrogen to atmospheric nitrous oxide since 1860. *Nature Geoscience,* 2**,** 659-662.

DE KLEIN, C. & HARVEY, M. 2012. *Nitrous Oxide Chamber Methodology Guidelines*, Ministry for Primary Industries, Pastoral House, 25 The Terrace, PO Box 2526, Wellington 6140, New Zealand.

DENGEL, S., LEVY, P. E., GRACE, J., JONES, S. K. & SKIBA, U. M. 2011. Methane emissions from sheep pasture, measured with an open-path eddy covariance system. *Global Change Biology,* 17**,** 3524-3533.

DENMEAD, O., LEUNING, R., JAMIE, I. & GRIFFITH, D. 2000. Nitrous oxide emissions from grazed pastures: measurements at different scales. *Chemosphere-Global Change Science,* 2**,** 301-312.

DRAXLER, R. R. 1976. Determination of atmospheric diffusion parameters. *Atmospheric Environment (1967),* 10**,** 99-105.

DRAXLER, R. R. & HESS, G. 1998. An overview of the HYSPLIT_4 modelling system for trajectories. *Australian meteorological magazine,* 47**,** 295-308.

E-PRTR. 2015. *The European Pollutant Release and Transfer Register* [Online]. European Comission. Available: http://prtr.ec.europa.eu/ [Accessed July 2015].

EDGAR 2011. Emission Database for Global Atmospheric Research (EDGAR), release version 4.2.: European Commission, Joint Research Centre (JRC)/Netherlands Environmental Assessment Agency (PBL).

ELKINS, J. & DUTTON, G. 2009. Nitrous oxide and sulfur hexafluoride. *Bull. Am. Meteorol. Soc,* 90**,** S38-S39.

ERISMAN, J. W., SUTTON, M. A., GALLOWAY, J., KLIMONT, Z. & WINIWARTER, W. 2008. How a century of ammonia synthesis changed the world. *Nature Geoscience,* 1**,** 636-639.

EUGSTER, W. & PLÜSS, P. 2010. A fault-tolerant eddy covariance system for measuring CH 4 fluxes. *Agricultural and Forest Meteorology,* 150**,** 841-851.
EUROSTAT. 2015. Agri-environmental indicator - gross nitrogen balance Available from: http://ec.europa.eu/eurostat/statistics-explained/index.php/Agri-environmental_indicator_-_gross_nitrogen_balance [Accessed July 2015].
FAO. 2006. *FAO Statistical Database* [Online]. Available: http://faostat.fao.org/default.aspx [Accessed July 2015].
FLEMING, E. L., JACKMAN, C. H., STOLARSKI, R. & DOUGLASS, A. 2011. A model study of the impact of source gas changes on the stratosphere for 1850–2100. *Atmospheric chemistry and physics,* 11**,** 8515-8541.
FLÜCKIGER, J., BLUNIER, T., STAUFFER, B., CHAPPELLAZ, J., SPAHNI, R., KAWAMURA, K., SCHWANDER, J., STOCKER, T. F. & DAHL-JENSEN, D. 2004. N2O and CH4 variations during the last glacial epoch: Insight into global processes. *Global Biogeochemical Cycles,* 18.
FLUXNET. 2015. *FLUXNET website* [Online]. Available: http://fluxnet.ornl.gov/ [Accessed July 2015].
FORSYTHE, G. E., MOLER, C. B. & MALCOLM, M. A. 1977. Computer methods for mathematical computations.
GAŁKOWSKI, M. 2013. *A "front-flush" mode implementation in the GC system with a uECD detector in high-quality measurements of atmospheric N2O mixing ratios.,* Kraków, Faculty of Physics and Applied Computer Science, AGH University of Science and Technology.
GALLOWAY, J. N., ABER, J. D., ERISMAN, J. W., SEITZINGER, S. P., HOWARTH, R. W., COWLING, E. B. & COSBY, B. J. 2003. The nitrogen cascade. *Bioscience,* 53**,** 341-356.
GALLOWAY, J. N. & COWLING, E. B. 2002. Reactive nitrogen and the world: 200 years of change. *AMBIO: A Journal of the Human Environment,* 31**,** 64-71.
GALLOWAY, J. N., DENTENER, F. J., CAPONE, D. G., BOYER, E. W., HOWARTH, R. W., SEITZINGER, S. P., ASNER, G. P., CLEVELAND, C., GREEN, P. & HOLLAND, E. 2004. Nitrogen cycles: past, present, and future. *Biogeochemistry,* 70**,** 153-226.
GALLOWAY, J. N., TOWNSEND, A. R., ERISMAN, J. W., BEKUNDA, M., CAI, Z., FRENEY, J. R., MARTINELLI, L. A., SEITZINGER, S. P. & SUTTON, M. A. 2008. Transformation of the nitrogen cycle: recent trends, questions, and potential solutions. *Science,* 320**,** 889-892.
GERBIG, C., LIN, J., WOFSY, S., DAUBE, B., ANDREWS, A., STEPHENS, B., BAKWIN, P. & GRAINGER, C. 2003. Toward constraining regional-scale fluxes of CO2 with atmospheric observations over a continent: 2. Analysis of COBRA data using a receptor-oriented framework. *Journal of Geophysical Research: Atmospheres (1984–2012),* 108.
GERLAND, P., RAFTERY, A. E., ŠEVČÍKOVÁ, H., LI, N., GU, D., SPOORENBERG, T., ALKEMA, L., FOSDICK, B. K., CHUNN, J. & LALIC, N. 2014. World population stabilization unlikely this century. *Science,* 346**,** 234-237.
GHG-EUROPE. 2015. *GHG-Europe project website* [Online]. Available: http://www.ghg-europe.eu/ [Accessed 2015].
GIFFORD JR, F. A. 1961. Use of routine meteorological observations for estimating atmospheric dispersion. *Nuclear Safety,* 2**,** 47-51.
HALL, S. J., HUBER, D. & GRIMM, N. B. 2008. Soil N2O and NO emissions from an arid, urban ecosystem. *Journal of Geophysical Research: Biogeosciences (2005–2012),* 113.
HANNA, S. R. 1979. Some statistics of Lagrangian and Eulerian wind fluctuations. *Journal of Applied Meteorology,* 18**,** 518-525.
HERRIDGE, D. F., PEOPLES, M. B. & BODDEY, R. M. 2008. Global inputs of biological nitrogen fixation in agricultural systems. *Plant and Soil,* 311**,** 1-18.
HORABIK, J. & NAHORSKI, Z. 2015. Improving resolution of a spatial air pollution inventory with a statistical inference approach. *Uncertainties in Greenhouse Gas Inventories.* Springer.
HSU, J. & PRATHER, M. J. 2010. Global long-lived chemical modes excited in a 3-D chemistry transport model: Stratospheric N2O, NOy, O3 and CH4 chemistry. *Geophysical Research Letters,* 37.
HUTCHINSON, G. & MOSIER, A. 1981. Improved soil cover method for field measurement of nitrous oxide fluxes. *Soil Science Society of America Journal,* 45**,** 311-316.
ICOS. 2015. *Integrated Carbon Observation System website* [Online]. Available: https://www.icos-ri.eu/ [Accessed July 2015].
INGOS. 2015. *Integrated Greenhouse gas Observing System (InGOS) website* [Online]. Available: http://www.ingos-infrastructure.eu/ [Accessed August 2015].
IPCC 2006. 2006 IPCC Guidelines for National Greenhouse Gas Inventories. *In:* H.S., E., L., B., K., M., T., N. & K., T. (eds.). Kamiyamaguchi Hayama, Japan: National Greenhouse Gas Inventories Programm.
IPCC 2013. *Climate Change 2013: The Physical Science Basis. Contribution of Working Group I to the Fifth Assessment Report of the Intergovernmental Panel on Climate Change,* Cambridge, United Kingdom and New York, NY, USA, Cambridge University Press.
ISHIJIMA, K., SUGAWARA, S., KAWAMURA, K., HASHIDA, G., MORIMOTO, S., MURAYAMA, S., AOKI, S. & NAKAZAWA, T. 2007. Temporal variations of the atmospheric nitrous oxide concentration and its δ15N and δ18O for the latter half of the 20th century reconstructed from firn air analyses. *Journal of Geophysical Research: Atmospheres (1984–2012),* 112.
JACKOWICZ-KORCZYŃSKI, M., CHRISTENSEN, T. R., BÄCKSTRAND, K., CRILL, P., FRIBORG, T., MASTEPANOV, M. & STRÖM, L. 2010. Annual cycle of methane emission from a subarctic peatland. *Journal of Geophysical Research: Biogeosciences (2005–2012),* 115.
JÄRVI, L., NORDBO, A., RANNIK, Ü., HAAPANALA, S., RIIKONEN, A., MAMMARELLA, I., PIHLATIE, M. & VESALA, T. 2014. Urban nitrous-oxide fluxes measured using the eddy-covariance technique in Helsinki, Finland. *Boreal Environment Research,* 19.
JASEK, A., ZIMNOCH, M., GORCZYCA, Z., SMULA, E. & ROZANSKI, K. 2014. Seasonal variability of soil CO2 flux and its carbon isotope composition in Krakow urban area, Southern Poland. *Isotopes in environmental and health studies,* 50**,** 143-155.
JONES, A., THOMSON, D., HORT, M. & DEVENISH, B. 2007. The UK Met Office's next-generation atmospheric dispersion model, NAME III. *Air Pollution Modeling and its Application XVII.* Springer.
JONES, S., FAMULARI, D., DI MARCO, C., NEMITZ, E., SKIBA, U., REES, R. & SUTTON, M. 2011. Nitrous oxide emissions from managed grassland: a comparison of eddy covariance and static chamber measurements. *Atmospheric Measurement Techniques,* 4**,** 2179-2194.
KHALIL, M. A. K. & RASMUSSEN, R. 1989. Climate-induced feedbacks for the global cycles of methane and nitrous oxide. *Tellus B,* 41**,** 554-559.
KOWALSKA, N., CHOJNICKI, B., RINNE, J., HAAPANALA, S., SIEDLECKI, P., URBANIAK, M., JUSZCZAK, R. & OLEJNIK, J. 2013. Measurements of methane emission from a temperate wetland by the eddy covariance method. *International Agrophysics,* 27**,** 283-290.
KUTZBACH, L., SCHNEIDER, J., SACHS, T., GIEBELS, M., NYKÄNEN, H., SHURPALI, N., MARTIKAINEN, P., ALM, J. & WILMKING, M. 2007. CO2 flux determination by closed-chamber methods can be seriously biased by inappropriate application of linear regression. *Biogeosciences,* 4**,** 1005-1025.
LAMB, R., HOGO, H. & REID, L. 1979. A Lagrangian approach to modeling air pollutant dispersion: Development and testing in the vicinity of a roadway.
LEIP, A., ACHERMANN, B., BILLEN, G., BLEEKER, A., BOUWMAN, A., DE VRIES, W., DRAGOSITS, U., DORING, U., FERNALL, D. & GEUPEL, M. 2011. Integrating nitrogen fluxes at the European scale.

LEUENBERGER, M. & FLÜCKIGER, E. 2008. Research at Jungfraujoch. *Science of the Total Environment,* 391**,** 169-176.
LEVY, P., GRAY, A., LEESON, S., GAIAWYN, J., KELLY, M., COOPER, M., DINSMORE, K., JONES, S. & SHEPPARD, L. 2011. Quantification of uncertainty in trace gas fluxes measured by the static chamber method. *European Journal of Soil Science,* 62**,** 811-821.
LGR. 2015. *Los Gatos Research Website* [Online]. Available: http://www.lgrinc.com/ [Accessed August 2015].
LIAO, T., CAMP, C. D. & YUNG, Y. L. 2004. The seasonal cycle of N2O. *Geophysical Research Letters,* 31.
LIN, J., GERBIG, C., WOFSY, S., ANDREWS, A., DAUBE, B., DAVIS, K. & GRAINGER, C. 2003. A near-field tool for simulating the upstream influence of atmospheric observations: The Stochastic Time-Inverted Lagrangian Transport (STILT) model. *Journal of Geophysical Research: Atmospheres (1984–2012),* 108.
LIVINGSTON, G. P., HUTCHINSON, G. L. & SPARTALIAN, K. 2006. Trace gas emission in chambers. *Soil Science Society of America Journal,* 70**,** 1459-1469.
LYNCH, P. 2008. The origins of computer weather prediction and climate modeling. *Journal of Computational Physics,* 227**,** 3431-3444.
MAMMARELLA, I., WERLE, P., PIHLATIE, M., EUGSTER, W., HAAPANALA, S., KIESE, R., MARKKANEN, T., RANNIK, Ü. & VESALA, T. 2010. A case study of eddy covariance flux of N 2 O measured within forest ecosystems: quality control and flux error analysis. *Biogeosciences,* 7**,** 427-440.
MANNING, A., O'DOHERTY, S., JONES, A., SIMMONDS, P. & DERWENT, R. 2011. Estimating UK methane and nitrous oxide emissions from 1990 to 2007 using an inversion modeling approach. *Journal of Geophysical Research: Atmospheres (1984–2012),* 116.
MATTHIAS, A. D., YARGER, D. N. & WEINBECK, R. S. 1978. A numerical evaluation of chamber methods for determining gas fluxes. *Geophysical Research Letters,* 5**,** 765-768.
MERBOLD, L., EUGSTER, W., STIEGER, J., ZAHNISER, M., NELSON, D. & BUCHMANN, N. 2014. Greenhouse gas budget (CO2, CH4 and N2O) of intensively managed grassland following restoration. *Global Change Biology,* 20**,** 1913-1928.
MOLGA, M. 1983. *Meteorologia rolnicza: podręcznik dla studentów akademii rolniczych*, Państwowe Wydawnictwa Rolnicze i Leśne.
MONTZKA, S., FRASER, P., BUTLER, J., CUNNOLD, D., DANIEL, J., DERWENT, R., LAL, S., MCCULLOCH, A., ORAM, D. & REEVES, C. 2003. Controlled substances and other source gases, Chapter 1 of the Scientific Assessment of Ozone Depletion: 2002. *Scientific Assessment of Ozone Depletion: 2002*.
MOONEY, H. A., VITOUSEK, P. M. & MATSON, P. A. 1987. Exchange of materials between terrestrial ecosystems and the atmosphere. *Science,* 238**,** 926-932.
MPAS. 2015. *Model for Prediction Across Scales website* [Online]. Available: https://mpas-dev.github.io/ [Accessed July 2015].
NASULEWICZ, M. 2009. *Automatyzacja systemu dozowania próbki do chromatografu gazowego.* Eng., AGH University of Science and Technology.
NCDC. 2015. *National Climatic Data Center - Climate Data Online* [Online]. Available: https://www.ncdc.noaa.gov/cdo-web/ [Accessed July 2015].
NCGG7. 2014. *Seventh International Symposium on Non-CO2 Greenhouse Gases (NCGG7) website* [Online]. Available: http://www.ncgg.info/ [Accessed July 2015].
NECKI, J., SCHMIDT, M., ROZANSKI, K., ZIMNOCH, M., KORUS, A., LASA, J., GRAUL, R. & LEVIN, I. 2003. Six-year record of atmospheric carbon dioxide and methane at a high-altitude mountain site in Poland. *Tellus B,* 55**,** 94-104.
NECKI, J. M., CHMURA, L., ZIMNOCH, M. & ROZANSKI, K. 2013. Impact of emissions on atmospheric composition at Kasprowy Wierch based on results of carbon monoxide and carbon dioxide monitoring. *Polish Journal of Environmental Studies,* 22.
NEHRKORN, T., ELUSZKIEWICZ, J., WOFSY, S. C., LIN, J. C., GERBIG, C., LONGO, M. & FREITAS, S. 2010. Coupled weather research and forecasting–stochastic time-inverted lagrangian transport (WRF–STILT) model. *Meteorology and Atmospheric Physics,* 107**,** 51-64.
NEON. 2015. *National Ecological Observatory Network website* [Online]. Available: http://www.neoninc.org/ [Accessed August 2015].
NEVISON, C., DLUGOKENCKY, E., DUTTON, G., ELKINS, J., FRASER, P., HALL, B., KRUMMEL, P., LANGENFELDS, R., O'DOHERTY, S. & PRINN, R. 2011. Exploring causes of interannual variability in the seasonal cycles of tropospheric nitrous oxide. *Atmospheric Chemistry and Physics,* 11**,** 3713-3730.
NEVISON, C., KINNISON, D. & WEISS, R. 2004. Stratospheric influences on the tropospheric seasonal cycles of nitrous oxide and chlorofluorocarbons. *Geophysical Research Letters,* 31.
NEVISON, C. D., MAHOWALD, N. M., WEISS, R. F. & PRINN, R. G. 2007. Interannual and seasonal variability in atmospheric N2O. *Global Biogeochemical Cycles,* 21.
NICOLINI, G., CASTALDI, S., FRATINI, G. & VALENTINI, R. 2013. A literature overview of micrometeorological CH4 and N2O flux measurements in terrestrial ecosystems. *Atmospheric Environment,* 81**,** 311-319.
NOAA, E. 2015. *Global Monitoring Division: Nitrous Oxide (N2O) — Combined Data Set* [Online]. Available: http://www.esrl.noaa.gov/gmd/hats/combined/N2O.html [Accessed July 2015].
OBUKHOV, A. 1959. Description of turbulence in terms of Lagrangian variables. *Adv. Geophys,* 6**,** 113-115.
PARK, S.-U., CHOE, A. & PARK, M.-S. 2013. Atmospheric Dispersion and Deposition of Radionuclides (137 Cs and 131 I) Released from the Fukushima Dai-ichi Nuclear Power Plant. *Computational Water, Energy, and Environmental Engineering,* 2**,** 61.
PARK, S., CROTEAU, P., BOERING, K., ETHERIDGE, D., FERRETTI, D., FRASER, P., KIM, K.-R., KRUMMEL, P., LANGENFELDS, R. & VAN OMMEN, T. 2012. Trends and seasonal cycles in the isotopic composition of nitrous oxide since 1940. *Nature Geoscience,* 5**,** 261-265.
PARKIN, T., VENTEREA, R. & HARGREAVES, S. 2012. Calculating the detection limits of chamber-based soil greenhouse gas flux measurements. *Journal of environmental quality,* 41**,** 705-715.
PARKIN, T. B. 2008. Effect of sampling frequency on estimates of cumulative nitrous oxide emissions. *Journal of environmental quality,* 37**,** 1390-1395.
PASQUILL, F. 1971. Atmospheric dispersion of pollution. *Quarterly Journal of the Royal Meteorological Society,* 97**,** 369-395.
PAWLAK, W., FORTUNIAK, K. & SIEDLECKI, M. 2011. Carbon dioxide flux in the centre of Łódź, Poland—analysis of a 2-year eddy covariance measurement data set. *International Journal of Climatology,* 31**,** 232-243.
PÉREZ, T., GARCIA-MONTIEL, D., TRUMBORE, S., TYLER, S., CAMARGO, P. D., MOREIRA, M., PICCOLO, M. & CERRI, C. 2006. Nitrous oxide nitrification and denitrification 15N enrichment factors from Amazon forest soils. *Ecological Applications,* 16**,** 2153-2167.
PHILLIPS, F., LEUNING, R., BAIGENT, R., KELLY, K. & DENMEAD, O. 2007. Nitrous oxide flux measurements from an intensively managed irrigated pasture using micrometeorological techniques. *Agricultural and Forest Meteorology,* 143**,** 92-105.
PICARRO. 2015. *Picarro Inc. website* [Online]. Available: http://www.picarro.com/ [Accessed August 2015].
PIHLATIE, M. K., CHRISTIANSEN, J. R., AALTONEN, H., KORHONEN, J. F., NORDBO, A., RASILO, T., BENANTI, G., GIEBELS, M., HELMY, M. & SHEEHY, J. 2013. Comparison of static chambers to measure CH 4 emissions from soils. *Agricultural and forest meteorology,* 171**,** 124-136.

PILLAI, D., GERBIG, C., AHMADOV, R., RÖDENBECK, C., KRETSCHMER, R., KOCH, T., THOMPSON, R., NEININGER, B. & LAVRIÉ, J. 2011. High-resolution simulations of atmospheric CO 2 over complex terrain–representing the Ochsenkopf mountain tall tower. *Atmospheric Chemistry and Physics,* 11**,** 7445-7464.

POPA, M., GLOOR, M., MANNING, A., JORDAN, A., SCHULTZ, U., HAENSEL, F., SEIFERT, T. & HEIMANN, M. 2010. Measurements of greenhouse gases and related tracers at Bialystok tall tower station in Poland. *Atmospheric Measurement Techniques,* 3**,** 407-427.

PRATHER, M. J. 2007. Lifetimes and time scales in atmospheric chemistry. *Philosophical Transactions of the Royal Society of London A: Mathematical, Physical and Engineering Sciences,* 365**,** 1705-1726.

PRATHER, M. J., HOLMES, C. D. & HSU, J. 2012. Reactive greenhouse gas scenarios: Systematic exploration of uncertainties and the role of atmospheric chemistry. *Geophysical Research Letters,* 39.

PREGGER, T., SCHOLZ, Y. & FRIEDRICH, R. 2007. Documentation of the anthropogenic GHG emission data for Europe provided in the Frame of CarboEurope GHG and CarboEurope IP. *Institut für Energiewirtschaft und Rationelle Energieanwendung, Universität Stuttgart, Stuttgart, Germany*.

PRIESTLEY, J. 1776. *Experiments and observations on different kinds of air*, Cambridge University Press.

PRINN, R., CUNNOLD, D., RASMUSSEN, R., SIMMONDS, P., ALYEA, F., CRAWFORD, A., FRASER, P. & ROSEN, R. 1990. Atmospheric emissions and trends of nitrous oxide deduced from 10 years of ALE–GAGE data. *Journal of Geophysical Research: Atmospheres (1984–2012),* 95**,** 18369-18385.

PRINN, R., WEISS, R., FRASER, P., SIMMONDS, P., CUNNOLD, D., ALYEA, F., O'DOHERTY, S., SALAMEH, P., MILLER, B. & HUANG, J. 2000. A history of chemically and radiatively important gases in air deduced from ALE/GAGE/AGAGE. *Journal of Geophysical Research: Atmospheres (1984–2012),* 105**,** 17751-17792.

PRUD'HOMME, M. 2007. Global Fertilizers and Raw Materials Supply and Supply/Demand Balances: 2007-2011. Paris, France: International Fertilizer Industry Association (IFA).

PUMPANEN, J., KOLARI, P., ILVESNIEMI, H., MINKKINEN, K., VESALA, T., NIINISTÖ, S., LOHILA, A., LARMOLA, T., MORERO, M. & PIHLATIE, M. 2004. Comparison of different chamber techniques for measuring soil CO2 efflux. *Agricultural and Forest Meteorology,* 123**,** 159-176.

RAPSON, T. D. & DACRES, H. 2014. Analytical techniques for measuring nitrous oxide. *TrAC Trends in Analytical Chemistry,* 54**,** 65-74.

RAVISHANKARA, A., DANIEL, J. S. & PORTMANN, R. W. 2009. Nitrous oxide (N2O): the dominant ozone-depleting substance emitted in the 21st century. *science,* 326**,** 123-125.

RCT 2014. R: A language and environment for statistical computing. R Foundation for Statistical Computing, Vienna, Austria, 2012. ISBN 3-900051-07-0.

REIMANN, S., VOLLMER, M., FOLINI, D., STEINBACHER, M., HILL, M., BUCHMANN, B., ZANDER, R. & MAHIEU, E. 2008. Observations of long-lived anthropogenic halocarbons at the high-Alpine site of Jungfraujoch (Switzerland) for assessment of trends and European sources. *Science of The Total Environment,* 391**,** 224-231.

ROCHETTE, P. & ERIKSEN-HAMEL, N. S. 2008. Chamber measurements of soil nitrous oxide flux: are absolute values reliable? *Soil Science Society of America Journal,* 72**,** 331-342.

RÖCKMANN, T. & LEVIN, I. 2005. High-precision determination of the changing isotopic composition of atmospheric N2O from 1990 to 2002. *Journal of Geophysical Research: Atmospheres (1984–2012),* 110.

ROY, A. H. & HAMMOND, L. L. 2004. Challenges and opportunities for the fertilizer industry. *SCOPE,* 65**,** 233-243.

RÓŻAŃSKI, K., NĘCKI, J., CHMURA, Ł., ŚLIWKA, I., ZIMNOCH, M., BIELEWSKI, J., GAŁKOWSKI, M., BARTYZEL, J. & ROSIEK, J. 2014. Anthropogenic changes of CO2, CH4, N2O, CFCl3, CF2Cl2, CCl2FCClF2, CHCl3, CH3CCl3, CCl4, SF6 and SF5CF3 mixing ratios in the atmosphere over southern Poland. *Geological Quarterly,* 58**,** 673-684, doi: 10.7306/gq. 1163.

RYALL, D., DERWENT, R., MANNING, A., SIMMONDS, P. & O'DOHERTY, S. 2001. Estimating source regions of European emissions of trace gases from observations at Mace Head. *Atmospheric Environment,* 35**,** 2507-2523.

SAKABE, A., HAMOTANI, K., KOSUGI, Y., UEYAMA, M., TAKAHASHI, K., KANAZAWA, A. & ITOH, M. 2012. Measurement of methane flux over an evergreen coniferous forest canopy using a relaxed eddy accumulation system with tuneable diode laser spectroscopy detection. *Theoretical and Applied Climatology,* 109**,** 39-49.

SCHMIDT, M., LOPEZ, M., YVER KWOK, C., MESSAGER, C., RAMONET, M., WASTINE, B., VUILLEMIN, C., TRUONG, F., GAL, B. & PARMENTIER, E. 2014. High-precision quasi-continuous atmospheric greenhouse gas measurements at Trainou tower (Orléans forest, France). *Atmospheric Measurement Techniques,* 7**,** 2283-2296.

SCHULZE, E., LUYSSAERT, S., CIAIS, P., FREIBAUER, A., JANSSENS, I., SOUSSANA, J., SMITH, P., GRACE, J., LEVIN, I. & THIRUCHITTAMPALAM, B. 2009. Importance of methane and nitrous oxide for Europe's terrestrial greenhouse-gas balance. *Nature Geoscience,* 2**,** 842-850.

SEITZINGER, S., HARRISON, J. A., BÖHLKE, J., BOUWMAN, A., LOWRANCE, R., PETERSON, B., TOBIAS, C. & DRECHT, G. V. 2006. Denitrification across landscapes and waterscapes: a synthesis. *Ecological Applications,* 16**,** 2064-2090.

SHERIDAN, P. & VOSPER, S. 2012. High-resolution simulations of lee waves and downslope winds over the Sierra Nevada during T-REX IOP 6. *Journal of Applied Meteorology and Climatology,* 51**,** 1333-1352.

SHIN, H. H. & HONG, S.-Y. 2011. Intercomparison of planetary boundary-layer parametrizations in the WRF model for a single day from CASES-99. *Boundary-Layer Meteorology,* 139**,** 261-281.

SINGER, I. & SMITH, M. 1968. A SUMMARY OF THE RECOMMENDED GUIDE FOR THE PREDICTION OF THE DISPERSION OF AIRBORNE EFFLUENTS. Brookhaven National Lab., Upton, NY.

SMIL, V. 2002. Nitrogen and food production: proteins for human diets. *AMBIO: A Journal of the Human Environment,* 31**,** 126-131.

SMIL, V. 2004. *Enriching the earth: Fritz Haber, Carl Bosch, and the transformation of world food production*, MIT press.

SMITH, F. 1968. Conditioned particle motion in a homogeneous turbulent field. *Atmospheric Environment (1967),* 2**,** 491-508.

SMITH, K. A. 2010. *Nitrous oxide and climate change,* London ; Washington, DC, Earthscan.

SMITH, K. A. & DOBBIE, K. E. 2001. The impact of sampling frequency and sampling times on chamber-based measurements of N2O emissions from fertilized soils. *Global Change Biology,* 7**,** 933-945.

STILT. 2015. *STILT information page* [Online]. Available: http://www.stilt-model.org/pmwiki/pmwiki.php [Accessed July 2015].

STOHL, A., FORSTER, C., FRANK, A., SEIBERT, P. & WOTAWA, G. 2005. Technical note: The Lagrangian particle dispersion model FLEXPART version 6.2. *Atmospheric Chemistry and Physics,* 5**,** 2461-2474.

STOHL, A., PRATA, A., ECKHARDT, S., CLARISSE, L., DURANT, A., HENNE, S., KRISTIANSEN, N., MINIKIN, A., SCHUMANN, U. & SEIBERT, P. 2011. Determination of time-and height-resolved volcanic ash emissions and their use for quantitative ash dispersion modeling: the 2010 Eyjafjallajökull eruption. *Atmospheric Chemistry and Physics,* 11**,** 4333-4351.

STOHL, A., SEIBERT, P., ARDUINI, J., ECKHARDT, S., FRASER, P., GREALLY, B., LUNDER, C., MAIONE, M., MÜHLE, J. & O'DOHERTY, S. 2009. An analytical inversion method for determining regional and global emissions of greenhouse gases: Sensitivity studies and application to halocarbons. *Atmospheric Chemistry and Physics,* 9**,** 1597-1620.

SUTKA, R. L., OSTROM, N., OSTROM, P., BREZNAK, J., GANDHI, H., PITT, A. & LI, F. 2006. Distinguishing nitrous oxide production from nitrification and denitrification on the basis of isotopomer abundances. *Applied and environmental microbiology,* 72**,** 638-644.

SUTTON, M. A., ERISMAN, J. W., DENTENER, F. & MÖLLER, D. 2008. Ammonia in the environment: from ancient times to the present. *Environmental Pollution,* 156**,** 583-604.

SUTTON, M. A., HOWARD, C. M., ERISMAN, J. W., BILLEN, G., BLEEKER, A., GRENNFELT, P., VAN GRINSVEN, H. & GRIZZETTI, B. 2011a. *The European nitrogen assessment: sources, effects and policy perspectives*, Cambridge University Press.

SUTTON, M. A., OENEMA, O., ERISMAN, J. W., LEIP, A., VAN GRINSVEN, H. & WINIWARTER, W. 2011b. Too much of a good thing. *Nature,* 472**,** 159-161.

SWINBANK, W. 1951. The measurement of vertical transfer of heat and water vapor by eddies in the lower atmosphere. *Journal of Meteorology,* 8**,** 135-145.

SYAKILA, A. & KROEZE, C. 2011. The global nitrous oxide budget revisited. *Greenhouse Gas Measurement and Management,* 1**,** 17-26.

THOMPSON, R., MANNING, A., GLOOR, E., SCHULTZ, U., SEIFERT, T., HÄNSEL, F., JORDAN, A. & HEIMANN, M. 2009. In-situ measurements of oxygen, carbon monoxide and greenhouse gases from Ochsenkopf tall tower in Germany. *Atmospheric Measurement Techniques,* 2**,** 573-591.

THOMPSON, R. L., CHEVALLIER, F., CROTWELL, A. M., DUTTON, G., LANGENFELDS, R. L., PRINN, R. G., WEISS, R. F., TOHJIMA, Y., NAKAZAWA, T. & KRUMMEL, P. B. 2014. Nitrous oxide emissions 1999 to 2009 from a global atmospheric inversion. *Atmospheric Chemistry and Physics,* 14**,** 1801-1817.

THOMSON, D. 1987. Criteria for the selection of stochastic models of particle trajectories in turbulent flows. *Journal of Fluid Mechanics,* 180**,** 529-556.

THOMSON, D., PHYSICK, W. & MARYON, R. 1997. Treatment of interfaces in random walk dispersion models. *Journal of Applied Meteorology,* 36**,** 1284-1295.

ULIASZ, M. 1993. The atmospheric mesoscale dispersion modeling system. *Journal of Applied Meteorology,* 32**,** 139-149.

ULIASZ, M. & PIELKE, R. 1990. Receptor-oriented Lagrangian-Eulerian model of mesoscale air pollution dispersion. *Computer techniques in environmental studies***,** 57-68.

UNFCCC. 2014. *GHG Data from UNFCCC* [Online]. Available: http://unfccc.int/ghg_data/ghg_data_unfccc/items/4146.php [Accessed July 2015].

URBANIAK, M. 2006. Ocena sezonowej zmienności strumieni dwutlenku węgla i pary wodnej na terenach podmokłych metodą kowariancji wirów. *Praca doktorska. Poznań. Katedra Agrometeorologii, Wydział Melioracji i Inżynierii Środowiska, AR. Maszynopis ss,* 103.

VAN EGMOND, K., BRESSER, T. & BOUWMAN, L. 2002. The European nitrogen case. *AMBIO: A Journal of the Human Environment,* 31**,** 72-78.

VELTHOF, G., JARVIS, S., STEIN, A., ALLEN, A. & OENEMA, O. 1996. Spatial variability of nitrous oxide fluxes in mown and grazed grasslands on a poorly drained clay soil. *Soil Biology and Biochemistry,* 28**,** 1215-1225.

VENTEREA, R. & PARKIN, T. 2012. Quantifying biases in non-steady state chamber measurements of soil-atmosphere gas exchange. *Managing agricultural greenhouse gases. Elsevier, Boston***,** 327-343.

VENTEREA, R. T. 2010. Simplified method for quantifying theoretical underestimation of chamber-based trace gas fluxes. *Journal of environmental quality,* 39**,** 126-135.

VENTEREA, R. T. 2013. Theoretical comparison of advanced methods for calculating nitrous oxide fluxes using non-steady state chambers. *Soil Science Society of America Journal,* 77**,** 709-720.

VENTEREA, R. T. & BAKER, J. M. 2008. Effects of soil physical nonuniformity on chamber-based gas flux estimates. *Soil Science Society of America Journal,* 72**,** 1410-1417.

VENTEREA, R. T., SPOKAS, K. A. & BAKER, J. M. 2009. Accuracy and precision analysis of chamber-based nitrous oxide gas flux estimates. *Soil Science Society of America Journal,* 73**,** 1087-1093.

VESTRENG, V. 2005. *Inventory Review 2005: Emission Data Reported to LRTAP Convention and Under the NEC Directive: Initial Review for HMs and POPs*, Meteorological synthesizing centre-west.

VITOUSEK, P. M., CASSMAN, K., CLEVELAND, C., CREWS, T., FIELD, C. B., GRIMM, N. B., HOWARTH, R. W., MARINO, R., MARTINELLI, L. & RASTETTER, E. B. 2002. Towards an ecological understanding of biological nitrogen fixation. *Biogeochemistry,* 57**,** 1-45.

VITOUSEK, P. M. & HOWARTH, R. W. 1991. Nitrogen limitation on land and in the sea: how can it occur? *Biogeochemistry,* 13**,** 87-115.

VOLK, C., ELKINS, J., FAHEY, D., DUTTON, G., GILLIGAN, J., LOEWENSTEIN, M., PODOLSKE, J., CHAN, K. & GUNSON, M. 1997. Evaluation of source gas lifetimes from stratospheric observations. *Journal of Geophysical Research: Atmospheres (1984–2012),* 102**,** 25543-25564.

WAGNER, S. W., REICOSKY, D. C. & ALESSI, R. S. 1997. Regression models for calculating gas fluxes measured with a closed chamber. *Agronomy journal,* 89**,** 279-284.

WŁODARCZYK, T., STĘPNIEWSKI, W. & BRZEZIŃSKA, M. 2002. Dehydrogenase activity, redox potential, and emissions of carbon dioxide and nitrous oxide from Cambisols under flooding conditions. *Biology and Fertility of Soils,* 36**,** 200-206.

WMO 2013. GAW Report No. 213, 17th WMO/IAEA Meeting on Carbon Dioxide, Other Greenhouse Gases and Related Tracers Measurement Techniques (GGMT-2013) (Beijing, China, 10-13 June 2013). World Meteorological Organization, Global Atmosphere Watch.

WMO. 2015. *World Meteorological Organization Global Atmosphere Watch website* [Online]. Available: http://www.wmo.int/gaw/ [Accessed July 2015].

WOLF, B., MERBOLD, L., DECOCK, C., TUZSON, B., HARRIS, E., SIX, J., EMMENEGGER, L. & MOHN, J. 2015. First on-line isotopic characterization of N2O emitted from intensively managed grassland. *Biogeosciences Discussions,* 12**,** 1573-1611.

WOLFF, E. & SPAHNI, R. 2007. Methane and nitrous oxide in the ice core record. *Philosophical Transactions of the Royal Society of London A: Mathematical, Physical and Engineering Sciences,* 365**,** 1775-1792.

XIONG, X., MADDY, E. S., BARNET, C., GAMBACORTA, A., PATRA, P. K., SUN, F. & GOLDBERG, M. 2014. Retrieval of nitrous oxide from Atmospheric Infrared Sounder: Characterization and validation. *Journal of Geophysical Research: Atmospheres,* 119**,** 9107-9122.

XU, R., PRENTICE, I. C., SPAHNI, R. & NIU, H. S. 2012. Modelling terrestrial nitrous oxide emissions and implications for climate feedback. *New Phytologist,* 196**,** 472-488.

ZAEHLE, S. & DALMONECH, D. 2011. Carbon–nitrogen interactions on land at global scales: current understanding in modelling climate biosphere feedbacks. *Current Opinion in Environmental Sustainability,* 3**,** 311-320.

ZIMNOCH, M., GODLOWSKA, J., NECKI, J. & ROZANSKI, K. 2010. Assessing surface fluxes of CO2 and CH4 in urban environment: a reconnaissance study in Krakow, Southern Poland. *Tellus B,* 62**,** 573-580.

ZIMNOCH, M., WACH, P., CHMURA, L., GORCZYCA, Z., ROZANSKI, K., GODLOWSKA, J., MAZUR, J., KOZAK, K. & JERIČEVIĆ, A. 2014. Factors controlling temporal variability of near-ground atmospheric 222 Rn concentration over central Europe. *Atmospheric Chemistry and Physics,* 14**,** 9567-9581.